VOLUME 35 FEBRUARY 1957 NUMBER 2

Canadian Journal of Physics

Published by THE NATIONAL RESEARCH COUNCIL
OTTAWA CANADA

CANADIAN JOURNAL OF PHYSICS

(Formerly Section A, Canadian Journal of Research)

Under the authority of the Chairman of the Committee of the Privy Council on Scientific and Industrial Research, the National Research Council issues THE CANADIAN JOURNAL OF PHYSICS and six other journals devoted to the publication, in English or French, of the results of original scientific research. Matters of general policy concerning these journals are the responsibility of a joint Editorial Board consisting of: members representing the National Research Council of Canada; the Editors of the Journals; and members representing the Royal Society of Canada and four other scientific societies.

Manuscripts for publication should be submitted to Dr. Léo Marion, Editor-in-Chief Canadian Journal of Physics, National Research Council, Ottawa 2, Canada.

(For instructions on preparation of copy, see **Notes to Contributors** (inside back cover).)

Proof, correspondence concerning proof, and orders for reprints should be sent to the Manager, Editorial Office (Research Journals), Division of Administration, National Research Council, Ottawa 2, Canada.

Subscriptions, renewals, requests for single or back numbers, and all remittances should be sent to Division of Administration, National Research Council, Ottawa 2, Canada. Remittances should be made payable to the Receiver General of Canada, credit National Research Council.

The journals published, frequency of publication, and prices are:

Canadian Journal of Biochemistry and Physiology	Monthly	$3.00 a year
Canadian Journal of Botany	Bimonthly	$4.00 a year
Canadian Journal of Chemistry	Monthly	$5.00 a year
Canadian Journal of Microbiology	Bimonthly	$3.00 a year
Canadian Journal of Physics	Monthly	$4.00 a year
Canadian Journal of Technology	Bimonthly	$3.00 a year
Canadian Journal of Zoology	Bimonthly	$3.00 a year

The price of single numbers of all journals is 75 cents.

Canadian Journal of Physics

Issued by THE NATIONAL RESEARCH COUNCIL OF CANADA

VOLUME 35 FEBRUARY 1957 NUMBER 2

THE FLASH PHOTOLYSIS OF DIACETYLENE[1]

J. H. CALLOMON[2] AND D. A. RAMSAY

ABSTRACT

A brief description is given of a "microsecond" flash photolysis apparatus in which a 40 μf. condenser charged to 8000 v. is discharged through a photolysis flash tube in ~20 microseconds. Absorption spectra of transient species are photographed with a second flash tube which provides a source of continuum by discharging a 2 μf. condenser charged to 10,000 v., in 3–5 microseconds. A circuit for controlling the time interval between the two flashes is given.

Experiments on the flash photolysis of diacetylene are discussed. With diacetylene at 0.5 mm. Hg pressure several well-known band systems were photographed in absorption 20 microseconds after the beginning of the photolysis flash, viz., the C_2 Swan bands, the C_2 Phillips bands, the C_2 Deslandres–d'Azambuja bands, the 4050 Å bands of C_3, and the CH band at 3143 Å. The rotational temperature of these bands was ~3000°–5000° K. The C_2 Swan bands were also recorded in emission after a single photolysis flash. When a considerable excess (100:1) of helium was added to the diacetylene, all the above band systems disappeared with the exception of the C_3 bands.

In the absence of helium it is probable that the reaction is mainly thermal and that the high temperature is produced by a thermal explosion of the diacetylene triggered by the photolysis flash. The thermal reaction is suppressed by the addition of excess helium and the photochemical reaction becomes dominant. Under these conditions it is interesting to note that C_3, but no C_2, is produced. It appears therefore that C_3 is a product of the photochemical decomposition of diacetylene. Possible mechanisms are discussed.

INTRODUCTION

The near ultraviolet absorption spectrum of diacetylene was first investigated by Woo and Chu (1935, 1937), who observed many sharp and narrow bands in the region 2970–2650 Å and many more diffuse bands in the region below 2650 Å. The bands in the region 3000–2500 Å have recently been reinvestigated (Callomon 1956) using the very high resolving power afforded by a 35 ft. concave grating spectrograph. No rotational fine structure was observed, although the slit width used was comparable to the rotational line width due to Doppler and collision broadening. The diacetylene molecule, therefore, appears to be predissociated by radiation of these wavelengths and it is interesting to inquire into the nature of the predissociation process and the primary dissociation products.

No previous photochemical experiments appear to have been carried out

[1]Manuscript received September 28, 1956.
Contribution from the Division of Pure Physics, National Research Council, Ottawa, Canada.
Issued as N.R.C. No. 4186.
[2]National Research Laboratories Postdoctorate Fellow 1953–1955; present address: Department of Chemistry, University College, London, England.

with diacetylene. A preliminary experiment on the flash photolysis of diacetylene indicated that considerable decomposition was produced by a single photolysis flash. Further experiments were therefore carried out to study this reaction in more detail and are the subject of the present paper.

APPARATUS

The experiments were carried out with a "microsecond" flash photolysis apparatus (Ramsay 1956), the essential features of which are as follows:

Reaction cell.—Quartz tube, 25 cm. long, 2 cm. diameter, quartz windows.

Photolysis lamp.—Quartz tube, 25 cm. long, 1.5 cm. diameter, duralumin electrodes, filled with xenon to 75 mm. Hg, fired by a 40 μf. condenser charged to 8000 v. using a triggered spark gap in series; duration of the flash ~20 microseconds.

"Source" lamp.—Quartz capillary tube, ~5 cm. long, 3 mm. internal diameter, expanding into two end sections containing tungsten electrodes, lamp filled with xenon to 75 mm. Hg, fired by a 2 μf. condenser charged to 10,000 v. by means of a 5C22 hydrogen thyratron in series; duration of the flash 5–10 microseconds.

The time delay between the photolysis flash and the "source" flash which provided the continuum for the absorption experiments was controlled by means of the circuit given in Fig. 1. Light from the photolysis flash falls on

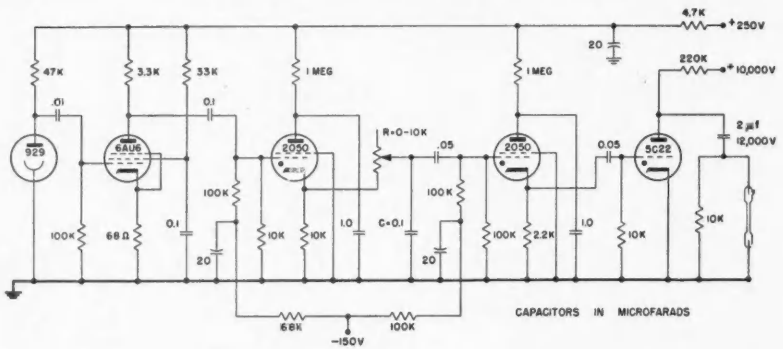

FIG. 1. Circuit used for controlling the time delay between the photolysis and the "source" flashes.

a 929 phototube producing a pulse which is amplified by a 6AU6 tube and triggers the first of a series of three thyratrons. The voltage pulse across the cathode resistor of the first 2050 thyratron charges a condenser C through a variable resistor R and fires a second 2050 thyratron after a time determined by RC. The pulse from the second 2050 thyratron in turn fires the 5C22 hydrogen thyratron causing the voltage across the 2 μf. condenser to appear across the "source" flash tube which then breaks down. It may be noted that there is no voltage across the "source" flash tube until the instant of firing.

The time delay is variable from 2 to ~250 microseconds and is reproducible to a few microseconds. The circuit is similar in some respects to one which has been published earlier by Marshall and Davidson (1953).

The waveform of the photolysis and "source" flashes and the time delay between them were observed by means of a 929 phototube in series with a 1000 ohm resistor. The voltage pulse across the latter was applied to the vertical plates of a Dumont Type 303 AH cathode ray oscilloscope. Experiments with light pulses reflected from a high-speed rotating mirror indicated that this simple recording circuit had a time constant of ~1–2 microseconds.

EXPERIMENTAL

Diacetylene was prepared from 2-butyne-1,4-diol in the way described in an earlier paper (Callomon 1956). Preliminary flash photolysis experiments were carried out using pressures of diacetylene from 10 to 100 mm. Hg. Absorption spectra were recorded in a single flash using a Hilger E1 spectrograph. Spectra taken 20 microseconds after the beginning of the photolysis flash showed a continuous absorption below 4000 Å. A considerable black deposit was formed in each experiment, making it necessary to clean the reaction cell between flashes.

At pressures of diacetylene of only 0.5 mm. Hg the black deposit was less troublesome and the continuous absorption considerably reduced, so that absorption spectra could be recorded down to ~2500 Å. The C_2 Swan bands then appeared strongly in absorption together with other band systems. The region from 2500 to 9000 Å was investigated with a 21 ft. grating spectrograph, the band systems observed and their approximate intensities being given in Table I. The C_2 Swan bands were sufficiently intense that the $C^{12}C^{13}$

TABLE I

BAND SYSTEMS OBSERVED DURING THE FLASH PHOTOLYSIS OF DIACETYLENE

Band system	Estimated relative intensity	Bands observed
C_2 Swan bands		
$A\ ^3\Pi_g$–$X\ ^3\Pi_u$	100	(0, 2), (1, 3), (2, 4) (0, 1), (1, 2), (2, 3) (0, 0), (1, 1), (2, 2) (1, 0), (2, 1), (3, 2), (4, 3), (5, 4) (2, 0), (3, 1), (4, 2)
C_2 Phillips bands		
$b\ ^1\Pi_u$—$a\ ^1\Sigma_g^+$	10	(2, 0), (3, 0)
C_2 Deslandres–d'Azambuja bands		
$c\ ^1\Pi_g$—$b\ ^1\Pi_u$	20	(0, 1), (0, 0), (1, 0), (2, 0), (3, 1)
C_2 4050 Å bands	10	
CH 3143 Å band	10	(0, 0)

head of the (1, 0) band was observed (see Fig. 2). The Deslandres–d'Azambuja system of C_2 has not been previously reported in absorption.

Experiments were carried out varying the time delay between the photolysis and the "source" flashes. It was found, however, that the most intense absorp-

tion spectra were obtained immediately after the photolysis flash, i.e., ~20 microseconds after its beginning. In the case of the C_2 Swan bands, it was found that these could also be observed *in emission* after a single photolysis flash without the "source" flash, suggesting that the system was being raised to a high temperature.

Further experiments were carried out using the same pressure of diacetylene and adding increasing amounts of helium to lower the temperature of the system. With a ratio of helium to diacetylene of 100:1, it was found that all the band systems listed in Table I disappeared with the exception of the C_3 bands, which remained with about the same intensity. The half-intensity lifetime of the bands under these conditions was about 25–50 microseconds.

DISCUSSION

The observation of the C_2 Swan bands in emission during the flash photolysis of diacetylene indicates that the system is being raised to a very high temperature. From the intensity distributions of the rotational structure in the C_2 and CH band systems in absorption, the temperature of the system immediately after the photolysis flash was estimated to be in the region of 3000°–5000° K. Under these conditions, C_2 absorption bands are observed not only from the lowest triplet and singlet states (the Swan and Phillips bands, respectively), but also from the first excited singlet state 8392 cm^{-1} above the lowest singlet state (the Deslandres–d'Azambuja bands). It is interesting to note that while in experiments with carbon furnaces the Swan and Phillips bands are readily obtained, the Deslandres–d'Azambuja bands have not been observed, and it is possible that the Deslandres–d'Azambuja bands are observed in the present experiments because the temperature of the system is higher than that which can be achieved in a carbon furnace.

The high temperature is probably produced by a thermal explosion of the diacetylene initiated by the photolysis flash. Diacetylene is an endothermic compound and, although its heat of formation has not yet been reported, it is probable that the energy liberated in its thermal decomposition is sufficient to raise the temperature of the system to the observed value.

When a considerable excess of helium is added to the diacetylene, the thermal reaction is suppressed and the photochemical reaction becomes dominant. Under these circumstances, it is interesting to note that C_3 bands, but no C_2 bands, are observed. Furthermore, the rotational temperature of the C_3 bands corresponds approximately to room temperature. It appears, therefore, that C_3 is a product of the photochemical decomposition of diacetylene.

It is interesting to inquire into the mechanism of the photodissociation process. The fact that diacetylene has a relatively weak central C—C bond in the ground state may be important in a discussion of the thermal decomposition of diacetylene, but it is not necessarily relevant to a discussion of the photochemical decomposition. In the latter case, the important factors are the nature of the excited state of diacetylene and the repulsive state producing

PLATE I

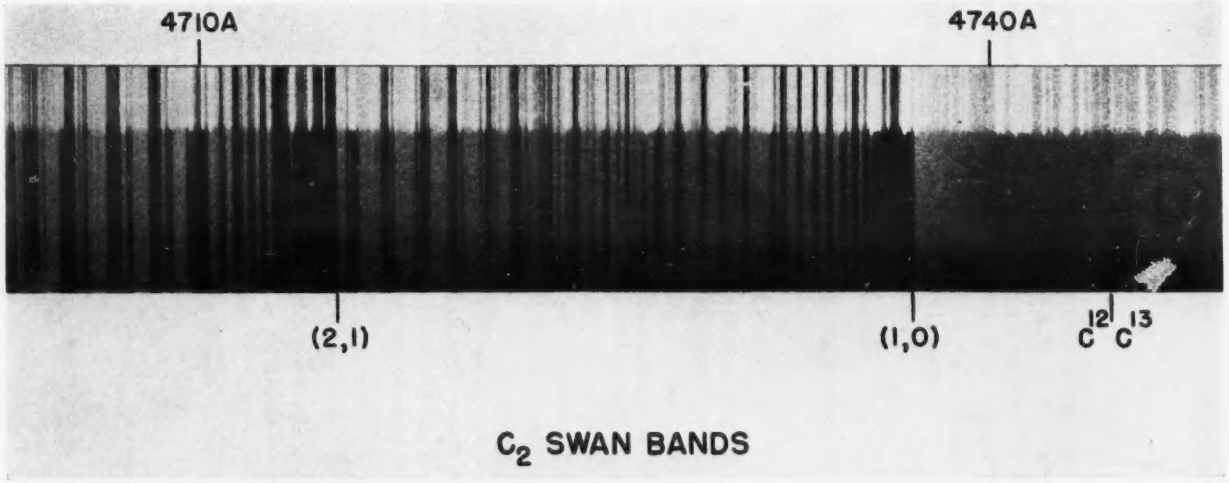

FIG. 2. Part of the (1, 0) sequence of the C_2 Swan bands observed in absorption during the flash photolysis of diacetylene. The $C^{12}C^{13}$ head of the (1, 0) band is also visible.

predissociation. About these, little is known. There are, however, only three ways by which diacetylene can dissociate into two fragments, viz.,

$$C_4H_2 \rightarrow 2C_2H,$$
$$C_4H_2 \rightarrow C_3H+CH,$$
$$C_4H_2 \rightarrow C_4H+H.$$

Since no C_2 radicals are observed in the photochemical reaction, it is unlikely that the primary split is into two C_2H radicals since it would be necessary to postulate that these radicals react further to produce C_3 and not C_2. The most attractive mechanism for explaining the formation of C_3 and not C_2 is to assume that the molecule dissociates into C_3H+CH and that the C_3 radicals are produced by a secondary reaction such as

$$C_3H+CH \rightarrow C_3+CH_2,$$

or

$$C_3H \rightarrow C_3+H.$$

There is insufficient evidence, however, to determine the mechanism unambiguously.

CONCLUDING REMARKS

The production of C_3 radicals by the photolysis of diacetylene is of interest since this is the first example of a molecule which produces C_3 by photodecomposition. This result may have a bearing on the question of the method of production of C_3 in comets. Although it does not follow that diacetylene is the molecule responsible for the production of C_3 radicals in comets, nevertheless the present experiments do establish that it is possible to produce these radicals photochemically and raise the possibility that there may be other hydrocarbon molecules which produce C_3 by photodecomposition. The present results are of interest also in problems connected with carbon formation since they provide a system in which carbon formation can be studied photochemically and also raise the question whether carbon formed by the polymerization of C_3 has the same properties as carbon formed by the polymerization of C_2. Clearly it would be interesting to carry out further experiments on the photochemistry of diacetylene.

ACKNOWLEDGMENTS

The authors are indebted to Dr. G. Herzberg for critical discussion of this manuscript and to Drs. C. C. Costain and R. S. Richards for helpful suggestions concerning the time delay circuit.

REFERENCES

CALLOMON, J. H. 1956. Can. J. Phys. **34**, 1046.
MARSHALL, R. and DAVIDSON, N. 1953. J. Chem. Phys. **21**, 659.
RAMSAY, D. A. 1956. Ann. N. Y. Acad. Sci. (In press).
WOO, S. C. and CHU, T. C. 1935. J. Chem. Phys. **3**, 541.
——— 1937. J. Chem. Phys. **5**, 786.

IONIC MOBILITIES IN ARGON AND HELIUM LIQUIDS[1]

R. L. WILLIAMS[2]

ABSTRACT

The mobilities of ions and electrons have been measured in liquid argon at 90° K., and in liquid helium from 4.2° to 1.4° K. The electron behavior in liquid argon can be explained in terms of gas kinetic theory, while the positive ion behavior in both liquids cannot. Stokes' law predicts the ionic behavior at the boiling points of the two liquids. Electrons in liquid helium have very small mobilities, approximately one-quarter the value for the positive ions, suggesting a wide departure from the electron behavior in argon. Below 2.19° K. both the electronic and ionic mobilities become temperature and electric field dependent.

INTRODUCTION

The feasibility of using alpha particle induced currents to study the properties of liquid argon was first demonstrated by Davidson and Larsh (1948). They, as well as Hutchinson (1948), were unsuccessful in measuring the mobility of the charge carriers released in the ionization process. Malkin and Shultz (1951), using a very wide band amplifier, found the mobility of electrons at 25 kv./cm. to be 20 cm.^{2}/v-sec., and inversely proportional to the square root of the applied field. However, they could make measurements only over a restricted range of fields (10–85 kv./cm.) because of limitations in their measuring equipment. The cross section for collision of electrons with argon atoms, based on the kinetic theory of gases, was of the order of one hundredth the gaseous value. By reducing the noise of the electronic equipment, it has been possible to extend the field range of electron mobility observations and to measure the positive ion mobility. These results have been used to determine some of the characteristics of liquid argon, and similar observations made in liquid helium provided a useful comparison.

THEORY

To interpret the results of their mobility measurements, Malkin and Shultz used gas kinetic theory. The significant equations involved, along with some theories related to liquids, are summarized below.

Langevin (see e.g. Loeb 1939) showed that ions of mass M_i and charge e, moving in a medium of atoms of mass M, having a mean free path L and a root mean square velocity C_i, have a mobility of

$$\mu_i = \frac{0.815eL}{M_i C_i}\sqrt{\frac{M+M_i}{M}}. \tag{1}$$

In small electric fields, the root mean square velocity is equal to the thermal velocity $(3kT/M)^{\frac{1}{2}}$ where k is Boltzmann's constant and T is the absolute temperature of the particles considered.

[1]Manuscript received August 15, 1956.
Contribution from the Department of Physics, University of British Columbia, Vancouver, B.C.

[2]Present address: Canadian Armament Research and Development Establishment, Valcartier, Que.

As electrons have much smaller masses m than atoms, equation (1) gives for their mobility

$$\mu_e = 0.815e\lambda/mc \tag{2}$$

where λ is the mean free path of electrons of root mean square velocity c. In the presence of an electric field the root mean square velocity is greater than the thermal velocity. In all but the highest electric fields the deviation of C_i from the thermal velocity is small for ions, and equation (1) is generally applicable. For electrons, even small electric fields cause substantial changes in c and equation (2) must be modified.

Electrons lose on the average a small fraction f of their energy $\mathscr{E}$ in collisions with atoms. The electrons accumulate energy even in a moderate electric field so that $\mathscr{E} \gg kT$. The average fraction of energy lost per collision is given by Cravath (1930) as

$$f = \frac{8mM}{3(M+m)^2}\left[1-\frac{3}{2}\frac{kT}{\mathscr{E}}\right] \simeq 2.66\,\frac{m}{M}. \tag{3}$$

In an electric field E, the average terminal energy $\frac{1}{2}mc^2$ becomes

$$\tfrac{1}{2}mc^2 = \frac{1}{2}\left[\tfrac{3}{2}kT+\left\{(\tfrac{3}{2}kT)^2+\frac{E^2\lambda^2e^2M}{1.5m}\right\}^{\frac{1}{2}}\right] \tag{4}$$

so that

$$\mu_e = \frac{0.815e\lambda}{\sqrt{m}\left[\tfrac{3}{2}kT+\left\{(\tfrac{3}{2}kT)^2+\dfrac{E^2\lambda^2e^2M}{1.5m}\right\}^{\frac{1}{2}}\right]^{\frac{1}{2}}}.$$

For most practical fields the factor M/m allows the equation

$$\mu_e = 0.815(1.5m/M)^{\frac{1}{2}}(e\lambda/mE)^{\frac{1}{2}} \tag{5}$$

to be used with negligible error. From this form the mean free path can be calculated from the observed mobility.

As the cross section, Q, for collisions of electrons with atoms is related to the mean free path of the electrons in a gas of N atoms per cc. by

$$QN\lambda = 1, \tag{6}$$

the collision cross section of the atoms of the gas can be calculated from the mobility.

Electrons in argon gas experience a strong energy-dependent collision cross section with a pronounced minimum which was investigated by Ramsauer (1921). This has been explained by Holtzmark (1929) and is discussed by Massey and Burhop (1952, p. 113). At energies slightly less than one electron volt the electrons experience very small cross sections, but at 12 electron volts there is a maximum. A graph of the cross section is given in Fig. 5, along with the values of cross section deduced from the present experiments in liquid argon.

Another interpretation of the ion mobility measurements can be based on the macroscopic properties of liquids. Stokes' law relates the viscosity η of the liquid with the mobility and the radius a of a diffusing particle by

$$\text{velocity/force} = \mu E/eE = 1/6\pi\eta a. \tag{7}$$

This formula is applicable to particles which are not small by comparison with atoms of the liquid, i.e. for ions, but not electrons.

The theory of diffusion developed by Eyring (1936) can be applied to the ion mobilities. As the diffusion coefficient D is related to the mobility by the Einstein relationship $\mu/D = e/kT$, the theory can be applied to mobility measurements. The Eyring theory is based on a mechanism of ion trapping in potential wells, and thermal ion excitation resulting in an ion drift in the direction of the applied field. Both the Eyring theory and Stokes' law predict a temperature-dependent, field-independent mobility.

APPARATUS

The electrode system used for measurement in liquid argon is illustrated in Fig. 1. Alpha particles are emitted from a polonium source in the center

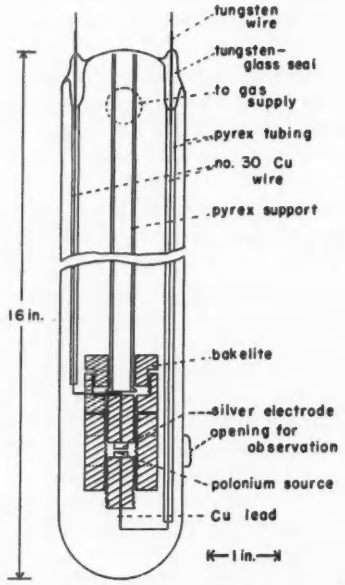

FIG. 1. Electrode system used for measuring collecting time of electrons and ions.

of one electrode. Each alpha particle in passing through the liquid produces a small densely ionized column. The range of the alpha particles in the liquids used is generally much smaller than the electrode spacing so that the alpha particle can be considered as producing instantaneously a cluster of positive and negative ions at the surface of one of the electrodes. The ions then drift to the electrodes under the influence of an applied electric field and produce a rectangular pulse of current (Fig. 2(*a*)). The drift velocity of the ions is equal to the ratio of the electrode spacing to the measured duration of the current pulse. The mobility of both the positive and negative ions can be determined by changing the polarity of the electrodes.

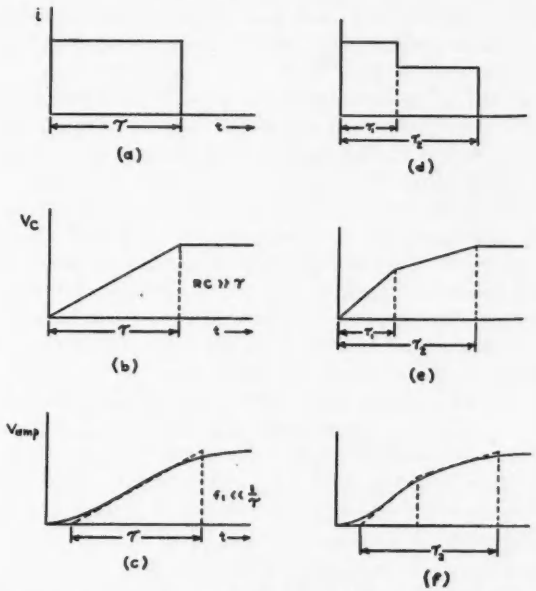

FIG. 2. Idealized pulse forms in argon (*a*, *b*, *c*) and helium (*d*, *e*, *f*).

Commercial argon was liquefied and maintained in the sealed tube enclosing the electrodes by immersion in liquid oxygen. For experiments in liquid helium the bottom half of the outer glass tube was removed and the electrode system suspended in a bath of helium by an 'O' ring seal at the head of the dewar system.

Travelling telescope measurements of electrode spacing made with the system cooled to near the working temperatures indicated that the electrodes were parallel to at least 2% across the dimensions of the polonium alpha source. Restriction of the source to a small central region eliminated edge effects. The silver electrodes were polished to increase the breakdown field and the leads surrounded by glass tubing to prevent any currents in the gas above the electrodes.

With this system the total capacitance of the signal leads and amplifier input was from 15 to 25 micromicrofarads. A block diagram of the electronic equipment is given in Fig. 3.

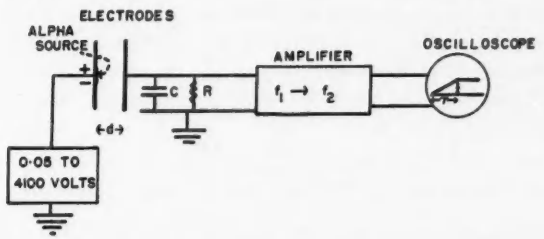

FIG. 3. Schematic diagram of measuring apparatus.

In determining the best electronic system the following idealized conditions were assumed. The current produced in a single event had a value i and lasted for a time τ, Fig. 2(a). With such a signal the largest voltage that could be obtained using an amplifier of input capacity C and resistance R was $i\tau/C$ if $RC \gg \tau$. Under such conditions the current of 2(a) was integrated as in 2(b) (the decay is not indicated) and passage of this voltage through an amplifier of bandwidth $f_2 \gg f_1$ modifies the signal to that shown in Fig. 2(c) ($f_1 \ll 1/\tau$). The upper and lower frequency limits of an amplifier are taken to be f_2 and f_1 respectively. To determine the time of the actual pulses, oscilloscope traces were photographed and the fastest rising portion of the photographed traces extrapolated to the maximum and zero amplitudes. Corrections were then applied for the rise time of the amplifier τ_a, using $\tau = (\tau_0^2 - \tau_a^2)^{\frac{1}{2}}$ where τ_0 is the observed rise time (Elmore and Sands 1949). For experiments in liquid argon the small effect of the range of the alpha particle was avoided by using the largest pulses only, while in helium the range effect was large enough to cause considerable trouble in analyzing the data.

For an electronic amplifier of equivalent noise resistance R_a, having frequency limits $f_2 \gg f_1$, a grid current I_g, and an input time constant CR, such that $2\pi f_1 CR$ is greater than unity, the mean square noise voltage referred to the input is given by

$$\overline{V^2} = 4kTf_2R_a + \frac{eI_g}{2\pi^2C^2f_1} + \frac{kT}{\pi^2C^2Rf_1} \tag{8}$$

where k is Boltzmann's constant, T is the absolute temperature at the input, and e the electronic charge (van der Ziel 1954). The third term was reduced to a negligible value by using $R = 10^9$ ohms. The value of R_a was reduced to approximately 500 ohms by the use of a 6AK5–6J4 cascode and selection of the input tubes. For experiments in liquid argon, the bandwidth required made the first term predominate as f_2 was from 2 to 18 Mc. with $f_1 \sim 100$ kc. In the case of liquid helium the second term also became important as low frequencies were required; $f_2 \sim 200$ kc., $f_1 \sim 10$ kc., and $I_g \sim 10^{-9}$ amp.

Using such a high input resistance required the use of d-c. filament supplies with the source and filament leads completely shielded. The electrode system, dewars, and preamplifier were enclosed in electrical shielding.

EXPERIMENTAL RESULTS

Argon

The values of mobility deduced from rise time measurements in liquid argon at 90° K. are plotted in Fig. 4. There is a systematic error dependent on spacing with estimated errors of individual points being 11%. The systematic error can be partially accounted for by the small but finite range of the alpha particle, but it is believed that part of this error is not caused by the experimental method. The electron mobility appears to obey a law of the form

$$\mu_e = 1/(A + BE)$$

where A and B are constants. A consequence of this mobility dependence is

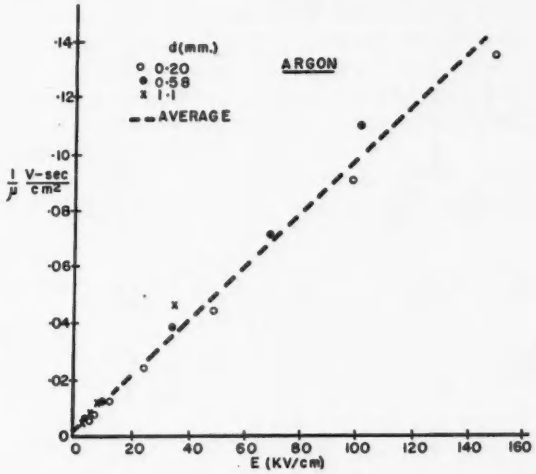

FIG. 4. Electronic mobility in liquid argon.

that the collecting time is very nearly independent of field, simplifying the experimental method. The field dependence disagrees with the result of Malkin and Shultz (1951), who found $\mu \propto E^{-\frac{1}{2}}$. The reduction of electronic noise and extension of measurements to a much wider range of field make the results of the present research more reliable. At high fields the values of mobility herein reported agree roughly with those of Malkin and Shultz.

In calculating values of the electron collision cross section, the values of mobility corresponding to the dashed line of Fig. 4 were used to calculate the cross section Q. These expressed as multiples of the cross section of the first Bohr orbit of hydrogen (of radius $a_0 = 0.58 \times 10^{-8}$ cm.) are plotted against the energy of the electrons calculated from equation (4) (Fig. 5). Plotted on the same graph but on a different scale is the electron collision cross section of argon atoms in the gaseous state. The cross section energy dependence in the liquid is quite different from that of the gaseous state, and the magnitude of the cross section is of the order of 100 times smaller in the liquid.

The mobility of the positive ions in liquid argon is given in Table I. It is seen that in the range 187 kv./cm. to 24 kv./cm., the mobility is apparently

TABLE I

MOBILITY OF POSITIVE IONS IN ARGON, $d = 0.11$ MM., AT 90° K.

E, kv./cm.	187	140	94	47	24
μ, cm.²/v-sec.	2.3	2.8	3.2	2.8	3.2

constant, having a value 2.8×10^{-3} cm.²/v-sec. The small value of ionic mobility necessitated a reduction of f_1 with the result that noise arising from

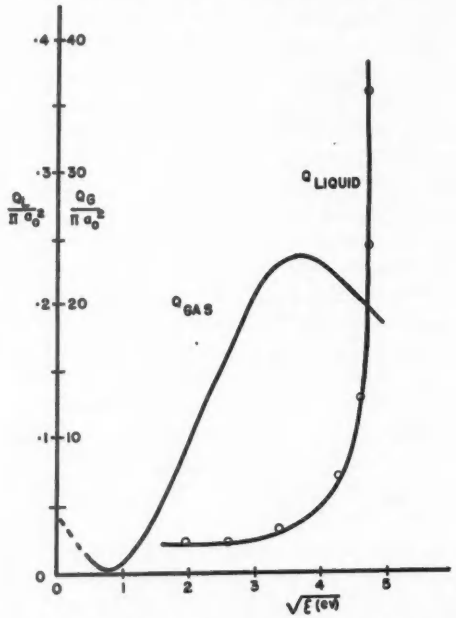

FIG. 5. Cross section for collision of electrons for atoms in argon gas and argon liquid.

the grid current became important (second term of equation (8)), so reducing the usable range of electric fields from 100:1 to 10:1.

On the basis of equation (1), this ionic mobility corresponds to a mean free path $L = 2.6\times10^{-14}$ cm., which is so short as to be meaningless in terms of ordinary kinetic theory. However application of Stokes' law in equation (7), using the gaseous thermal energy collision radius $a = 1.05\times10^{-8}$ (Massey and Burhop 1952, p. 116), together with the value of viscosity reported by Rudenko and Schubnikov (1934) 2.5×11^{-3} poise at 87.5° K., leads to $\mu_+ = 3.2 \times10^{-3}$ cm.^{2}/v-sec., in excellent agreement with the experimental result. The constant mobility is also predicted by the theory of Eyring, but agreement is not good between predicted and observed values of ion mobility, the former being a factor of 500 smaller than the latter.

Helium

The range of the alpha particles in liquid helium, as estimated from the known value in the gas, is 0.28 mm. Only if the range is much smaller than the electrode spacing will the current resulting from the alpha particle be very nearly a rectangular current pulse. Because of the small values of mobility observed in helium, low frequencies were required, and noise produced by the grid current of the amplifier predominated, cf. second term of equation (8). To reduce noise, small spacings were used so that the low frequency limit f_1 could be made as large as possible.

With spacings of the order of the range, the current pulses were not generally rectangular but of the form of Fig. 2(*d*), τ_1 being the collecting time of one type of ion, and τ_2 that of the oppositely charged ions. Of the pulses recorded from the oscilloscope screen, only those were used which had a single rate of rise, i.e. of form 2(*c*), thus corresponding to charge of one polarity travelling the total distance between the electrodes.

The values of the mobility of positive and negative ions are given in Table II. The mobility of both types of ions is apparently independent of field, but

TABLE II

MOBILITY OF POSITIVE AND NEGATIVE IONS IN HELIUM AT 4.2° K.

			d = 0.15 mm.			
E, kv./cm.	130	65	33	17	8.0	4.0
μ_+, cm.²/v-sec.	0.06	0.13	0.13	0.14	0.15	0.18
μ_-, cm.²/v-sec.	0.022	0.031	0.027	0.032	0.039	0.050
			d = 0.33 mm.			
E, kv./cm.	130	61	30	15	7.8	3.8
μ_+, cm.²/v-sec.	0.139	0.145	0.118	0.121	0.133	0.123
μ_-, cm.²/v-sec.	0.024	0.022	0.030	0.035	0.037	
			d = 0.44 mm.			
E, kv./cm.	46	23	12			
μ_+, cm.²/v-sec.	0.080	0.078	0.098			
μ_-, cm.²/v-sec.	0.021	0.024	0.024			

varies with electrode spacing in an unsystematic way with more than twice the expected experimental error. The variation in mobility found when experiments were repeated without altering the electrode spacing seemed to be quite close to the expected error. This suggests that the larger variation found for the various spacings may be caused by inability to distinguish those pulses corresponding to traversal of the complete electrode spacing. The most surprising feature is that the negative ion mobility μ_- is smaller than the positive ion mobility μ_+, their ratio μ_+/μ_- being equal to 4 (± 1) for all spacings. The average values, $\mu_+ = 8.5\times10^{-2}$ cm.²/v-sec. and $\mu_- = 2.0\times10^{-2}$ cm.²/v-sec., are not understandable in terms of kinetic theory as was μ_+ for liquid argon.

Application of Stokes' law gives $\mu_+ = 0.20$ cm.²/v-sec., using the following data: radius of helium atom = 1.34×10^{-8} cm., the gaseous electron collision cross section given by Massey and Burhop (1952, p. 410), and the viscosity of liquid helium at $T = 4.2°$ K., $\eta = 2.5\times10^{-5}$ poise (Daunt and Smith 1954). This value is more than twice the average value obtained experimentally. London (1954) pointed out that zero point energy will cause an apparent increase of the size of atoms. Using the value suggested by London of 3.3×10^{-8} cm. for the helium atom radius changes μ_+ to 0.12 cm.²/v-sec., a value in slightly better agreement with the experimental results.

As in the case of positive ions in liquid argon, the mobility is independent of field, as suggested by the Eyring theory. Here predicted mobilities are not as widely different as in argon but are still a factor of 4 too small.

As the viscosity of liquid helium decreases rapidly below the λ point, Stokes' law (equation (7)) predicts a rapid rise of mobility in this temperature region. Fig. 6 indicates that below the λ point there is indeed a strong tempera-

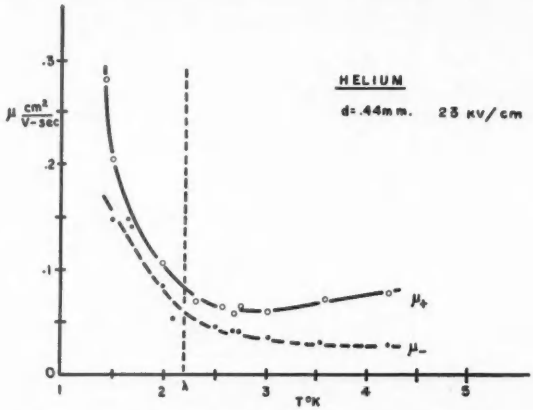

FIG. 6. Mobility of ions in liquid helium as a function of absolute temperature.

ture dependence which is found to be a function of applied field, and different for positive and negative ions. The flattening-off of the viscosity–temperature curve found below 1.85° K. (Gorter 1955) appears to have no counterpart

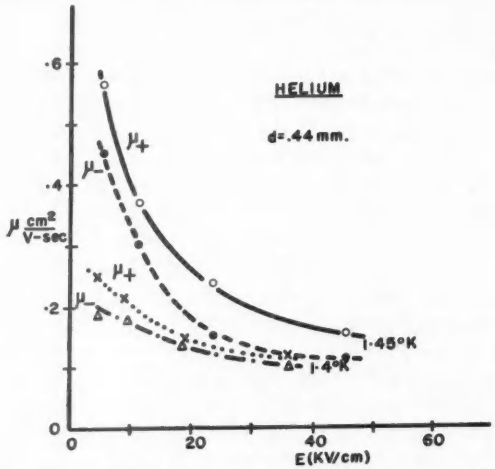

FIG. 7. Mobility of ions in liquid helium at temperatures below the λ point.

in the mobility curves. The temperature dependence, which is strongest for weak fields and negative ions, is inconsistent with the theory of Eyring.

As shown in Fig. 6, the mobility is not strongly dependent on field above the λ point temperature, but develops a definite field dependence below this region. One rather surprising feature is that there is no evidence of a different field dependence for μ_+ and μ_- at a specific temperature, while the ratio μ_+/μ_- changes from 4 at the boiling point to approximately 1.3 at 1.4° K., the mobilities are roughly proportional to $E^{-\frac{1}{2}}$ (Fig. 7).

Lack of reproducibility in the mobility measurements suggested that impurities might be present, or that external radiation might be influencing the results. During one experiment the helium dewar was opened to air until particles of solid air could be seen suspended in the liquid. There was no observed change in the mobilities, but this brief test was not conclusive since even if air had been the effective impurity, the liquid may have been saturated already. Extreme care had not been taken to prevent air entering the system during the helium transfer.

Illumination of the area between the electrodes with a hundred watt light bulb 6 cm. away had no effect on the mobilities.

CONCLUSIONS

(*a*) *General*

The extremely low values of ionic mobility in argon and helium most emphatically indicate that the liquids can not be considered as compressed gases. The agreement obtained with the predictions of Stokes' law for positive ions suggests that the theory is applicable to particles of atomic size, but not to electrons. Unfortunately, Stokes' law, being macroscopic, does not provide any model which would help to illustrate the nature of the two liquids. The Eyring theory, although in less close agreement with the experimental results, does give a crude model of the structure of the liquid.

(*b*) *Argon*

The rough agreement of the ionic mobility measurements with the form of the Eyring theory (i.e. mobility apparently independent of field) suggests that there are indeed potential wells in liquid argon. Thus the atoms of the liquid cannot be considered as independent as required by kinetic theory, but if the electrons do accumulate energy owing to their small masses, they may suffer collisions with the potential wells without being trapped. Under such conditions the electrons could be considered to have a mean free path and an average kinetic theory.

That kinetic theory may still be applicable is suggested by the Shockley theory of "hot electrons" in semiconductors (Shockley 1951) where scattering theory is used to determine the mobility when the total energy is determined by field and thermal components. For germanium a form $\mu = 1/(C_1+C_2E)$ can be fitted to the experimental data (Ryder 1953).

The small cross section found for liquid argon compared with the gas cannot satisfactorily be explained on the basis of an effective mass. A value 10^{-4}

times the rest mass would be required to give gaseous cross sections. Another feature of graph 3 is that the highest value of energy plotted is very near 20 ev., or about 4 ev. above the ionization energy of argon. Measurements of the average number of electrons released per alpha particle ionization (Williams and Stacey 1957) suggest that some multiplication may be taking place.

On the basis of all the above considerations, it seems not unreasonable that there is indeed a change in the value of the cross section and its energy dependence in passing from the gaseous to the liquid phase.

An explanation can be given for the change in cross section energy dependence by considering the theory of the Ramsauer effect in gases. Fig. 8 (Massey

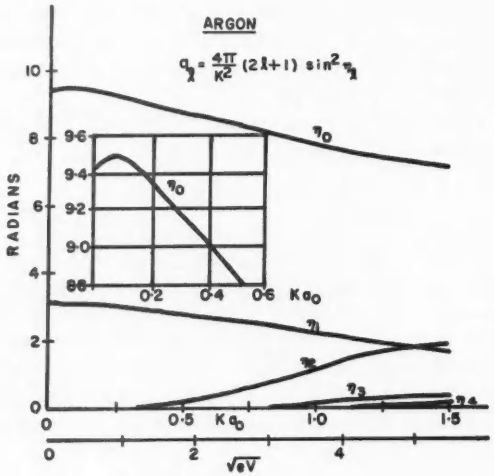

FIG. 8. Phase shift of partial waves in argon gas: a_0 is the radius of the first Bohr orbit of the hydrogen atom.

and Burhop 1952, p. 115) is a plot of the phase shift η_l experienced during the collision by the partial waves of which the incident particle is considered to be composed. The partial cross section q_l, a partial wave of orbital angular momentum l, is

$$q_l = \frac{4\pi}{k^2}(2l+1)\sin^2\eta_l$$

where k is the wave vector of the partial wave considered. For electrons in gaseous argon the contribution to the total cross section

$$Q = \sum_{l=0}^{\infty} q_l$$

of the partial waves with $l > 0$ is very small for values of energy in the region 1 to 1.5 ev. The minimum of the gaseous total cross section, Fig. 5, is then

produced by q_0 passing through a zero at an energy of approximately 0.9 ev. (see insert Fig. 8). The suggestion is offered that in liquid argon η_0 is changed slightly by the influence of the neighboring atoms so that the minimum is much broader. The sharp rise of Q (Fig. 5) in the vicinity of 16 ev. is then due to η_l for $l > 0$ beginning to have values different from $n\pi$.

(*c*) *Helium*

The positive ion behavior above the λ point seems to be reasonably similar to that of positive ions in argon. The negative ions in this temperature region are anomalous in that they have mobilities of the order of the positive ions. Three possible explanations of this low mobility can be examined:

1. The formation of negative helium ions.
2. The formation of negative impurity ions.
3. Electrons not forming massive ions but behaving similarly to the positive ions.

The formation of He^- in helium gas is highly improbable. Haloein and Midtdal's (1955) theory demonstrated that there is a metastable state which would produce He^- with a lifetime of 10^{-3} sec. in helium gas at low pressure; in liquid helium the lifetime is likely to be very much shorter. Hiby (1939) was able to detect He^- with a mass spectrograph where Tuxon (1936) had failed. Unless there is some marked change from the gaseous state which makes the negative ion more stable in the liquid phase, the possibility of He^- explaining the low values of mobility seems unlikely.

For negative ions to obey Stokes' law, their radii must be of the order of 4 times that of the positive ion.

If impurity atoms were present in the liquid helium used for mobility measurements it is possible that their numbers need only have been one in 10^5 to 10^6 to have had an effect. As it is not known how easily impurities dissolve or can be suspended in liquid helium, little can be said concerning this possibility.

The small value of μ_- could occur if electrons in liquid helium are trapped by potential wells. It would be expected that the well depth would be different from that experienced by the positive ions, leading to a different value and temperature variation of the mobility from that of the positive ions. Illumination of the electrode area indicated that variation of room intensity illumination, causing variation of photon excitation of electrons out of the wells, could not produce the discrepancies found in mobility measurements of different experiments.

At this point the author would like to mention an unexplained anomalous result found in liquid helium. The slow electron mobility changes from approximately 0.03 cm.^{2}/v-sec. to 15 cm.^{2}/v-sec. as the field changes from 30 kv./cm. to 60 kv./cm. Using kinetic theory, this gives an atomic radius of approximately 0.6 Å as compared with the gaseous value of 1.3 Å. This transition was observed for three different experiments in which the electrode spacing was not changed. However, in the next experiment, when the

electrode spacing was changed, this effect did not occur and it could not be repeated in any subsequent experiment.

The temperature effects in liquid helium find little explanation. The general trend of mobility is predicted by Stokes' law and the known viscosity of helium, except below 1.85° K., but this law cannot explain the field dependence of the mobility. As the features of liquid helium at and below the λ point can at least be partially explained by Bose statistics, it may be significant that both the positive and negative ions obey Fermi–Dirac statistics.

Using the results of Goldstein and Reekie (1955), an explanation of the ionic mobility below the λ point cannot be made by a simple modification of the Eyring potentials with temperature. Goldstein and Reekie found that the change at the λ point in the potential experienced by atoms of liquid helium is very small.

ACKNOWLEDGMENTS

The author would like to express his gratitude to R. E. Burgess and Dr. F. D. Stacey for their discussions concerning the experimental results, and to acknowledge the assistance of the Defence Research Board, who supported the research, and the Ontario Research Foundation for a Fellowship 1954–55.

REFERENCES

CRAVATH, A. M. 1930. Phys. Rev. **36**, 248.
DAUNT, J. G. and SMITH, R. S. 1954. Revs. Mod. Phys. **26**, 172.
DAVIDSON, N. and LARSH, A. E. 1948. Phys. Rev. **72**, 220.
ELMORE, W. C. and SANDS, M. 1949. Electronics (McGraw-Hill Book Co., Inc., Toronto), p. 139, eq. 19.
EYRING, H. 1936. J. Chem. Phys. **4**, 283.
GOLDSTEIN, L. and REEKIE, J. 1955. Phys. Rev. **98**, 857.
GORTER, C. J. 1955. Progress in low temperature physics (North-Holland Pub. Co., Amsterdam), p. 65.
HALOIEN, E. and MIDTDAL, J. 1955. Proc. Phys. Soc. A, **68**, 815.
HIBY, J. W. 1939. Ann. Physik, **34**, 473.
HOLTZMARK, J. 1929. Z. Physik, **55**, 437.
HUTCHINSON, G. W. 1948. Nature, **162**, 610.
LOEB, L. 1939. Fundamental process of electrical discharges in gases (John Wiley & Sons, Inc., New York), p. 86.
LONDON, F. 1954. Superfluids (John Wiley & Sons, Inc., New York), p. 31.
MALKIN, M. S. and SHULTZ, H. L. 1951. Phys. Rev. **83**, 1051.
MASSEY, H. S. W. and BURHOP, E. H. S. 1952. Electronic and ionic impact phenomena (Oxford University Press, London.)
RAMSAUER, C. 1921. Ann. Physik, **64**, 513.
RUDENKO, N. S. and SCHUBNIKOV, I. W. 1934. Physik. Z. Sowjetunion, **6**, 470.
RYDER, E. J. 1953. Phys. Rev. **90**, 766.
SHOCKLEY, W. 1951. Bell System Tech. J. **30**, 990.
TUXON, O. 1936. Z. Physik, **163**, 463.
VAN DER ZIEL, A. 1954. Noise (Prentice-Hall, Inc., New York), pp. 8, 30, 32.
WILLIAMS, R. L. and STACEY, F. D. 1957. To be published shortly.

THE NEUTRON CAPTURE CROSS SECTIONS OF Pu^{238}, Pu^{242}, AND Am^{243} IN THE THERMAL AND EPICADMIUM REGIONS[1]

J. P. Butler, M. Lounsbury, and J. S. Merritt

ABSTRACT

Thermal neutron capture cross sections of 403±8 b. for Pu^{238}, 18.6±0.8 b. for Pu^{242}, and 73.6±1.8 b. for Am^{243} have been measured by the activation method assuming 36.4 b. for the thermal neutron cross section of Co^{59}. Samples of plutonium (90% Pu^{242} – 10% Pu^{238}) were irradiated for 1 to 5 months in the NRX reactor. The growth of Pu^{239}, Am^{243} (the daughter of the 5 hr. Pu^{243}), and Cm^{244} (the daughter of the 25 min. Am^{244}) was determined by mass analysis and by alpha spectrum analysis and total alpha counting. Resonance capture integrals (from 0.5 ev. to ∞) of 3260±280 b. for Pu^{238}, 1275±30 b. for Pu^{242}, and 2290±50 b. for Am^{243} were found using cobalt and U^{238} as standards. Values of 48.6 b. and 282 b. were taken as the resonance integrals of Co^{59} and U^{238} respectively.

The fission cross section of Pu^{242} was zero within experimental error.

I. INTRODUCTION

Average cross sections are generally used in nuclear reactor calculations rather than detailed cross section data. For a thermal neutron reactor two averages for most materials suffice, the thermal cross section and the resonance capture integral. The thermal value is averaged over a Maxwell–Boltzmann velocity distribution of neutrons and the resonance value is averaged over the slowing-down flux distribution. The slowing-down distribution has equal flux per ln e energy interval and thus the resonance capture integral can be defined as $\int \sigma_a(E)\, dE/E$, with the integral evaluated from a lower cutoff energy (cadmium cutoff, 0.5 ev.) to fission energies.

In the literature various values have been reported for the pile neutron capture cross sections of Pu^{242}, Pu^{238}, and Am^{243}. In view of the differences and lack of precision in these values and since the values are for "pile neutrons" only, it was considered that a further investigation would be worth while. In the present experiments, the thermal neutron capture cross sections of these nuclides and their resonance capture integrals have been determined.

Preliminary values for the neutron capture cross sections of Pu^{238}, Pu^{242}, and Am^{243} were reported at the Chemical Institute of Canada Symposium on Nuclear Chemistry and Radiochemistry, Montreal, Sept., 1955, and at the Tripartite Reactor Core Conference, Chalk River, Jan., 1956 (Butler, Lounsbury, and Merritt 1956*a*, *b*). Since these conferences several more irradiations have been performed and the resonance flux has been measured for the irradiation position used in this work, so that the values reported here supersede those given previously.

II. METHOD

To determine the neutron capture cross section of Pu^{238}, Pu^{242}, and Am^{243}, samples of plutonium containing initially about 90% Pu^{242}, 10% Pu^{238}, and

[1]Manuscript received October 16, 1956.
Contribution from Research Chemistry Branch, Atomic Energy of Canada Limited, Chalk River, Ontario.
Issued as A.E.C.L. No. 387.

0.15% Pu^{239} have been irradiated in a high flux position for several months in the NRX reactor. Plutonium of this isotopic composition was prepared by recovering the plutonium produced in 2-week irradiations of Am^{241} (Butler, Lounsbury, and Merritt 1956*a*, *b*). The integrated neutron flux received by the plutonium samples was measured by placing cobalt wires in close proximity.

The nuclear reactions occurring in the irradiation of a mixture of Pu^{238} and Pu^{242} are as follows:

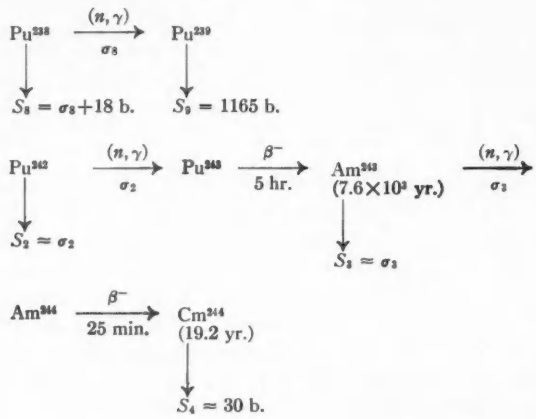

Since the irradiations were long in comparison to the β half-lives it will be assumed that all β processes are instantaneously accomplished. For a sample irradiated in a uniform flux of F neutrons cm.$^{-2}$ sec.$^{-1}$, for a period of t sec., the ratio of the number of atoms of Pu^{239}, P_9, to the number of atoms of Pu^{238}, P_8, is given by:

$$(1) \qquad \frac{P_9}{P_8} = \frac{\sigma_8 F}{S_9 F-(S_8 F+\lambda)}\left(\frac{e^{-S_8 F t}e^{-\lambda t}-e^{-S_9 F t}}{e^{-S_8 F t}e^{-\lambda t}}\right)+\frac{P_9{}^0}{P_8{}^0}\,\frac{e^{-S_9 F t}}{e^{-S_8 F t}e^{-\lambda t}}$$

where $P_9{}^0/P_8{}^0$ is the initial mass ratio of Pu^{239} to Pu^{238}, λ is the decay constant of Pu^{238}, and σ_8 is the capture cross section of Pu^{238}. S_8 and S_9 are the total destruction cross sections of Pu^{238} and Pu^{239} respectively. The second term of this expression accounts for the small amount of Pu^{239} initially present in the sample of plutonium. S_8 is numerically equal to σ_8 plus 18 barns (Hughes and Harvey 1955) for the fission cross section of Pu^{238}. The total destruction cross section of Pu^{239} was taken as 1165 barns (Hughes and Harvey 1955), a value calculated for the neutron temperature in the irradiation position.

From a measurement of the integrated thermal neutron flux and the mass ratio of the Pu^{239} and Pu^{238} before and after the irradiation, the capture cross section of Pu^{238} was calculated from equation (1) by successive approximations.

From the amount of Am^{243} (A_3 atoms) and Cm^{244} (C_4 atoms) produced, the capture cross sections of Pu^{242}, σ_2, and Am^{243}, σ_3, were evaluated from the following equations in which the exponential terms have been expanded:

$$\frac{A_3}{P_2} = \frac{\sigma_2 Ft}{e^{-S_2 Ft}}\left[1-(S_2+S_3)\frac{Ft}{2!}+\ldots\right], \tag{2}$$

$$\frac{C_4}{A_3} = \sigma_3 Ft\,\frac{\left[\frac{1}{2}-(S_2+S_3+S_4)\frac{Ft}{3!}+\ldots\right]}{\left[1-(S_2+S_3)\frac{Ft}{2!}+\ldots\right]}, \tag{3}$$

where S_2, S_3, and S_4 are the total destruction cross sections of Pu^{242}, Am^{243}, and Cm^{244} respectively. P_2 is the number of atoms of Pu^{242} present at the end of the irradiation. Fission in Pu^{242} and Am^{243} was assumed to be negligible, that is the total destruction cross sections of these nuclides were assumed to be equal to their neutron capture cross sections.

The contributions to the neutron capture cross sections of these nuclides from neutrons in the epicadmium region (i.e. of energy greater than 0.5 ev.) were obtained experimentally by irradiating, in the same position, plutonium samples and monitors in small cadmium boxes. The contributions for thermal neutrons (energy less than 0.5 ev.) were obtained by subtracting the "cadmium covered" contributions from the "uncovered" contributions.

III. EXPERIMENTAL

(*a*) *Irradiations*

Samples of plutonium (90% Pu^{242} – 10% Pu^{238}) varying in weight from 40 to 450 μg. were irradiated in aluminum containers for 1 to 5 months in the NRX reactor.

The samples were irradiated in a lattice position in which the longitudinal gradient of the neutron flux was very low, 0.2% per inch. Cobalt flux monitors were placed within a half inch of the sample. The plutonium was irradiated as the fluoride, rather than the oxide, since this compound had the advantage of being easily dissolved after the irradiation. To eliminate self-shielding the plutonium fluoride was spread over an area of about 2 sq. cm.

Samples of plutonium inside cadmium boxes of an average wall thickness 0.028 in. were irradiated in the same position in the reactor. During the irradiations about 0.007 in. of cadmium was burnt out. The cadmium box was so placed that the thermal flux depression at the unshielded monitor in the same irradiation capsule was only 1%, for which the appropriate corrections were made. Cobalt monitors were also placed inside the cadmium boxes to obtain a measure of the epicadmium flux.

(*b*) *Determination of Pu^{239}, Am^{243}, and Cm^{244} Formed*

After the irradiation the plutonium fluoride was dissolved in a boric–nitric acid mixture. A small amount of lanthanum carrier was added and the plutonium, americium, and curium were precipitated as the hydroxides. The hydroxides were dissolved in concentrated hydrochloric acid and the plutonium was separated from the americium and curium by absorption on a Dowex A–1 anion exchange resin column (Diamond, Street, and Seaborg 1954). In the chemical separation the yields of Am, Cm, and Pu were 98–99%. The yield of

Am–Cm relative to Pu, which is necessary to calculate the neutron capture cross section of Pu^{242}, was determined with an estimated error of $\pm 0.5\%$.

The samples of plutonium were mass analyzed before and after the irradiations with a 60° deflection, 8 in. radius mass spectrometer with a mass resolution of 0.3% (Lounsbury 1952). A surface ionization ion source was employed. For each analysis a sample of about 15 μg. of plutonium was used. The mass spectrum was scanned magnetically and the ion current amplified by a vibrating reed electrometer and recorded with a type G Speedomax pen recorder. For each sample some 10 determinations were made of the abundance of plutonium isotopes and the standard deviations from the mean varied from ± 0.4 to $\pm 0.9\%$.

The relative amount of Pu^{239} formed was determined from the mass analysis. The amount of Pu^{242} at the end of the irradiation was determined from the mass analysis and the weight of the plutonium fraction. The absolute weight of the plutonium was deduced from the Pu^{238} α activity, 99.7% of the total, and the Pu^{238} α half-life, 89.6 ± 0.4 years (Joffey and Lerner 1950).

The amount of Am^{243} and Cm^{244} produced in the irradiations was determined from a total α count and an α spectrum analysis of the Am–Cm fraction. The alpha spectrum of the Am–Cm fraction was determined with a gridded ion chamber (Harvey, Jackson, and Eastwood, to be published) and a 30 channel pulse height analyzer (Moody, Battell, Howell, and Taplin 1951). The resolution of the chamber was 0.6% full width at half maximum. Half-lives of 7.6×10^3 years (Butler, Eastwood, and Schuman, unpublished results) and 19.2 years (Friedman *et al.* 1954) for Am^{243} and Cm^{244} respectively were used to calculate the number of atoms of these isotopes. The half-life used for Am^{243} is a value that has been determined recently in our laboratories from a mass analysis and an α spectrum analysis of a sample of americium containing Am^{241} and Am^{243}.

(*c*) *Determination of the Integrated Neutron Flux*

The thermal integrated neutron flux was determined with weighed pieces of pure cobalt wire 0.005 in. in diameter and 1 cm. in length. Several cobalt monitors wrapped in aluminum foil were placed in the irradiation container. After the irradiation the gamma activity of the monitors was measured with a high pressure argon ionization chamber. The disintegration rate of the monitor was determined by comparison with a standard cobalt monitor whose disintegration rate had been determined by coincidence counting. The observed activity was corrected for epicadmium neutrons and for self-shielding in the wire. The self-shielding correction for thermal neutrons of 2.1% for 0.005 in. Co wire was determined experimentally by measuring the thermally induced activity per mg. of cobalt in wires of various thicknesses and extrapolating to zero thickness. The activity was also corrected for decay. Integrated neutron fluxes calculated from the several monitors associated with each irradiation deviated less than $\pm 0.3\%$.

The thermal integrated flux was calculated from the corrected activity of the cobalt monitor using 36.4 ± 0.9 barns (Hughes and Harvey 1955) for the

capture cross section of Co^{59} and 5.27±0.2 years (Brownell and Maletskoss 1950) for the half-life of Co^{60}. It was estimated that the accuracy of the flux determination was ±2%. Recent experiments carried out in our laboratories comparing cobalt and gold wire monitors have shown that the integrated thermal neutron flux obtained with cobalt monitors agrees within 0.5% with that obtained with gold monitors. A value of 99.0 barns (Carter *et al.* 1953; Egelstaff 1954) was used for the thermal neutron capture cross section of Au^{197}. The Au^{198} disintegration rate was determined by coincidence counting. Corrections were made for self-shielding and epicadmium neutron flux.

IV. RESULTS AND DISCUSSION

The capture cross sections of Pu^{238}, Pu^{242}, and Am^{243} were calculated for pile neutrons using equations (1), (2), and (3), and the results obtained in four irradiations are summarized in Table I. The errors quoted are standard deviations of the determinations and do not include any error in the cobalt cross section.

The agreement of the values for the different irradiations is good and on the bottom line of the table average values are listed. The values are relative to 36.4 barns for the cobalt (n, γ) cross section, which in turn is relative to 99.0 barns for the gold (n, γ) cross section. Previous values for these capture cross sections were 425±75 barns for Pu^{238} (Hughes and Harvey 1955), 100, 150, and 30 barns for Pu^{242} (Sullivan *et al.* 1951; Neutron Cross Section Compilation 1952; Studier *et al.* 1954), and 50, 115, and 140 barns for Am^{243} (Neutron Cross Section Compilation 1952; Stevens *et al.* 1954; Harvey *et al.* 1954).

In the first three irradiations, the measurement of the capture cross section of Pu^{238} is rather insensitive to the value of the total destruction cross section of Pu^{239}, S_9. An error of 30 barns in S_9 causes an error of only 2 barns in the capture cross section of Pu^{238}. However, in the fourth irradiation S_9 can be calculated from equation (1) with reasonable precision. A value of 1166±40 barns was obtained for S_9, assuming 489±6 barns, the average of the first three irradiations, for the capture cross section of Pu^{238}. This value agrees very well with the calculated value (see Section II), thus justifying taking the neutron temperature as the temperature of the heavy water moderator.

From the mass analysis of the plutonium before and after the irradiation and from the measured destruction cross section of Pu^{238}, S_8 (which is equal to σ_8+18 barns), the total destruction cross section of Pu^{242}, S_2, can be calculated from the following equation:

$$\left(\frac{P_8}{P_2}\right)\left(\frac{P_2^0}{P_8^0}\right)\frac{1}{e^{-\lambda t}} = e^{-(S_8-S_2)Ft}. \tag{4}$$

In these irradiations the destruction of Pu^{242} was small so that S_2 could be determined in this manner with a precision of only 20%. The values obtained for S_2 are listed in the last column of Table I. The average value of 55±15 barns for the total destruction cross section of Pu^{242} is in reasonable agreement with the value for the neutron capture cross section determined from the

production of Am^{243}. This indicates that the fission cross section of Pu^{242} is small, as would be predicted.

TABLE I

CAPTURE CROSS SECTIONS OF Pu^{238}, Pu^{242}, AND Am^{243} FOR PILE NEUTRONS

Irradiation	μg. of Pu irradiated	Thermal $Ft\times10^{20}$	(n,γ) Pu^{238}, barns	(n,γ) Pu^{242}, barns	(n,γ) Am^{243}, barns	Total Pu^{242}, barns
1	151	3.059	492 ±6	52.1±0.7	133.5±1.6	64±15
2	130	3.874	488.5±6	51.6±0.7	133.5±1.6	41±20
3	460	4.026	487 ±5	52.6±0.7	134.4±1.6	65±16
4	136	6.933	489 ±5			51±11
	Mean values		489 ±3	52.1±0.7	133.8±0.8	55±15

The results of the irradiations performed with cadmium shielding are listed in Table II in which the results for the various isotopes are listed as "effective capture cross sections" under cadmium. The effective cross sections were calculated from the thermal integrated flux so that the thermal neutron cross sections of these nuclides could be obtained by subtracting the effective cross sections under cadmium from the pile neutron cross sections. In the calculations, the destruction cross sections of Pu^{242} and Am^{243} were taken as their effective neutron capture cross sections under cadmium. The destruction cross section of Pu^{239} was taken as 22 barns, which corresponds to a cadmium ratio of 53 for Pu^{239} (Cornish and Lounsbury 1956).

TABLE II

EFFECTIVE CAPTURE CROSS SECTIONS UNDER CADMIUM FOR Pu^{238}, Pu^{242}, AND Am^{243}

Irradiation	μg. of Pu irradiated	σ_{eff} Pu^{238}	σ_{eff} Pu^{242}	σ_{eff} Am^{243}
1	40	—	33.0±0.6	58.6±1.0
2	49	85.4±7	33.6±0.5	63.9±0.8
3	48	86.0±18	33.9±0.5	58.1±0.8
		85.7±7	33.5±0.5	62.0±1.0

The resonance capture integral is related to the cadmium ratio, R_{Cd}, by the following expression:

$$R_{Cd}-1=\left(\frac{F_{th}}{F_r}\right)\sigma_{th}\Big/\int_{0.5}^{\infty}\sigma_c\,\frac{dE}{E} \tag{5}$$

in which σ_{th} is the thermal neutron cross section and (F_{th}/F_r) is the ratio of the thermal flux to the resonance flux per ln e energy interval. Values of (F_{th}/F_r) were calculated from the activities of the cobalt monitors inside and outside of the cadmium box. Self-shielding corrections were applied to the observed activities of the monitors, 2.1% for the thermal induced activity and 5.5% for the epicadmium activity. A value of 36.4 barns was used for the thermal neutron cross section of cobalt and 48.6 barns (Macklin and Pomerance 1955) for the resonance integral inside a cadmium box of wall thickness 0.028 in.

Independent values of (F_{th}/F_r) were obtained by irradiating thin samples of uranium (30 μg./cm.^{2}) in the same assembly with the cobalt monitors. From the ratio of the alpha activity, Pu^{239}, induced in wrapped and unwrapped uranium samples, values of (F_{th}/F_r) were calculated using 2.75 barns (Hughes and Harvey 1955) for the thermal cross section of U^{238} and 282 barns (Macklin and Pomerance 1955) for the resonance integral.

The value of the ratio of the thermal flux to the resonance flux per ln e energy interval, (F_{th}/F_r), obtained from the cobalt monitors was 38.2±0.5 and from the uranium samples was 37.7±0.6. The errors quoted are the standard deviations of the determinations and do not include any errors in the cross sections. Using an average value of 38.0±0.5 for (F_{th}/F_r) the resonance capture integrals of Pu^{238}, Pu^{242}, and Am^{243} were calculated from equation (5). The thermal neutron (2200 m./sec.) cross sections of these nuclides were obtained from the results of Tables I and II assuming that these nuclides and cobalt have the same cross section versus energy dependence (e.g. both are "$1/v$"). The results are summarized in Table III.

TABLE III

SUMMARY OF RESULTS

Nuclide	$\sigma(n,\gamma)$ for pile neutrons, barns	R_{Cd}	σ at 2200 m./sec., barns	Resonance integral, barns $\int_{0.5}^{\infty} \sigma_a \, dE/E$
Pu^{239}	489 ±3	5.71±0.54	403 ±8	3260±280
Pu^{242}	52.1±0.7	1.55±0.03	18.6±0.8	1275±30
Am^{243}	133.8±0.8	2.22±0.04	73.6±1.8	2290±50

The results for Pu^{242} and Am^{243} show that there is very strong resonance capture in these nuclides. This probably accounts for the disagreement between the previously reported values for the pile neutron capture cross sections of these nuclides. Resonance capture in Pu^{238}, although appreciable, is not nearly as pronounced.

ACKNOWLEDGMENTS

The authors are indebted to Dr. C. H. Westcott and Dr. D. G. Hurst for many valuable discussions and to Mr. J. A. Giordmaine for his assistance in several of the irradiations. The standardization of a Co^{60} source by β–γ coincidence counting by Dr. P. J. Campion is gratefully acknowledged.

REFERENCES

BROWNELL, G. L. and MALETSKOSS, C. J. 1950. Phys. Rev. **80**, 1102.
BUTLER, J. P., EASTWOOD, T. A., and SCHUMAN, R. P. Unpublished results.
BUTLER, J. P., LOUNSBURY, M., and MERRITT, J. S. 1956*a*. Atomic Energy of Canada Limited Report, C.R.C. 628.
——— 1956*b*. Can. J. Chem. **34**, 253.
CARTER, R. S., PALEVSKY, H., MYERS, V. W., and HUGHES, D. J. 1953. Phys. Rev. **92**, 716.
CORNISH, F. W. and LOUNSBURY, M. 1956. Atomic Energy of Canada Limited Report, C.R.C. 633.
DIAMOND, R. M., STREET, K., and SEABORG, G. T. 1954. J. Am. Chem. Soc. **76**, 1461.

EGELSTAFF, P. A. 1954. J. Nuclear Energy, **1**, 57.
FRIEDMAN, A. M., HARKNESS, A. L., FIELDS, P. R., STUDIER, M. H., and HUIZENGA, J. R. 1954. Phys. Rev. **95**, 1501.
HARVEY, B. G., JACKSON, H. G., and EASTWOOD, T. A. To be published.
HARVEY, B. G., ROBINSON, H. P., THOMPSON, S. G., GHIORSO, A., and CHOPPIN, G. R. 1954. Phys. Rev. **95**, 581.
HUGHES, D. J. and HARVEY, J. A. 1955. Brookhaven National Laboratory Report, BNL-325.
JOFFEY, A. H. and LERNER, J. 1950. Argonne National Laboratory Report, ANL-4411.
LOUNSBURY, M. 1952. Proc. Roy. Soc. Can. **46**, 128.
MACKLIN, R. L. and POMERANCE, H. S. 1955. Geneva Conference Paper 833.
MOODY, N. F., BATTELL, W. J., HOWELL, W. D., and TAPLIN, R. H. 1951. Rev. Sci. Instr. **22**, 551.
Neutron Cross Section Compilation. 1952. U.S. Atomic Energy Commission Report, AECU-2040.
STEVENS, C. M., STUDIER, M. H., FIELDS, P. R., MECH, J. F., SELLERS, P. A., FRIEDMAN, A. M., DIAMOND, H. D., and HUIZENGA, J. R. 1954. Phys. Rev. **94**, 974.
STUDIER, M. H., FIELD, P. R., SELLERS, P., FRIEDMAN, A. M., STEVENS, C. M., MECH, J. F., DIAMOND, H. D., SEDLET, J., and HUIZENGA, J. R. 1954. Phys. Rev. **93**, 1433.
SULLIVAN, J. C., PYLE, G. L., STUDIER, M. H., FIELDS, P. R., and MANNING, W. M. 1951. Phys. Rev. **83**, 1267.

THE ANGULAR DISTRIBUTION AND YIELD OF THE REACTION $F^{19}(p, \alpha_0)O^{16}$ [1]

R. L. Clarke and E. B. Paul[2]

ABSTRACT

The yield of the ground state alpha particles from the $F^{19}(p, \alpha_0)O^{16}$ reaction has been studied from an energy of 1.3 Mev. to 2.7 Mev. The observed angular distributions were analyzed in terms of a Legendre polynomial expansion by the method of least squares. Six resonances were found in the energy region studied, at bombarding energies of 1.358 Mev., 1.709 Mev., 1.853 Mev., 2.11 Mev., 2.31 Mev., and 2.58 Mev. The widths and peak cross sections of these resonances are respectively: (54±10 kev., 46±5 mb.), (140±5 kev., 55±6 mb.), (132±5 kev., 77±8 mb.), (75±25 kev., 10±2 mb.), (80±25 kev., 32±5 mb.), and (300±25 kev., 51±10 mb.). Their spins, parities, channel spin mixtures, and partial widths are discussed.

INTRODUCTION

When fluorine is bombarded by protons, the $F^{19}(p, \alpha)O^{16}$ reaction, elastic and inelastic proton scattering, and proton capture followed by gamma ray emission have all been observed. The results of previous studies are summarized in the review of Ajzenberg and Lauritsen (1955).

In the (p, α) reaction several groups of alpha particles are observed, corresponding to Q values of 8.117 (Ajzenberg and Lauritsen 1955), 2.06, 1.98, 1.21, and 1.00 Mev. The Q values correspond respectively to reactions leading to the ground state and excited states at 6.06, 6.14, 6.91, and 7.12 Mev. of O^{16}.

A study of the $F^{19}(p, \alpha)O^{16}$ reaction gives information both on the excited states of O^{16} and on the excited states of Ne^{20} above 12.9 Mev. An examination of the excitation function gives the positions and widths of the excited states of Ne^{20}. A study of the angular distribution of the emerging particles with respect to the incident protons may give information on the spins and parities of these excited states.

The excitation function of the ground state alpha particles has been observed by Streib *et al.* (1941) from 0.3 to 1.45 Mev. Resonances were reported at 0.72, 0.78, 0.84, 1.1, and 1.38 Mev. The 1.38 Mev. state is believed to be the same as the state at 1.358 Mev. observed in the present work. Angular distributions were studied by Rubin (1947) near the 1.1 and 1.38 Mev. states.

The purpose of the present work was to extend the work of Rubin to higher energies. To this end, detailed measurements of the angular distributions have been made at intervals of from 20 to 50 kev. in the range of proton energy from 1.31 to 1.94 Mev. Less accurate measurements of the angular

[1]Manuscript received October 23, 1956.
Contribution from Physics Division, Atomic Energy of Canada Limited, Chalk River Laboratory, Chalk River, Ontario.
Issued as A.E.C.L. No. 389.
[2]Present address: Department of Physics, Atomic Energy Research Establishment, Harwell, England.

distributions have been made from 1.94 to 2.7 Mev. In addition, observations of the yield of alpha particles at 90° to the proton beam as a function of proton energy have been made from 0.8 to 2.7 Mev., using smaller energy intervals.

EXPERIMENTAL METHODS

(*1*) *90° Excitation Function*

For the excitation function taken at 90° to the proton beam, protons from the electrostatic accelerator passed through a single collimating aperture before striking the target. For this experiment the targets used were CaF_2 evaporated onto polished copper disks. These disks were mounted on a brass block which held them at 45° with respect to the beam and the outgoing alpha particles. It could be rotated so as to present any one of four targets to the beam.

The alpha particles resulting from the reaction were analyzed by means of a 60° magnet which separated the alpha particles from the scattered protons. The resolution was about five per cent in energy. The alpha particles were detected in a proportional counter.

In taking the data, a small portion of the alpha particle spectrum was taken for each value of the proton energy. Counts were taken for a given number of microcoulombs incident on the target, as measured with a current integrator of the type described by Gittings (1949). Since the energy spread of the alpha particles is much smaller than the energy resolution of the magnet, the yield at each energy was taken to be proportional to the counting rate at the peak of the spectrum.

During the course of any one run, the formation of a deposit of carbon on the surface of the target could be seen. However, frequent checking resonances at the beginning and end of a run failed to reveal any effect due to this deposit.

The thickness of each of the targets used in this experiment was not measured. The thickness of one target made in the same manner as those used in the course of the experiment was measured by comparing the yield of gamma rays from it at the 1.372 Mev. resonance with the increase in yield of a thick target due to this resonance, in the manner described by Fowler, Lauritsen, and Lauritsen (1948). In this way the target was found to be 1.7 kev. thick for 1 Mev. protons.

During these experiments the energy of the electrostatic accelerator was stabilized to within ±2 kev. The calibration of the voltage scale was done by observation of the $(p, \alpha\gamma)$ resonances in fluorine at 1.346 and 1.372 Mev.* (Chao, Tollestrup, Fowler, and Lauritsen 1950). The voltage scale of the accelerator depends on the calibration of the beam bending magnet, which is stabilized by means of a proton resonance fluxmeter. The ratio of the field in the region of the proton resonance system to the field in the region of the beam

*In earlier discussions of this work (Paul and Clarke 1953; Paul, Clarke, and Sharp 1953), it was assumed that these resonances were at 1.355 and 1.381 Mev. Recent work (Ajzenberg and Lauritsen 1955; Hunt and Firth 1955; Kingdon, Bair, Cohn, and Willard 1955) has shown that more accurate values are 1.346 and 1.372 Mev. The voltage scale used in the present discussion has been corrected accordingly. The values given in Ajzenberg and Lauritsen for the energies of the last six resonances listed in Table VI (20) should be altered accordingly.

trajectory was found by measurement of the whole field with a moveable fluxmeter probe. This ratio was found to be constant to 0.2% over the energy region used.*

The alpha particle yield curve at 90° obtained from these measurements is shown in Fig. 1. This curve was not used for the measurements of the positions

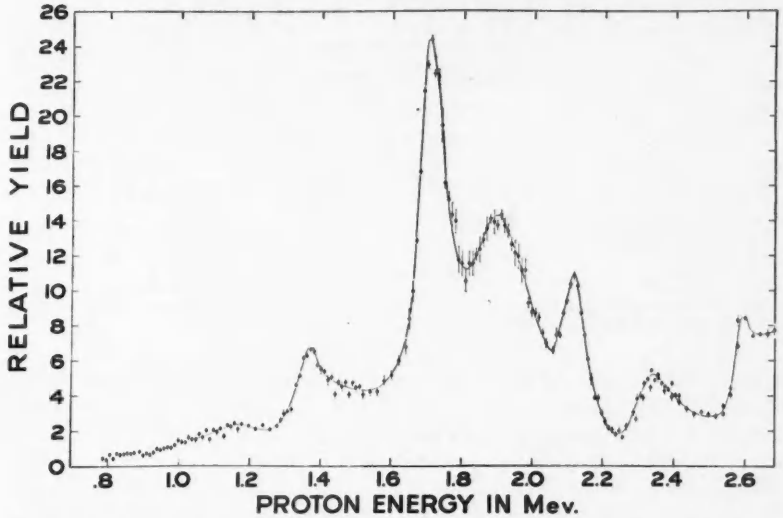

FIG. 1. The yield at 90° to the incident proton beam of the $F^{19}(p, \alpha_0)O^{16}$ reaction as a function of bombarding energy.

and yields of the resonances, but was used as a guide in the later parts of the experiment.

(2) *Angular Distributions*

Angular distributions for proton energies from 1.31 to 1.94 Mev. were obtained using the apparatus shown in Fig. 2. It consisted of a pill-box-shaped chamber made of two brass blocks. These blocks were sealed together with an O-ring so that the upper half of the chamber could be rotated with respect to the lower half. Two ports on the upper half carried the proportional counter with its absorbing foils and the window used in lining up the target. The ports on the lower half carried the beam collimator and, when used, the monitor counter. The target holder was supported by a lucite bushing which went through a hole in the center of the lower half. The angular position of the upper block could be read from a scale on its perimeter. The proportional counter made it possible to distinguish readily the ground state group of alpha particles from the short-range alpha particles, so that it was possible to be sure that only the ground state group was being counted. However, the proportional counter could not measure the reaction alpha particles in the

*We are indebted to Dr. A. J. Ferguson for carrying out these measurements.

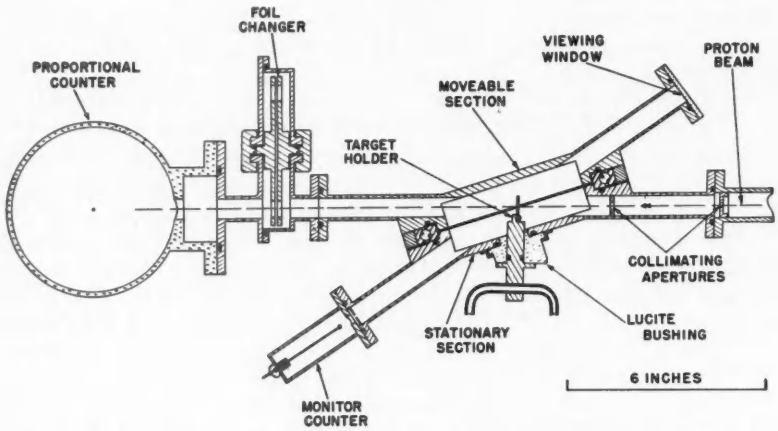

FIG. 2. Schematic diagram of the apparatus used to study angular distributions for bombarding energies between 1.3 Mev. and 1.94 Mev.

presence of the protons scattered from the target. By means of the wheels shown in Fig. 2 absorbers of aluminum foil of thicknesses ranging from 0.0002 to 0.005 in. were introduced between the target and counter to eliminate the scattered beam and the alpha particle groups of lower energy than the ground state group. At energies above 1.94 Mev. it was no longer possible to separate the scattered proton group and the α_0 group at angles near 0°. This set an upper limit of proton energy for this technique. Below this energy, in order to be sure that the separation was being done satisfactorily, the pulse height spectrum from the proportional counter was kept under observation during the experiment on a 30 channel pulse height analyzer.

The collimator consisted of a piece of 0.001 in. tantalum foil with a 3/16 in. diameter hole located at a distance of 4 in. from the target. The spread in energy of the incident protons was shown to be negligible by observations of the width of the 1.372 Mev. $(p, \alpha\gamma)$ resonance. The observed width was found to be 17 kev., which may be compared with the natural width of 15 kev. given by Ajzenberg and Lauritsen (1955).

The target consisted of CaF_2 evaporated onto 0.0002 in. aluminum foil. This foil was mounted on a small frame which was held in the middle of the chamber by the supporting post shown in Fig. 2. It was possible to line up the target with the center of the chamber by turning the wedge-shaped lucite bushing. This alignment was done at the beginning of each series of observations.

When the beam current integrator was connected to the target, a substantial current was observed, due partly to secondary emission of electrons under proton bombardment. On being checked against the yield of scattered protons in the monitor counter, this current was found to be proportional to the incident beam. The current was thereafter used as a measure of the incident beam.

The apparatus shown in Fig. 2 allowed the observation of reaction particles at angles from 0° to 146° in the laboratory system.

In taking observations from 0° to 100° the target was set with the normal to its face at an angle of 135° to the beam direction so that the observed alpha particles passed through the target backing. For observations from 80° to 150° the target was turned so that its normal again made an angle of 135° on the opposite side of the beam. In this position the observed alpha particles did not pass through the target backing. In both positions the incident beam struck the target material before passing through the backing. The values observed in both positions from 80° to 100° were used to normalize the forward position to the backward position readings.

Since the above apparatus could not be used for bombarding energies above 1.94 Mev., the apparatus shown in Fig. 3 was used to extend the data

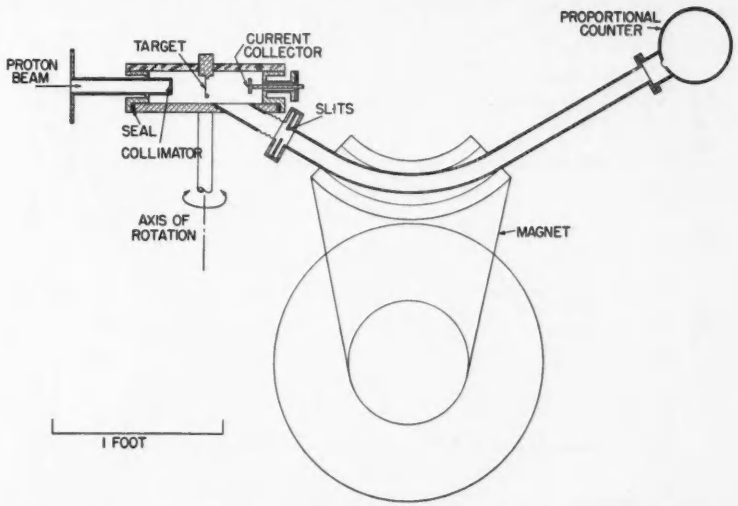

FIG. 3. Schematic diagram of the apparatus used to study angular distributions from 1.8 Mev. to 2.7 Mev. The whole device is mounted on a Bofors gun mount which can rotate the magnet, the counter, and the floor of the target chamber about the vertical axis shown.

to higher energies. The magnetic spectrometer used in the 90° yield studies described above was mounted on a Bofors gun mount so that it could be rotated about the target. The stationary (top) part of the target chamber was fixed to the beam entry port and collimator. The exit port was in the floor of the chamber, which rotated with the magnet. The frame carrying the target was mounted on the lucite lid of the chamber. The target, as before, was CaF_2 evaporated onto 0.0002 in. aluminum foil. The beam passed through the target to a beam stopper at the back of the chamber. The combined currents to the beam stopper and the target were passed through the current integrator to serve as a monitor of the incident beam. The system allowed observations to be made for angles between 30° and 150° in the laboratory system.

Because the target support for this apparatus was not rigidly fixed to the axis of rotation of the magnet, the accuracy of the observations was not as good as that of the apparatus of Fig. 2. Owing to the difficulty of collimating a beam in the variable fringing field of the spectrometer, only a crude collimator could be used. As a result, the presence of scattered beam hitting the target made the incident energy less well defined. In order to circumvent these diffi-

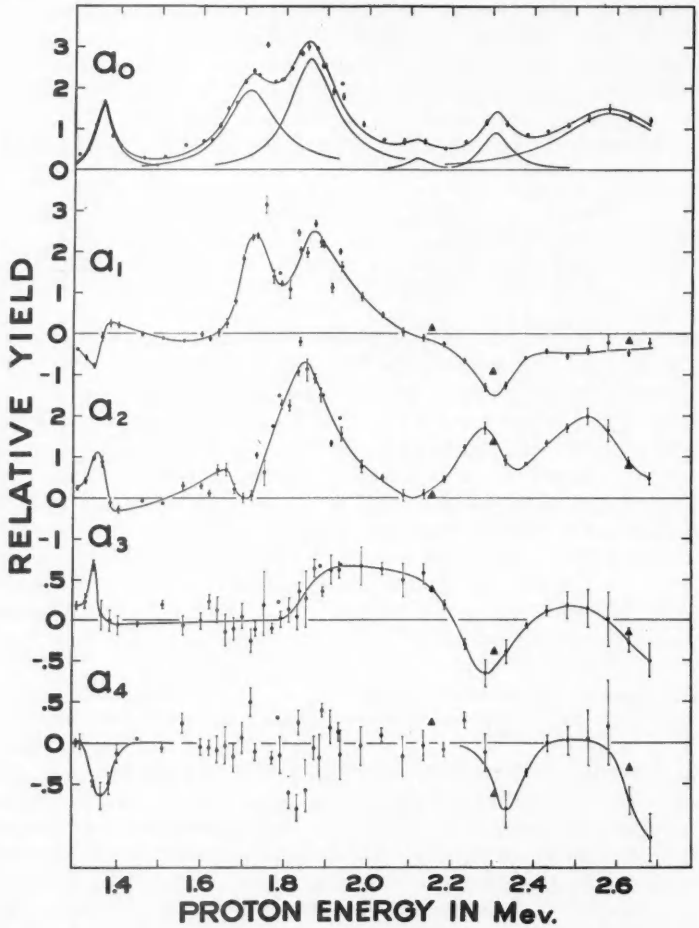

FIG. 4. The coefficients of the Legendre polynomial expansion of the observed angular distribution. The apparatus of Fig. 2 was used from 1.3 Mev. to 1.94 Mev., and that of Fig. 3 from 1.8 Mev. to 2.7 Mev. The points marked with triangles (▲) are check points taken using the apparatus of Fig. 3 with a different technique, described in the text. The errors shown are calculated from the scatter of the experimental data about the angular distribution curves calculated from the coefficients shown. The curve through the a_0 points is the sum of the individual resonance contributions. These contributions are calculated from the Breit–Wigner formula, using the constants given in Table IV.

culties a series of excitation curves was taken at laboratory angles of 30°, 54°, 70.1°, 109.9°, 126.0°, and 148.8°. These data were supplemented by those previously taken at 90°. These excitation functions extended from an energy of 1.8 Mev. to 2.7 Mev., the points being taken every 50 kev.

At each angle the excitation function taken with the magnet system in the region from 1.8 to 1.9 Mev. was normalized to the excitation function for the same angle and energy derived from the proportional counter system. The continuation of the normalized excitation functions into higher energy regions gave the required angular distributions, but with less accuracy than that obtained with the proportional counter system.

The data for both the proportional counter and magnet systems were corrected for the center-of-mass motion and analyzed in terms of Legendre polynomials up to order four. The fitting was done by the least squares method with all the points weighted equally. The coefficients of the terms in the expansion so obtained are shown plotted against energy in Fig. 4.

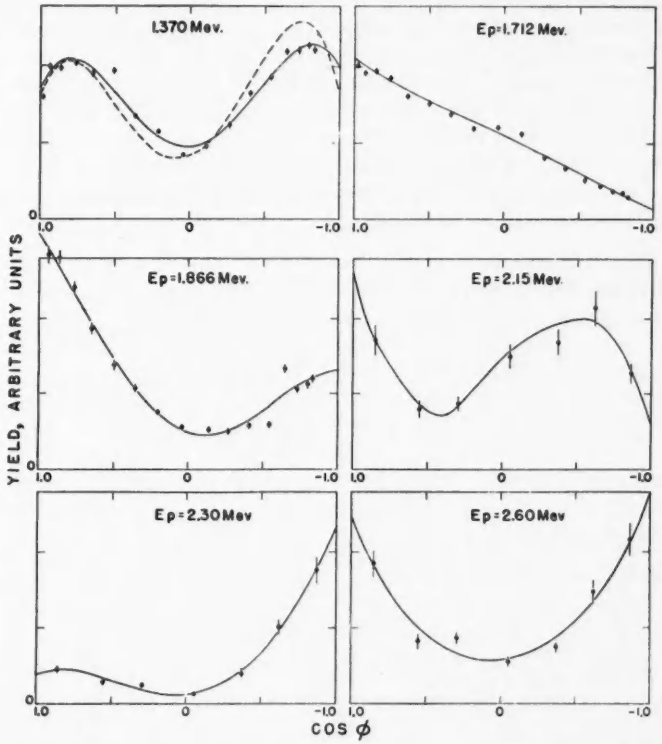

FIG. 5. Observed angular distributions taken near the resonances. The errors shown arise from counting statistics and the error in normalizing the cos $\phi > 0$ portion of the data to the cos $\phi < 0$ portion. The solid curves are the Legendre polynomial expansions fitted to the data by the method of least squares. The broken curve is the angular distribution observed by Rubin (1947) at an energy of 1.348 Mev.

The errors shown in Fig. 4 are the probable errors arising from the difference between the fitted curve and the experimental points as defined by Rose (1953). In the case of the proportional counter system, these errors are about the same as those to be expected on the basis of the statistical counting errors involved in normalizing the yields of the forward to the backward angles. Subsequent improvements in the apparatus of Fig. 3 made it possible to determine angular distributions directly with the magnet system. The results of spot checks taken in this way are shown by the triangles on Fig. 4.

Figure 5 shows angular distributions taken near the peaks of the resonances. The curves are calculated from the least squares fitted polynomials. The coefficients of the polynomial expansions for these energies are given in Table I. The angular distribution found by Rubin (1947) for this resonance is also shown by the dashed curve.

(3) Cross Section Measurements

Measurements of the total cross sections were made with the magnetic spectrometer set up in the same manner as for the 90° excitation function. The measurements were made using a thin target of CaF_2 on a polished copper backing. The yields of alpha particles from the $(p, \alpha\gamma)$ resonances at 1.346 and 1.372 Mev. were measured with the spectrometer and compared with the yield of alpha particles from the (p, α_0) resonance at 1.358 Mev. The value of the $(p, \alpha\gamma)$ cross section is known from the work of Streib, Fowler, and Lauritsen (1941). A value of 46±5 mb. was obtained for the cross section of the ground state reaction resonance at the 1.358 Mev. resonance, from which the cross sections of the other resonances observed can be deduced.

TABLE I

COEFFICIENTS OF THE LEGENDRE POLYNOMIAL FITS TO THE ANGULAR DISTRIBUTIONS OBSERVED NEAR RESONANCES IN THE $F^{19}(p, \alpha_0)O^{16}$ REACTION

E_p, Mev.	a_0	a_1	a_2	a_3	a_4
1.363	1653±55	−92±98	884±132	61±183	−627±179
1.701	1082±25	962±45	6±62	19±83	35±87
1.854	1510±502	984±87	1567±130	139±164	−288±192
2.14	714±47	−95±77	102±112	583±134	−32±188
2.28	1163±57	−1306±95	1701±138	−648±166	−118±233
2.583	1448±112	−208±190	1647±276	7±331	197±465

In addition, the cross section of the $(p, \alpha\gamma)$ resonance at 1.372 Mev. was determined by comparison of the gamma ray yield of this reaction with that from known RaTh and RaC″ sources, using the type of counter described by Fowler *et al.* (1948) and their calibration curve. The thickness of the target was measured by the thick target comparison technique of Fowler *et al.* (*loc. cit.*) and found to be 0.29 kev. For a thick target, CaF_2 powder pressed into a brass receptacle was used. A value of 550±300 mb. was obtained, to be compared with the value of 300 mb. obtained by Streib *et al.* (1941). The chief uncertainties in the present measurement were the absolute calibration of the current integrator and the absorption of the gamma rays in the brass well of the target chamber and the target mounting block.

RESULTS

The results are summarized in Table IV. The resonant energies, widths, and cross sections were found from the curve of total yield as a function of energy. The resonant energies are not corrected for level shift. In finding E_0, Γ, and σ from the yield for those resonances which overlap to a large extent, the parameters were adjusted until the areas under the experimental and calculated curves were equal, and the observed and calculated peaks coincided. The errors given in the first three columns of Table IV are estimated from the uncertainty in fitting the many parameters of overlapping levels. With the exception of the 1.358 Mev. state, this uncertainty overshadowed the counting rate statistics and errors in the calibrations of solid angles, current integrator, etc. No account has been taken of the possibility of other resonances not seen in this experiment.

In calculating the curves, account was taken of the penetrability of the Coulomb barrier for protons, using a radius of 4.0×10^{-13} cm. The results are not very sensitive to this choice of radius. The calculations were made from tables of Bloch *et al.* (1951), using values for the proton orbital angular momenta given in column 4 of Table IV. No correction was made for the penetrability of the emerging alpha particle, as this was found to be very close to unity for all energies and angular momenta under consideration. Since the correction for the change in observed width due to level shift (Thomas 1951) was less than the experimental error, it was also ignored. The calculated yield using the parameters of Table IV is shown in Fig. 4.

THEORY

Since both the alpha particle and the ground state of O^{16} have zero spin and even parity, only those states of the compound nucleus Ne^{20} having even spin and even parity or odd spin and odd parity can decay to the O^{16} ground state, and the angular momentum of the emerging alpha particle will be equal to the spin of the compound state. Because of this selection of states, only about half of the possible excited states of Ne^{20} can be studied by this reaction. Further, since both the proton and F^{19} have spin 1/2 and even parity, the angular momentum of the captured proton will be equal to that of the compound state when this is restricted to the properties given above. Consequently, in the fitting of an angular distribution for an isolated resonance to an assumed value of the spin of the compound state, there is only one adjustable parameter, the ratio t of the intensity of the channel spin 1 contribution to the channel spin 0 contribution.

The theoretical predictions for the angular distributions of (p, α) reactions have been expressed in convenient form by Blatt and Biedenharn (1952). The results for the present case are summarized in Tables II and III. Table II gives the results for isolated resonances. Table III gives the terms in the angular distributions arising from interference between levels. Since the experimental data have been fitted in terms of Legendre polynomials only up to P_4, the higher theoretical terms have not been listed.

From the known cross section and total width for a single resonance, the lower limit of the proton width can be calculated. Comparison of this lower

TABLE II

THEORETICAL ANGULAR DISTRIBUTIONS FOR THE $F^{19}(p, \alpha_0)O^{16}$ REACTION. THE FIRST COLUMN GIVES THE ASSIGNMENT OF THE STATE OF Ne^{20} INVOLVED. THE SECOND COLUMN GIVES THE CHANNEL SPIN OF THE INCIDENT PROTON PLUS F^{19} TARGET. THE NEXT THREE COLUMNS GIVE THE COEFFICIENTS IN THE LEGENDRE POLYNOMIAL EXPANSION OF THE DISTRIBUTION UP TO P_4

$J\pi$	S	P_0	P_2	P_4
0+	0	1	0.0	0.0
1−	0	3	6	0.0
	1	3	3	0.0
2+	0	5	7.14	12.86
	1	5	3.57	−8.57
3−	0	7	9.33	11.45
	1	7	7	1.91
4+	0	9	11.69	13.11
	1	9	9.94	6.55

TABLE III

INTERFERENCE TERMS IN THE THEORETICAL ANGULAR DISTRIBUTIONS ARISING FROM INTERFERING STATES IN THE $F^{19}(p, \alpha_0)O^{16}$ REACTION. THE FIRST TWO COLUMNS GIVE THE ASSIGNMENTS OF THE STATES OF Ne^{20} INVOLVED. THE THIRD COLUMN GIVES THE CHANNEL SPIN OF THE INCIDENT PROTON PLUS F^{19} TARGET. THE REMAINING COLUMNS GIVE THE COEFFICIENTS IN THE LEGENDRE POLYNOMIAL EXPANSION OF THE INTERFERENCE TERMS UP TO P_4

$J_1\pi_1$	$J_2\pi_2$	S	P_1	P_2	P_3	P_4
0+	1−	0	3	—	—	—
0+	3−	0	0	—	7	—
1−	2+	0	6	—	9	—
1−	2+	1	5.196	—	−5.196	—
1−	4+	0	—	—	12	—
1−	4+	1	—	—	3.49	—
2+	3−	0	9	—	1.62	—
2+	3−	1	8.50	—	−1.37	—
0+	2+	0	—	5	—	—
0+	4+	0	—	—	—	9
1−	3−	0	—	9	—	12
1−	3−	1	—	−7.35	—	−7.35
2+	4+	0	—	12.86	—	11.69
2+	4+	1	—	11.74	—	3.20

limit with the single particle limit rule (Wigner and Teichmann 1952) shows that only angular momenta of four or less need be considered. The narrowest resonance observed, having a $\Gamma_p > 0.52$ kev. (Table IV), is more than 10 times wider than the single particle limit for $l = 5$ protons.

DISCUSSION

The 1.358 Mev. Level

On the basis of the measurements of Rubin (1947), Chao (1950) gives this level an assignment $J = 2$, even parity. In addition he says there is interference with a $J = 1$, odd parity state located at 1.1 Mev. and a $J = 0$, even parity state which was not resonant in the region he investigated. This $J = 0$ state appears to be the one discussed below. Since this resonance has a width of 54 kev., it is reasonably certain that the corresponding state of the compound nucleus is distinct from that of the 1.372 Mev. resonance seen in the $(p, \alpha\gamma)$ reaction which has a width of 15 kev.

TABLE IV

SUMMARY OF RESULTS. THE FIRST THREE COLUMNS GIVE THE EXPERIMENTAL RESULTS. COLUMNS 4 AND 5 GIVE THE SPINS, PARITIES, AND CHANNEL SPIN MIXTURES ASSIGNED TO THE RESONANCES ON THE BASIS OF THE OBSERVED ANGULAR DISTRIBUTIONS. BRACKETED VALUES ARE TENTATIVE

E, Mev.	Γ, kev.	σ, mb,	$J\pi$	t	$\frac{\Gamma_p \Gamma_\alpha}{\Gamma}$, kev.
1.358±.010	54±10	46±5	2+	2.7	2.0
1.709±.010	148±5	55±6	0+	0	4.2
1.853±.010	132±5	77±8	1−	0.4	1.9
2.11 ±.025	75±25	10±2	(4+)		(0.52)
2.31 ±.025	80±25	32±5	(2+)		(3.6)
2.58 ±.025	300±25	51±10	(0+)		(119.3)

The most serious discrepancy between the present work and the earlier results is in the cross section for the peak of this resonance. Streib, Fowler, and Lauritsen (1941) give a value of 0.0031 barn for this cross section, to be compared with the value of 0.046 barn in the present work. In contrast to this, the cross section for the 1.372 Mev. $(p, \alpha\gamma)$ resonance, as seen above, agrees within the given errors with the value found by Streib *et al.* The reason for the discrepancy in the (p, α_0) cross section is not clear. Although it appears that the cross section of Streib *et al.* was derived from the yield of alpha particles due to this resonance from a thick target, possible errors from this source do not seem to be sufficient to account for a difference of a factor of 15. The value of 46 mb., which is based on the $(p, \alpha\gamma)$ cross section of Streib *et al.*, is used as a basis for further calculations.

The value of the channel spin mixture given in column 5 of Table IV is taken from the ratio a_4/a_0. Since the curve of a_2 with energy does not resemble the curve for a_0 either in width or in position of the peak, and since it is probable that some of the a_2 contribution arises from the interference with the $J = 0$ resonance, the ratio a_2/a_0 would not be expected to give a reliable value. The ratio a_4/a_0 does not suffer from these uncertainties.

The 1.709 and 1.854 Mev. Resonances

These resonances show a strong interference in the a_1 curve. The rise in the a_3 curve starting at 1.8 Mev. appears to be associated with interference between the 1.853 resonance and higher resonances. There does not seem to be any a_3 component associated with the interference of the 1.709 and 1.853 Mev. resonances. These observations can only be a result of interference between a $J = 1$ and a $J = 0$ level. Since the a_2 curve shows a maximum under the 1.853 Mev. resonance, the assignment $J = 1$, odd parity has been given to it. The 1.709 Mev. resonance has then the assignment $J = 0$, even parity. The value of t of 0.4 given in column 5 of Table IV for the 1.853 Mev. resonance is taken from the ratio a_2/a_0. Although the a_2 curve has not exactly the same shape as the a_0 curve, the difference is not large. Since a_2/a_0 is large, the contribution of interference effects is presumed to be negligible, although certainly present to some extent. The value of a_4/a_0 is zero within the limits of error in this region.

The Resonances above 2 Mev.

The most outstanding feature of these resonances is the presence of the strong a_2 term at the 2.31 and 2.58 Mev. resonances. The presence of a_1 and a_3 terms under the 2.31 Mev. resonance and their absence under the 2.58 Mev. resonance strongly suggest that these two resonances have the same parity, and that this parity is the opposite of that of the 1.853 Mev. resonance. Hence it may be reasonably concluded that they both have positive parity. Since the 2.31 Mev. resonance shows in all the terms up to a_4, it is unlikely that it has zero spin. Spin 4 is excluded by the sum rule. Hence it appears to have the assignment 2+.

Owing to the unknown effect of higher levels, any assignment of the 2.58 Mev. level must be of a tentative nature. From the best estimate of the width it might be either 0+ or 2+.

The rather weak level at 2.11 Mev. can by the sum rule have any spin up to four. The best indication of its assignment comes from indirect data. Since the 1.853 Mev. level and the 2.31 Mev. level interfere strongly, it may be expected that their t values are not too dissimilar. If the value of a_4 seen under the 2.31 Mev. resonance is due to the channel spin mixture of this state alone, then it must have a t value of about five. Since the t value of the 1.853 Mev. level is 0.4, this does not seem consistent. Thus it would appear that the a_4 contribution under the 2.31 Mev. level is due to interference. This would suggest a 4+ assignment for the 2.11 Mev. level.

On the basis of these qualitative arguments alone, the assignment of these states is rather uncertain. However, once a set of assignments has been arrived at, it should be possible to fit the data in detail by the application of the interference formula of Blatt and Biedenharn (1952, Eqs. 4.7 and 5.6). In such a calculation the resonant energies, resonance widths, and t values are the adjustable parameters. In addition, the signs of the resonance amplitudes, that is the "$g_{\alpha sl}$" of Blatt and Biedenharn, are arbitrary.

An attempt was made to fit the interference formula to the present data taking the resonant energies and approximate widths from the a_0 curve. It was then found impossible to fit the remaining curves a_1 to a_4 with any manipulation of the values of t and $g_{\alpha sl}$. Even the best theoretical fits to the experimental data had too large a discrepancy to be accounted for by experimental error. It is possible that these discrepancies could be removed by a suitable choice of contributions of distant resonances in each of the various spin channels. In view of the large numbers of additional arbitrary parameters so introduced, the present data do not merit such an analysis, and the interpretation of the interference must remain uncertain. For this reason the assignments for the states above 2 Mev. are tentative.

It is of interest to note that the general features of the a_0 curve of Fig. 4 resemble the yield curve for the production of electron–positron pairs observed by Phillips and Heydenburg (1951). The relative yields at the peaks of the 1.853, 1.709, and 1.358 Mev. resonances in this work were 1.00: 0.75: 0.50 to be compared with relative yields at 1.00: 0.6: 0.2 found in the pair production

yield curve. Since the ground state of O^{16} and the pair emitting state have the same spin and parity, this similarity is not unexpected.

ACKNOWLEDGMENTS

It is a pleasure to acknowledge the help of Mr. R. A. Fraser in taking the data. We are indebted to Dr. W. T. Sharp for many helpful discussions. The analysis of the data in terms of Legendre polynomials was done by Dr. H. S. Gellman on FERUT at the University of Toronto.

REFERENCES

AJZENBERG, F. and LAURITSEN, T. 1955. Revs. Mod. Phys. **27**, 77.
BLATT, J. M. and BIEDENHARN, L. C. 1952. Revs. Mod. Phys. **24**, 258.
BLOCH, I., HULL, M. M., BROYLES, A. A., BORICIUS, W. G., FREEMAN, B. E., and BREIT, G. 1951. Revs. Mod. Phys. **23**, 147.
CHAO, C. Y. 1950. Phys. Rev. **80**, 1035.
CHAO, C. Y., TOLLESTRUP, A. V., FOWLER, W. A., and LAURITSEN, C. C. 1950. Phys. Rev. **79**, 108.
FOWLER, W. A., LAURITSEN, C. C., and LAURITSEN, T. 1948. Revs. Mod. Phys. **20**, 236.
GITTINGS, H. T. 1949. Rev. Sci. Instr. **20**, 325.
HUNT, S. E. and FIRTH, K. 1955. Phys. Rev. **99**, 786.
KINGDON, J. D., BAIR, J. K., COHN, H. O., and WILLARD, H. B. 1955. Phys. Rev. **99**, 1393.
PAUL, E. B. and CLARKE, R. L. 1953. Phys. Rev. **89**, 892A.
PAUL, E. B., CLARKE, R. L., and SHARP, W. T. 1953. Phys. Rev. **90**, 381A.
PHILLIPS, G. C. and HEYDENBURG, N. P. 1951. Phys. Rev. **83**, 184.
ROSE, M. E. 1953. Phys. Rev. **91**, 610, Eq. 30.
RUBIN, S. 1947. Phys. Rev. **72**, 1176.
STREIB, J. F., FOWLER, W. A., and LAURITSEN, C. C. 1941. Phys. Rev. **59**, 253.
THOMAS, R. G. 1951. Phys. Rev. **81**, 148.
WIGNER, E. P. and TEICHMANN, T. 1952. Phys. Rev. **87**, 123.

MOMENTUM DISTRIBUTION OF METALLIC ELECTRONS BY POSITRON ANNIHILATION[1]

A. T. STEWART

ABSTRACT

The angular correlation of photons from the two-photon decay of positrons has been measured for positrons annihilating in some 34 elements, mostly metals. These data give the momentum distribution of photons and hence of the center of mass of the annihilating electron–positron pairs. The momentum distributions are discussed in terms of the velocity dependence of the annihilation probability. It is concluded that the observed momentum distributions are primarily the momentum distributions of the conduction electrons in the metals. A higher momentum component is observed, which is attributed to ion core effects.

INTRODUCTION

The annihilation of free electron–positron pairs usually occurs by the emission of two photons, which, to conserve momentum, are emitted at 180° to each other in the center of mass of the annihilating particles. If the center of mass is in motion with respect to an observer the angle between the photon directions departs from 180° by an amount of the order of $v_{c.m.}/c$, where $v_{c.m.}$ is the velocity of the center of mass and c is the velocity of light. For the low velocities of interest here the departure of the angle between the photon directions from 180° is proportional to the component of momentum of the annihilating pair which is parallel to the bisector of the propagation directions.

The first measurements of the angular correlation of annihilation photons were made by Beringer and Montgomery in 1942. Following this Vlasov and Tsirelson (1948) showed that 95% of the photon pairs were emitted within $180° \pm 1°$, from which they concluded that the kinetic energies of most of the annihilating positrons were less than 80 ev. Soon after these experiments Dumond *et al.* (Dumond, Lind, and Watson 1949) showed that the line width of the (0.511 Mev.) annihilation radiation was slightly greater than their instrument resolution. The excess width could be accounted for by assuming that the electron or positron had a kinetic energy at annihilation of 10–20 ev. Following this, DeBenedetti *et al.* (DeBenedetti, Cowan, and Konneker 1949; DeBenedetti, Cowan, Konneker, and Primakoff 1950) arrived at a similar conclusion from their study of the angular correlation of the annihilation radiation. Warren and co-workers (Argyle and Warren 1951; Warren and Griffiths 1951; and Erdman 1955) also measured the angular correlation of photons from annihilations in various elements and compounds.

Maier-Leibnitz' measurements (1951) of the angular correlation of the radiation from positrons annihilating in several metals showed clearly that there were differences between various metals and that the mean momentum of the annihilating pairs in some heavy metals was greater than the momentum of conduction electrons.

[1]Manuscript received September 20, 1956.
Contribution from the Physics Division, Atomic Energy of Canada Ltd., Chalk River, Ontario.
Issued as A.E.C.L. No. 384.

In 1955 some measurements were made by Green and Stewart (1955, and Stewart and Green 1954) which showed that the half-width of the angular distribution was a good measure of the Fermi energy of light metals. Other experimenters (Page, Heinberg, Wallace, and Trout 1955; Page and Heinberg 1956) have shown that angular correlation measurements give information about the mechanism of positron annihilation in solids and in some cases about the electrons of the solid with which the positrons annihilate. Extensive work with metals done at Professor DeBenedetti's Laboratory (Lang, DeBenedetti, and Smoluchowski 1955) has given results similar to and in agreement with those presented in this paper.

Here we present* measurements of the angular distribution of photons from positron annihilation in 30 metals and four other closely related elements. It is shown that a simple transform of the angular distributions can yield the distribution in momentum of the annihilating electron–positron pairs. These derived distributions are presented for all the specimens and are discussed in terms of the momentum distribution of free electrons, which they often closely resemble.

EXPERIMENTAL

A schematic diagram of the apparatus is shown in Fig. 1. Radiation from annihilation of positrons in the specimen was detected in two 2 in. × 2 in.

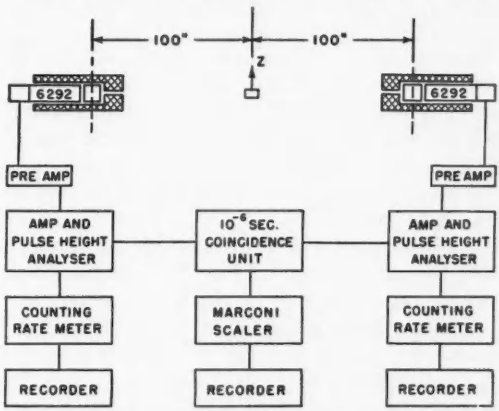

FIG. 1. Schematic diagram of the apparatus.

cylindrical NaI(Tl) crystals and RCA 6292 photomultipliers mounted behind 0.050 in. × 1.5 in. horizontal slits in lead shields. The rate of coincidences in the two detectors was measured as a function of the vertical displacement of the specimen from the mid-point between the counters. Automatic equipment moved the specimen at 5 minute intervals and recorded the counting rate. The pulse height analyzers selected pulses corresponding to photons in the energy range from about 200 to 600 kev.

*A preliminary report of this work was given in a letter to *The Physical Review* (Stewart 1955).

The positron emitter used was Cu^{64} (12.8 hr.) made by irradiating copper foils in the NRX reactor. Two methods of bombarding the approx. $\frac{5}{8}$ in. diam. specimen with positrons were used. In one, a multilayer sandwich was made from thin foils of the specimen metal alternating with approximately 1 mg./cm.^{2} copper leaf. The total thickness and vertical dimension of such a sandwich was usually about 0.06 in. With this technique only about 3% of the positrons annihilated in the copper. Because the shape and width of the angular correlation curve for positrons annihilating in copper were not very different from the results obtained for most of the metals examined by this method, no corrections were made for annihilations in the copper leaf.

In the other method a much thicker piece of copper foil was used as a positron emitter. It was mounted about $\frac{1}{2}$ in. from the specimen and was shielded by several inches of lead from the direct view of the detectors. This method was used for many specimens, including the chemically active metals, which were supported in the center of a vacuum chamber. Under these circumstances positrons entered from above through a thin mica window.

RESULTS

The angular correlation measurements for 34 specimens are shown in Fig. 2. The data shown for each element are the sum of many runs through the angular range indicated. A correction for source decay has been made. The total number of counts at the peak position is greater than 6000 for all except some heavy metals and is at least twice this value for most of the alkali metals.

Before the momentum distributions of annihilation photons are obtained from the angular distributions, two instrumental effects must be considered. The more important is the combined effect of detector slit width and specimen thickness. This produces an approximately Gaussian shaped angular resolution function of half-width about 0.6×10^{-3} radians for most of the runs, increasing to about 2×10^{-3} radians for some light metals. A correction for this instrumental resolution width was calculated by the parabolic method of Eckart (1937) and was applied to the observational points. The effect of the correction is to increase the height of the peak and to sharpen the corners of the angular correlation curves. The maximum correction was applied to measurements with the Mg specimen and amounted to only 4% at the peak.

The other is the effect of the finite length (1.5 in.) of the slits, which causes a loss in counting efficiency for photon pairs with large angular deviation from 180°. In terms of the total momentum of the annihilating particles the decrease in detection efficiency is found to be about 6% and 25% for total momenta 3 and 6 (times $2mc\times10^{-3}$) respectively. A correction has not been made for this effect because it is well within the experimental errors in the lower momentum region of interest.

The momentum distribution of the annihilation photons $N(k)$, and the corresponding momentum space density $\rho(k)$, were obtained using the relations

$$N(k) \propto dI/dz\cdot z, \qquad \rho(k) \propto dI/dz\cdot 1/z,$$

which are derived in the Appendix. In these expressions I is the coincidence counting rate as a function of z, the vertical displacement of the specimen

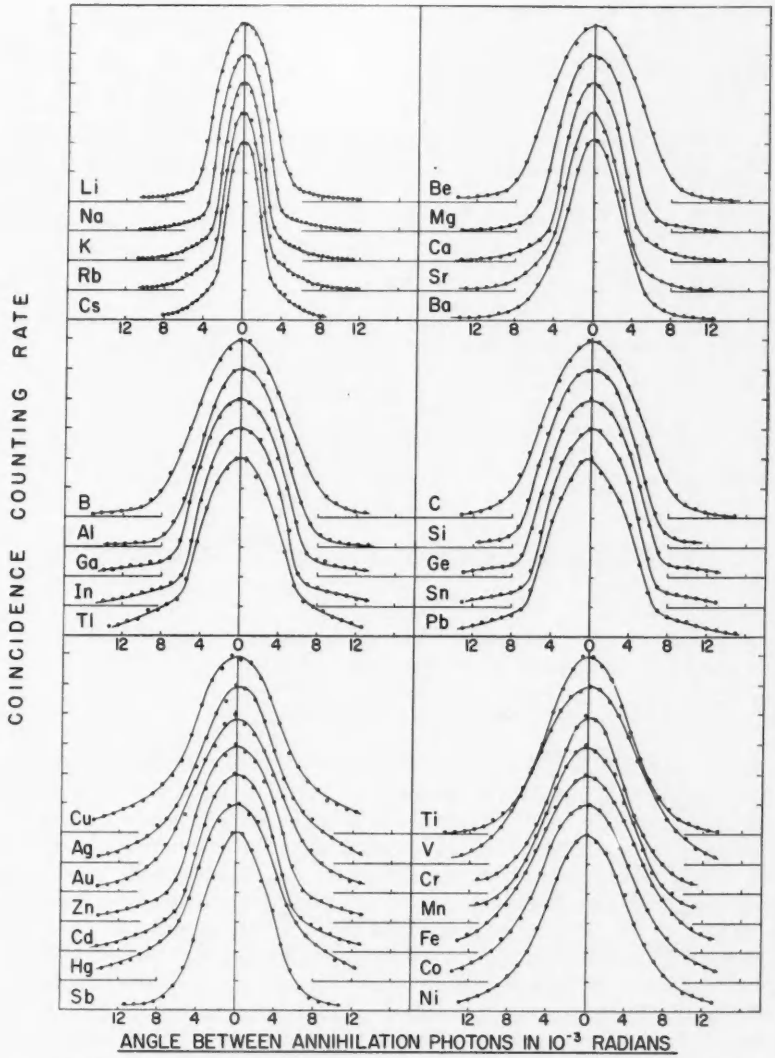

FIG. 2. Observed angular correlation of photons from positrons annihilating in various elements. The data have been normalized to make all curves the same height.

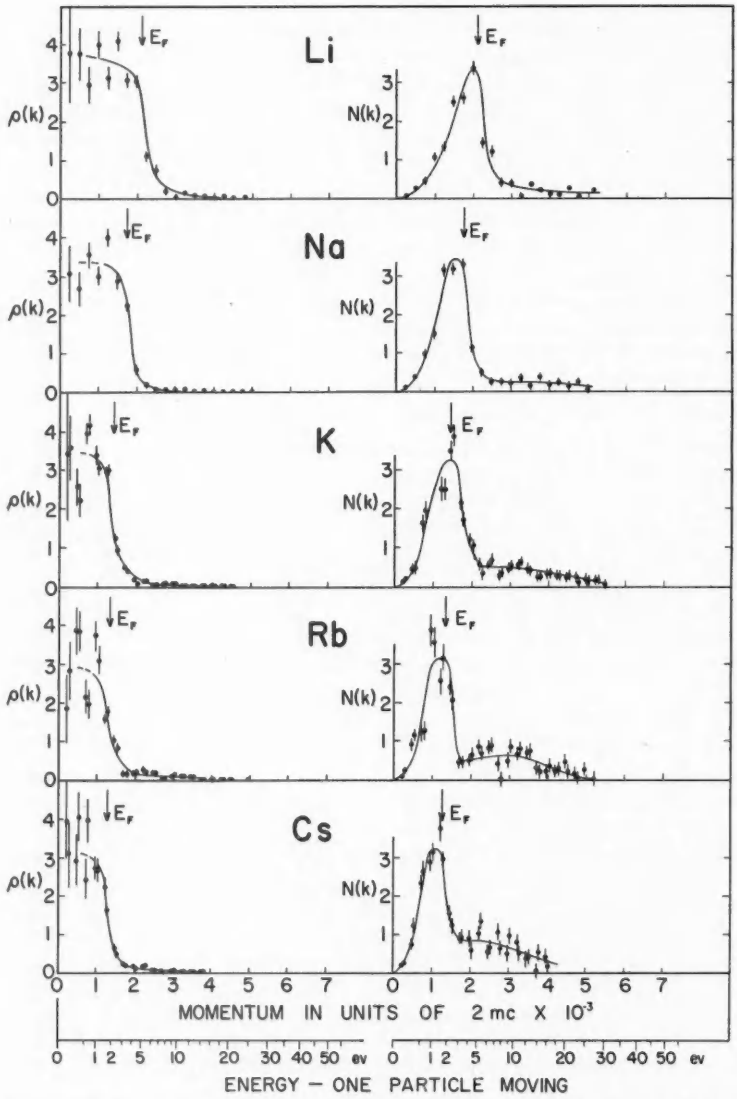

FIG. 3. Momentum distributions, $N(k)$, and momentum space densities, $\rho(k)$, of photons from positron annihilations in the alkali metals Li, Na, K, Rb, and Cs of Group Ia of the Periodic Table.

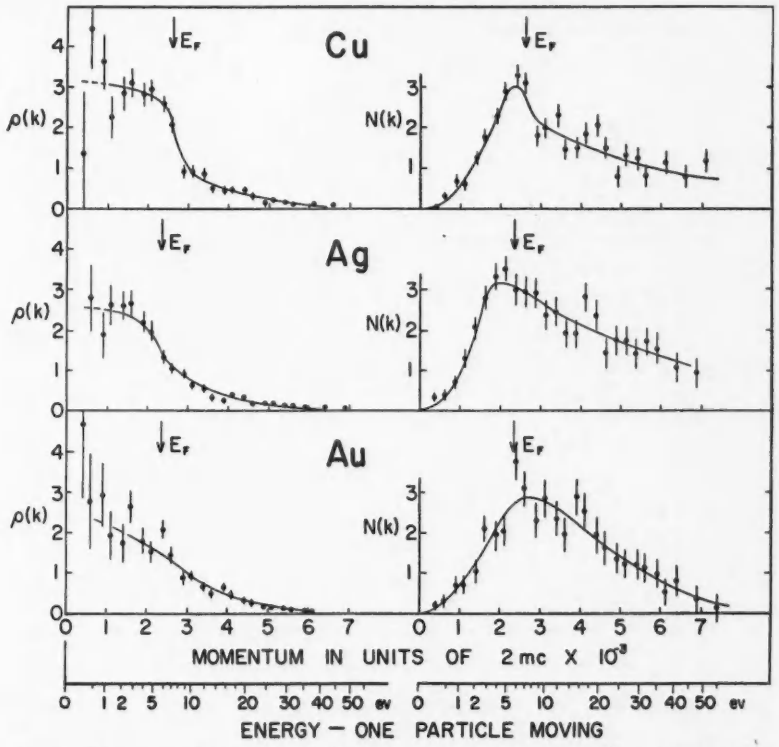

FIG. 4. Momentum distributions, $N(k)$, and momentum space densities, $\rho(k)$, of photons from positron annihilations in the noble metals Cu, Ag, and Au of Group Ib.

from the line joining the detector slits. The centers of the observed angular distributions were taken to be $z = 0$. The value of the chord $(I_1-I_2)/(z_1-z_2)$ was used for the derivative dI/dz at $z = (z_1+z_2)/2$, where I_1 and I_2 are the experimentally observed counting rates (with above correction) at z_1 and z_2 respectively. The momentum distribution and momentum space density so calculated are shown in Figs. 3 to 11. The errors indicated in the figures are the statistical errors of counting and an estimate of the effect of uncertainty in z. The full line has been arbitrarily drawn through the points. The arrows marked E_F indicate the momentum of an electron at the Fermi surface* for 1, 2, 3, and 4 electrons per atom in metals of Groups I, II, III, and IV respectively. In Fig. 11 (Fe, Co, and Ni) two arrows are shown for 0.5 and 1 electron per atom. The energy scale on each figure was calculated on the assumption that the momentum is due to the motion of one of the annihilating particles only.

*The Fermi energy was computed from the usual formula given for example in Mott and Jones, *Properties of Metals and Alloys*, Chap. II, Eq. 19.

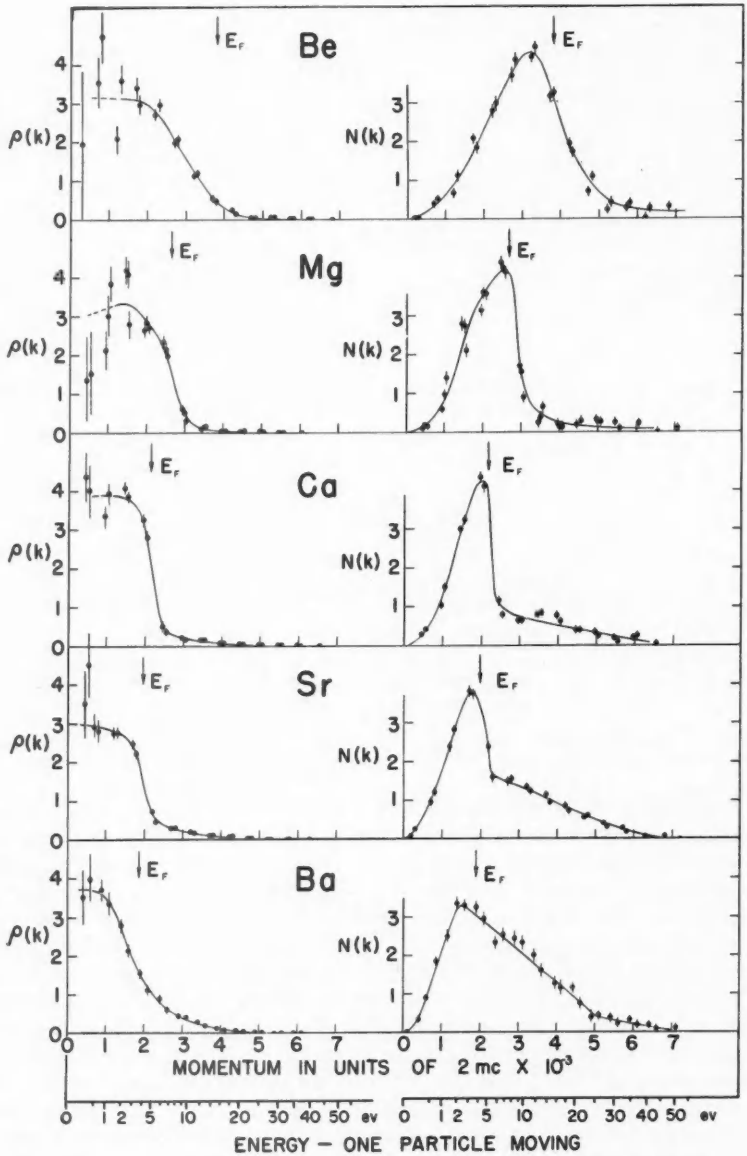

FIG. 5. Momentum distributions, $N(k)$, and momentum space densities, $\rho(k)$, of photons from positron annihilations in the alkali earth metals Be, Mg, Ca, Sr, and Ba of Group IIa.

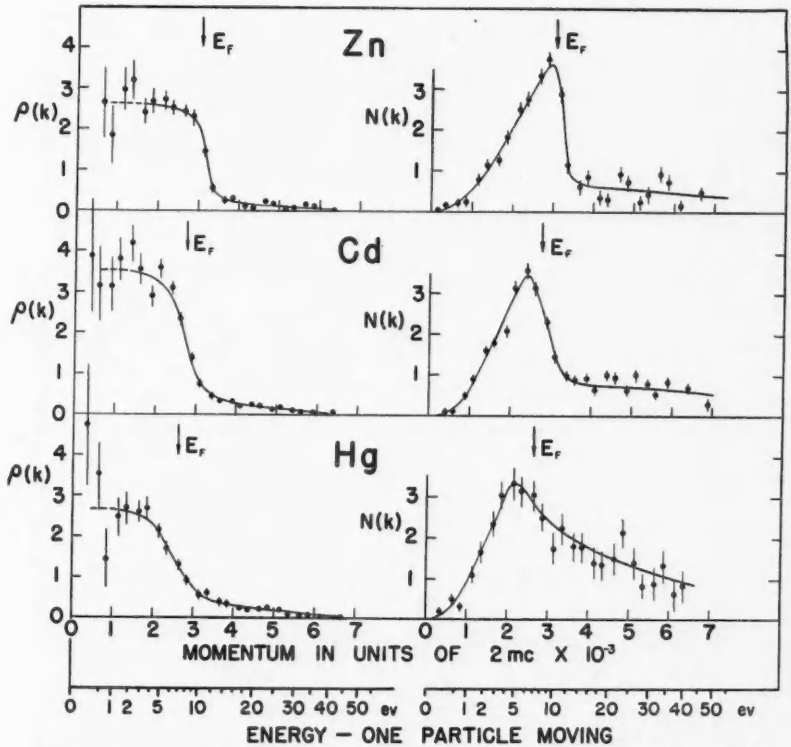

FIG. 6. Momentum distributions, $N(k)$, and momentum space densities, $\rho(k)$, of photons from positron annihilations in metals Zn, Cd, and Hg of Group IIb.

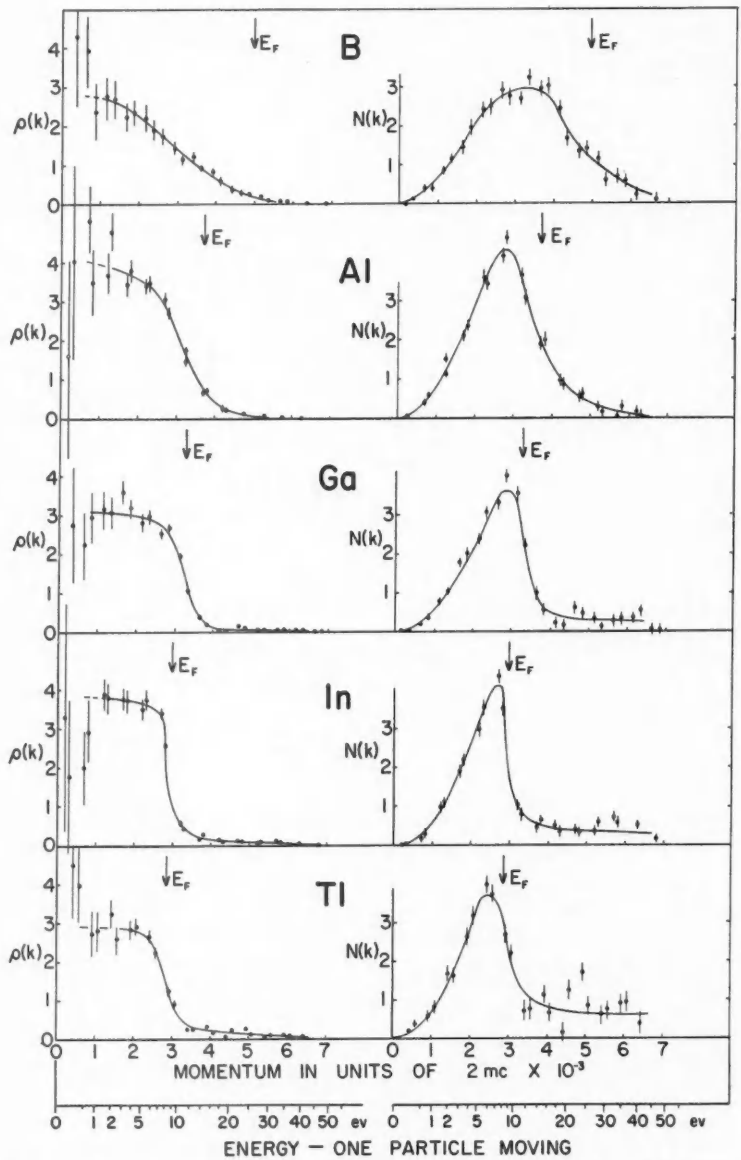

FIG. 7. Momentum distributions, $N(k)$, and momentum space densities, $\rho(k)$, of photons from positron annihilations in the metals B, Al, Ga, In, and Tl of Group III.

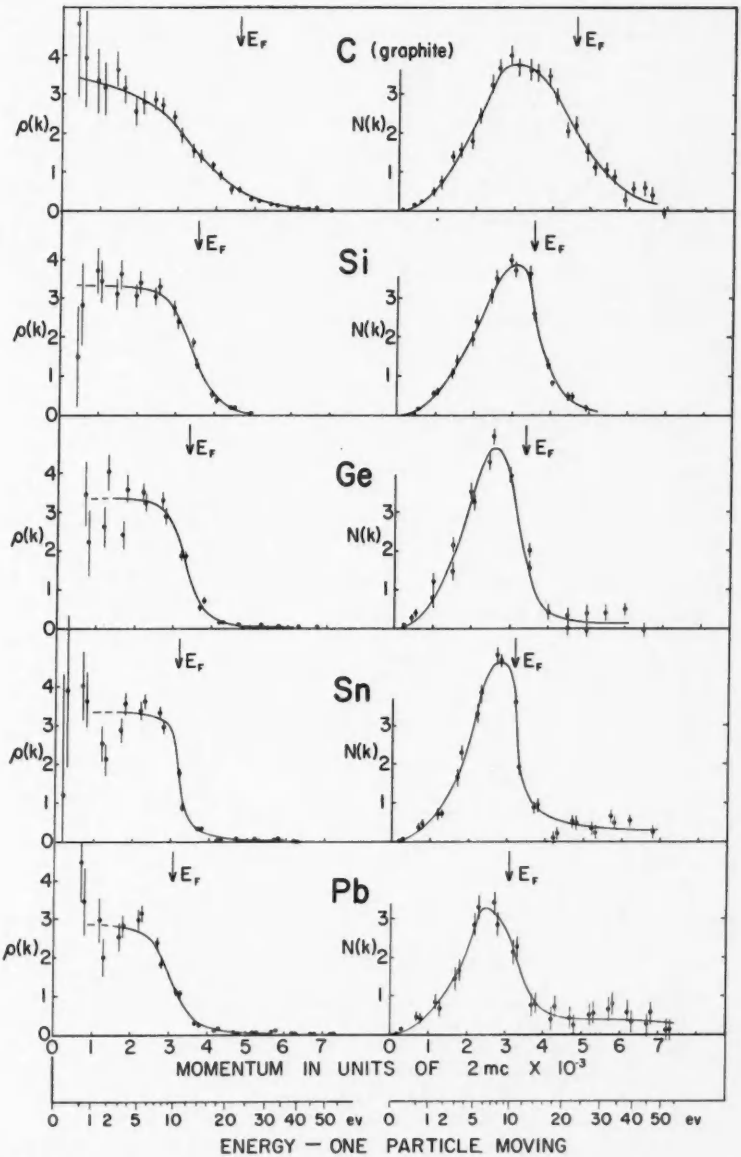

FIG. 8. Momentum distributions, $N(k)$, and momentum space densities, $\rho(k)$, of photons from positron annihilations in the elements C, Si, Ge, Sn, and Pb of Group IV.

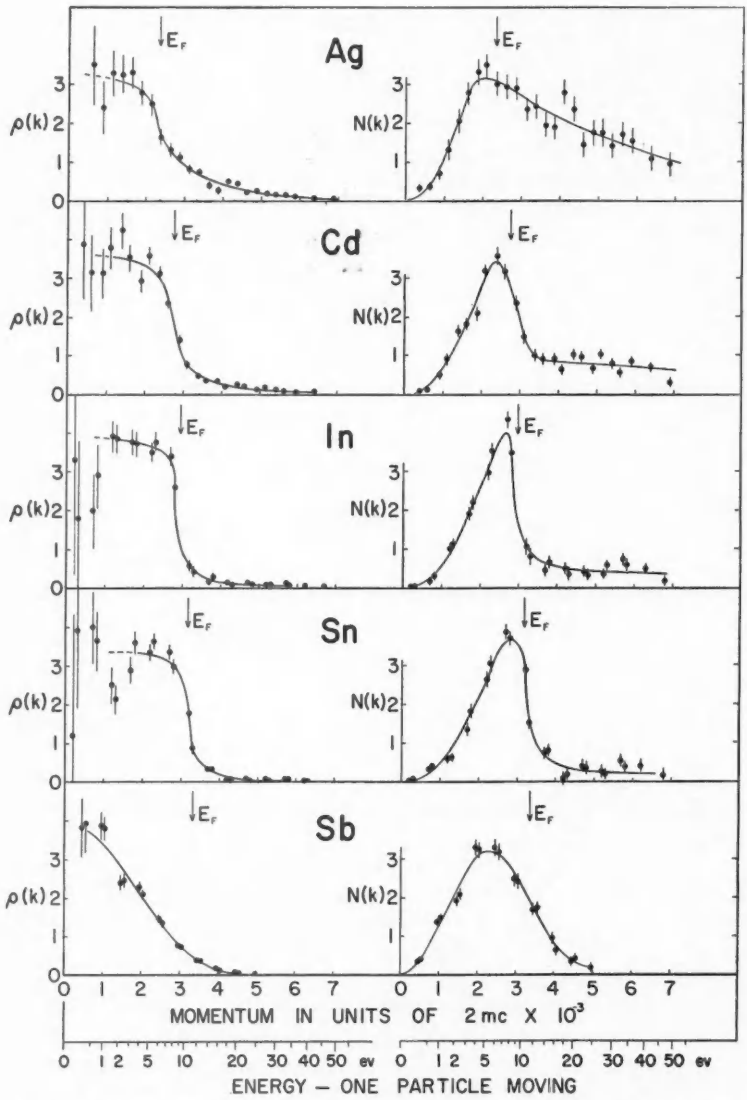

FIG. 9. Momentum distributions, $N(k)$, and momentum space densities, $\rho(k)$, of photons from positron annihilations in the metals Ag, Cd, In, Sn, and Sb of Period IVb.

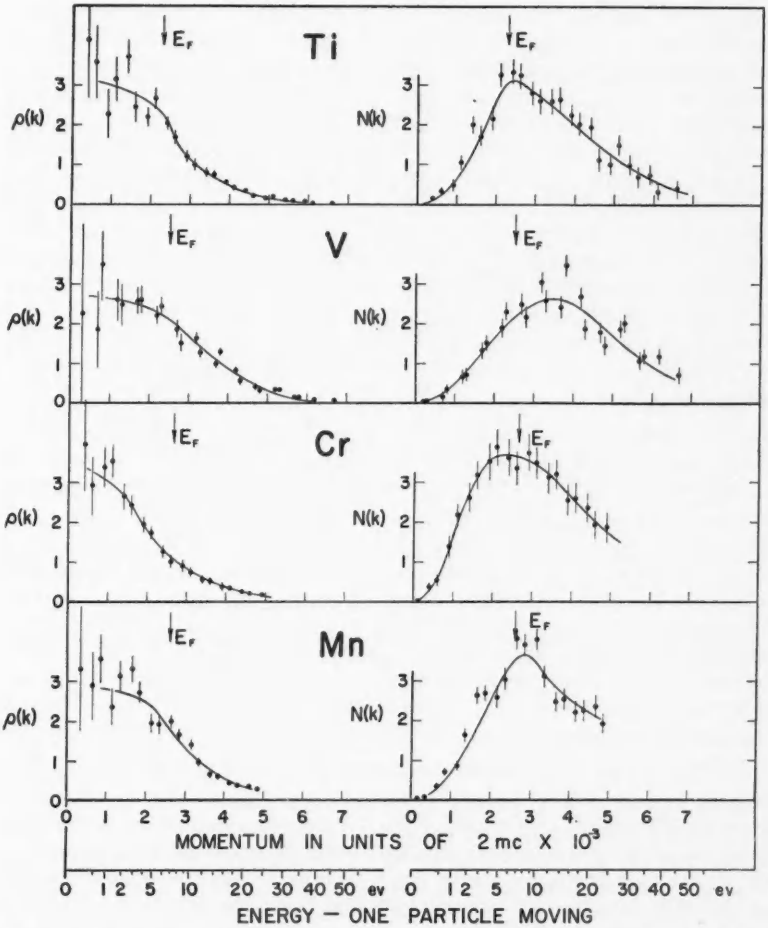

FIG. 10. Momentum distributions, $N(k)$, and momentum space densities, $\rho(k)$, of photons from positron annihilations in the transition metals Ti, V, Cr, and Mn.

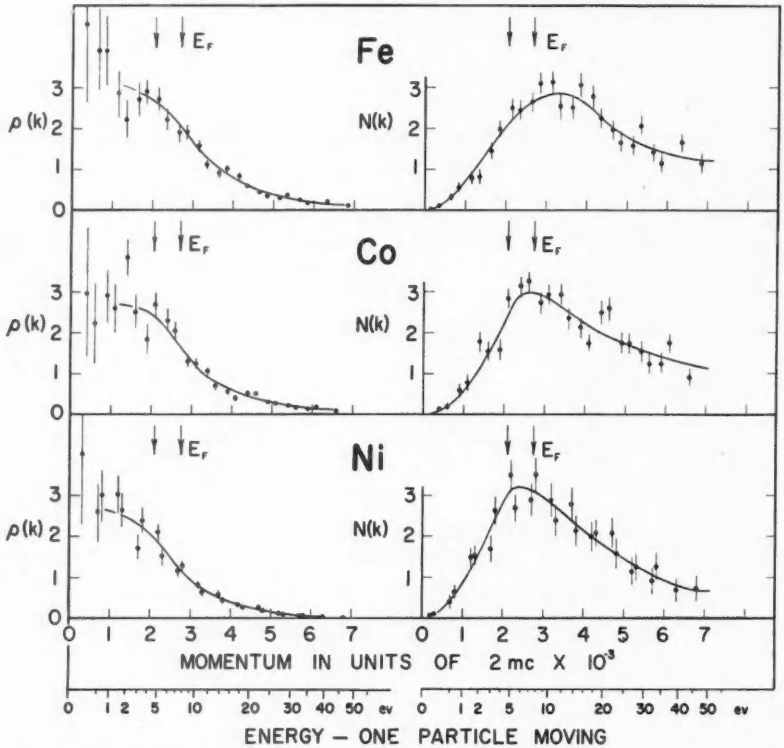

FIG. 11. Momentum distributions, $N(k)$, and momentum space densities, $\rho(k)$, of photons from positron annihilations in the transition metals Fe, Co, and Ni.

DISCUSSION

Momentum Distributions

The momentum distributions of annihilating electron–positron pairs appear to have two components, which are clearly seen in some of the alkali and alkali earth metals. The similarity between the lower momentum components of the momentum distributions obtained in this experiment and the momentum distributions expected for conduction electrons of the free electron metals, i.e. the alkali metals, is striking. (It should be remembered that $\rho(k)$ and $N(k)$ for electrons of a free electron gas are constant and quadratic respectively out to the Fermi cutoff, where they fall to zero.) That the maximum momentum cutoff occurs at the calculated Fermi limit provides experimental support for Lee-Whiting's (1955) calculation which showed that positrons in metals thermalize in a time short compared with annihilation lifetime. Thus the total momentum of the photons is very likely the momentum of the annihilation electron. The form of the momentum distribution below the cutoff is some-

what similar to the free electron theory momentum distribution and implies that the annihilation probability is not strongly velocity dependent. For example, an annihilation probability of the form $1/v$, which is predicted by a coulomb interaction between a free electron and positron, is precluded. The almost velocity independent annihilation probability calculated by Ferrell (1956) is in agreement with these results. For metals other than the alkalies the momentum distribution and the maximum momentum cutoff are not expected to resemble so closely the free electron theory but will contain lattice effects. For example the two-electron alkali earth metals have Fermi surfaces near the reciprocal lattice zone boundaries and thus the electron momentum near the Fermi limit is reduced below the free electron theory value, even being zero at some symmetry points on the faces of the zone. The result of lattice effects will be to change the quadratic function $N(k)$ of the free electron theory by reducing the number of high momentum electrons and increasing the number with lower momentum. For the three-electron Al structure the Fermi surface in most places extends past the first zone boundaries and in some places probably past the free electron Fermi sphere. It can be seen that a small number of electrons in Al have momenta greater than the Fermi limit, as indeed is the case for several others.

Higher Momentum Component

The higher momentum component of the distribution observed in this experiment is probably due to an effect of the ion cores. At first sight it might appear that this component is caused by positrons annihilating with electrons bound to the ion core, because the importance of the effect increases roughly as the volume of the core. However another explanation is also possible. DeBenedetti *et al.* (1950) showed that because the positron space wave function is excluded (by coulomb repulsion) from the interior of the ion cores, the momentum wave function is many valued having momenta which correspond to the wave numbers of the points of the reciprocal lattice. In this explanation too, the relative importance of the higher momentum components of the positron wave function increases with increase in core volume. Ferrell (1956) has shown that this excluded volume effect is probably the more important.

Lifetime

The rate of annihilation of positrons in metals has been discussed many times.* The measured lifetime is about $1.5\pm0.7\times10^{-10}$ sec.† whereas the expected lifetime for a non-coulomb interacting positron in a sea of electrons of density similar to the density of conduction electrons in metals is one or two orders of magnitude longer and varies with electron density. Inclusion of the coulomb interaction makes the calculation of annihilation probability difficult. The simplest improvement, the introduction of a coulomb interaction between the otherwise free annihilating pairs, increases the rate of annihilation almost enough but gives a $1/v$ annihilation probability, which, as discussed

*See for example the review article by Ferrell (1956).

†Recent experiments of Gerholm (1956) and Minton (1954) yield lifetimes of about 2.5×10^{-10} sec. which are not in agreement with most other measurements.

above, seems unlikely in view of the results of the present experiment. The more complicated case of allowing coulomb interaction between all particles and not only the annihilating pair has been discussed by Ferrell (1956). His calculations yield an annihilation probability which is approximately independent of velocity and give a lifetime in agreement with observation for the metals of higher conduction electron density (e.g. Al) but too low by a factor of about four for lower density metals (e.g. Na). As he points out, however, one would not expect the lifetime of an interacting positron in an electron sea to exceed the lifetime of the positronium ion, $e^-e^-e^+$, which is the bound (0.2 ev.) system of particles with the greatest density of electrons at the positron. The electron density in this system is about 50% greater than in the positronium atom, e^-e^+. The annihilation rates of the singlet and triplet positronium atom are 8.0×10^9/sec. and 7.1×10^6/sec. respectively (Ore and Powell 1949). The annihilation rate of the ion is then $1.5(\frac{1}{4}\times8.0\times10^9+\frac{3}{4}\times7.1\times10^6)$/sec. $= 3.0\times10^9$/sec. This rate corresponds to a lifetime of 3.4×10^{-10} sec., which is somewhat greater than the measured lifetime of positrons in metals. If one considers a positron located in a lattice defect or an interstitial positron in a crystal it is reasonable to expect that the wave functions of the valence band electrons are not much altered by its presence. The wave functions will be slightly increased at the positron and virtually unchanged in the remainder of the crystal. The sum of these small increases in each electron wave function may be sufficient to concentrate at the positron a negative charge density equivalent to that in the positronium ion. Hence we might expect the positron to have a short lifetime and to annihilate with an electron which has a momentum almost exactly that of the unperturbed valence electron. The observed momentum distributions are in agreement with this simple picture of positron annihilation in metals.

ACKNOWLEDGMENTS

I wish to thank Dr. R. H. Betts for the assistance and cooperation of the Research Chemistry Branch in the handling of copper sources; Mr. R. L. Brown and Mr. C. B. Falconer who operated the experiment for some time; and especially Miss A. R. Rutledge who did most of the considerable computations. I have had the pleasure of profitable discussions with many colleagues, especially Dr. B. N. Brockhouse and Dr. G. E. Lee-Whiting, as well as with Dr. R. A. Ferrell of the University of Maryland.

APPENDIX

Proportionality Constant between z and k_z

We define $\mathbf{k}$ to be the momentum of the center of mass of the electron–positron pair at the time of annihilation. If k_z is the z component of this momentum, a coincidence between the annihilation photons can be detected only when the source is displaced from a line joining the counter slits by an amount $z = k_z d/2mc$, where $2d$ is the distance between the counters, m is the electron mass, and c the velocity of light.

Derivation of Differentiation Relation

When the source is displaced an amount z the coincident counting rate $I(z)$ is proportional to the total number of pairs with $k_z = 2mc\,z/d$, that is

$$I(z) = \text{const.} \iint \rho(\mathbf{k})\, dk_x\, dk_y,$$

where $\rho(\mathbf{k})$ is the momentum space density of annihilating electron–positron pairs and the integral is taken over the plane of constant k_z. In this expression we assume that variations in $\rho(\mathbf{k})$ are small within a region Δk_z corresponding to the slit width, and that the length of the slits is much greater than the extent of $\rho(\mathbf{k})$, i.e. slit length $\gg k_{\max} d/2mc$. As discussed above small corrections for the finite slit width and slit length have been calculated and the former applied. If the distribution in momentum space is assumed isotropic and denoted by $\rho(k)$, the integral becomes

$$I(z) = \text{const.}\, 2\pi \int_{k_z}^{\infty} k\rho(k)\, dk,$$

from which we have by differentiating with respect to k_z

$$\rho(k) = \frac{-(d/2mc)^2}{2\pi\ \text{const.}} \frac{dI}{dz} \frac{1}{z},$$

and for momentum distribution

$$N(k) = 4\pi k^2 \rho(k)$$

$$= \frac{-2}{\text{const.}} \frac{dI}{dz}\, z.$$

REFERENCES

ARGYLE, P. E. and WARREN, J. B. 1951. Can. J. Phys. **29**, 32.
BERINGER, R. and MONTGOMERY, C. G. 1942. Phys. Rev. **61**, 222.
DEBENEDETTI, S., COWAN, C. E., and KONNEKER, W. R. 1949. Phys. Rev. **76**, 440(L).
DEBENEDETTI, S., COWAN, C. E., KONNEKER, W. R., and PRIMAKOFF, H. 1950. Phys. Rev. **77**, 205.
DUMOND, J. W. M., LIND, D. A., and WATSON, B. B. 1949. Phys. Rev. **75**, 1226.
ECKART, C. 1937. Phys. Rev. **51**, 735.
ERDMAN, K. L. 1955. Proc. Phys. Soc. **68**, 304.
FERRELL, R. A. 1956. Revs. Mod. Phys. **28**, 308.
GERHOLM, T. R. 1956. Arkiv Fysik, **10**, 523.
GREEN, R. E. and STEWART, A. T. 1955. Phys. Rev. **98**, 486.
LANG, G., DEBENEDETTI, S., and SMOLUCHOWSKI, R. 1955. Phys. Rev. **99**, 596(L).
LEE-WHITING, G. E. 1955. Phys. Rev. **97**, 1557.
MAIER-LEIBNITZ, H. 1951. Z. Naturforsch. **6a**, 663.
MINTON, G. E. 1954. Phys. Rev. **94**, 758.
ORE, A. and POWELL, J. L. 1949. Phys. Rev. **75**, 1696.
PAGE, L. A. and HEINBERG, M. 1956. Phys. Rev. **102**, 1545.
PAGE, L. A., HEINBERG, M., WALLACE, J., and TROUT, T. 1955. Phys. Rev. **98**, 206(L).
STEWART, A. T. 1955. Phys. Rev. **99**, 594(L).
STEWART, A. T. and GREEN, R. E. 1954. Bull. Am. Phys. Soc. **29**, No. 7, H12 (Phys. Rev. **98**, 232(A) (1955)).
VLASOV, N. A. and TSIRELSON, E. A. 1948. Doklady Akad. Nauk S.S.S.R. **59**, 879.
WARREN, J. B. and GRIFFITHS, G. M. 1951. Can. J. Phys. **29**, 325.

ELASTIC SCATTERING OF 20-MEV. PROTONS BY OXYGEN AND NITROGEN[1,2]

R. H. CHOW[3] AND BYRON T. WRIGHT

ABSTRACT

The absolute angular distributions for 20-Mev. protons elastically scattered by O^{16} and N^{14} were determined using the external beam of the frequency-modulated cyclotron at the University of California, Los Angeles. The distributions for the two elements were found to be similar except for the appearance of a more pronounced first minimum in the O^{16} distribution. The locations of the maxima and minima seem to indicate that simple diffraction effect is responsible for their presence. The cross sections range from about 1 barn per sterad. to 4 mb. per sterad. between 15° and 165° in the laboratory system. The standard deviations due to statistics range from 1½% to 10%.

I. INTRODUCTION

The interaction between a proton and a nucleus can be studied through the angular distribution of elastically scattered protons. The experiments of Burkig and Wright (1951), Cohen and Neidigh (1954), Dayton (1954), Schrank (1955), Bromley *et al.* (1956), and others have shown the interaction to be non-Coulomb when the incident energy of the proton is sufficient to penetrate the Coulomb barrier and encounter the short-range nuclear forces. The results also showed that at a bombarding energy of the order of 20 Mev. the angular distributions of various nuclei display a systematic trend as one proceeds from light to heavy nuclei. This trend has been reasonably well reproduced, particularly at not-too-large angles, by the optical model of Saxon *et al.* (1952, 1954, 1956).

In the present experiment the absolute angular distributions of 20-Mev. protons scattered elastically from N^{14} and O^{16} have been determined.

II. DESCRIPTION OF APPARATUS

Protons from the deflected beam of the U.C.L.A. synchrocyclotron, collimated into a beam ¼-in. in diameter, with ±0.3° angular divergence at the target, were introduced into a 32-in. I.D. aluminum scattering chamber in which the target, gaseous or solid, was located. The scattered protons were detected by a NaI(Tl) crystal, coupled to a Dumont-6292 multiplier phototube. The protons not scattered by the target nuclei were caught in a Faraday cup equipped with magnets and a guard ring which, together with the beam-integrating feedback circuit which held the cup voltage to within a few millivolts above ground, assured that the effects due to secondary electrons and residual ionization currents were negligible (Yntema and White 1954). The Faraday cup opening was sufficiently large so that multiple-scattering losses, according to the treatment of Dickenson and Dodder (1953) or Ashby (1951), were negligible.

[1]Manuscript received July 23, 1956.
Contribution from the Department of Physics, University of California, Los Angeles, California.
[2]Assisted in part by the joint program of the Office of Naval Research and the U.S. Atomic Energy Commission.
[3]Now at Atomic Energy of Canada, Ltd., Chalk River, Ontario, Canada.

At small angles where Coulomb scattering predominates, the error due to the finite width of the slit was eliminated by utilizing an equation derived by Breit, Thaxton, and Eisenbud (1939, Equation 7.2), viz., number of protons received is equal to:

$$\frac{NnA\sigma(\theta_0)}{R_0S_0}\frac{2b}{h}\left\{1+\frac{C_0x_{Av}}{S_0R_0}+\frac{C_0^2(x^2)_{Av}}{S_0^2R_0^2}+\frac{C_0^2-2(y^2)_{Av}}{2R_0^2S_0^2}-\frac{b^2}{6h^2}\right.$$
$$+\frac{(x^2)_{Av}}{2h^2}+\frac{\sigma'(\theta_0)}{\sigma(\theta_0)}\left[-\frac{x_{Av}}{h}+\frac{C_0(y^2)_{Av}}{2S_0R_0^2}-\frac{C_0(x^2)_{Av}}{S_0R_0h}\right]$$
$$\left.+\frac{\sigma''(\theta_0)}{\sigma(\theta_0)}\left[\frac{b^2}{6h^2}+\frac{(x^2)_{Av}}{2h^2}\right]\right\},$$

where (x, y) denote the coordinates of an elemental area dS of the detector slit,

N = number of protons that passed in the beam,
n = number of scattering nuclei per unit volume,
$\sigma(\theta_0)$ = scattering cross section per unit solid target,
θ_0 = scattering angle,
$2b$ = slit width (front slit),
A = area of rear slit,
$C_0 = \cos\theta_0$,
$S_0 = \sin\theta_0$.

The correction terms depending upon the geometry must be made to cancel. Since for sufficiently small angles

$$\frac{C_0}{S_0}\simeq\frac{1}{\theta_0}, \qquad C_0\simeq 1, \qquad \frac{\sigma'(\theta_0)}{\sigma(\theta_0)}=-\frac{4}{\theta_0}, \quad \text{and} \quad \frac{\sigma''(\theta_0)}{\sigma(\theta_0)}=\frac{20}{\theta_0^2}.$$

If rectangular slits are used with the front and rear slits equal in width, the two terms not containing the angle cancel and the remaining correction terms can be made to vanish if the ratio of the height l of the rear slit to its half width b is chosen to satisfy the following equation:

$$\frac{l^2}{b^2}=\frac{24}{5}\left(\frac{1}{3}+\frac{4}{3}\frac{R_0}{h}+\frac{20}{3}\frac{R_0^2}{h^2}\right).$$

The ratio R/h therefore determines the ratio $(l/b)^2$, and vice versa. In this experiment the slit dimensions were made as close as possible to specifications, then the distances R_0 and h were set to satisfy the above equation.

The effects of the front slit and baffles between the front and rear slit in causing uncompensated multiple-scattering losses were found from the expression of Worthington *et al.* (1953)

$$\epsilon=\frac{\pi n}{6}\left(\frac{Ze^2}{E}\right)^2\frac{L^3}{x_1^2-x_0^2}$$

to be negligible for 20-Mev. protons in oxygen at 5 cm. of Hg pressure. The effect in the vertical plane of the analyzer was less than 0.02%. In the horizontal plane, the effect was still lower, since the anti-scattering baffles were

of generous width and were located almost directly behind the front slit, which is regarded as a virtual source in this case.

In scattering experiments using a gas target, two slits are needed to define the solid angle, the scattering volume, and the direction of scattering. The solid angle is given by A/R_0^2, where A is the area of the rear slit and R_0 is the distance from the rear or furthermost slit to the scattering volume. At an angle θ_0, the scattering volume is easily shown to be $(2b/\sin\theta_0)R_0/h$. Obviously, the yield of scattered protons is proportional to the product of the above two factors. The factor $2bA/R_0h$ is characteristic of the slit-system geometry and is usually denoted by G in the literature (Herb *et al.* 1939). The differential scattering cross section can be easily shown to be

$$\sigma(\theta_0) = \frac{Y(\theta_0)\sin\theta}{nNG},$$

where N is the number of incident protons,

n is the density of target atoms,

and $Y(\theta_0)$ is the yield of scattered protons at angle θ_0.

In this experiment three separate analyzing slit-systems with values of G equal to 3.935×10^{-4} cm., 3.911×10^{-4} cm., and 1.675×10^{-4} cm. were used.

Tool steel with edges lap finished was used for making the slits. The components of the slit system were aligned using dial indicators. The collimator, analyzing slit-system, and Faraday cup were aligned with respect to the chamber axis and each other using a transit.

The output pulses from the photomultiplier were fed into a cathode follower, passed through about 80 ft. of RG-62U coaxial cable, clipped to 1 μsec. length by a shorted delay line at the input of a Bell and Jordan type linear amplifier with rise time of 0.13 μsec., sorted at the output of the amplifier by differential-integral pulse-analyzers, and finally recorded by binary scalers with a resolving time of 1 μsec. for pair pulses.

The resolution of the system was found to be about 2% full width at half maximum for 20-Mev. protons. The counting system was controlled remotely by the beam integrating system which shorted the polystyrene integrating condenser whenever a preset voltage was reached. The integrating system was calibrated by a time–current method discussed in an article by Caldwell and Royden (1956).

III. EXPERIMENTAL PROCEDURE

The constancy of the ratio of the counting yield at a given angle to the scattering gas pressure was first measured to determine the optimum pressure for scattering. Thus with a pressure of about 5 cm. of Hg, the absolute angular distribution of elastic protons from oxygen was determined from 15° to 60° (laboratory system), and that from nitrogen from 15° to 45°. To overcome the low counting rate at larger angles the relative angular distribution from 60° and beyond was determined for oxygen by resolving the protons scattered elastically from the oxygen nuclei in the solid C.P. LiOH targets made as thin

as 6.3 mg. per cm.^{2} thick (measured effective thickness of 0.19 Mev. for 20-Mev. protons). The front slit of the analyzing slit-system was removed for this part of the experiment. The relative distribution was then normalized at 60°. For large-angle scattering from nitrogen, the gas was confined at one-atmosphere pressure in a gas cell constructed of 0.0005-in. duraluminum and 0.001-in. mylar polyester film. When the cell was evacuated the background was found to be negligible.

Spectroscopically pure and tank oxygen were used without any discernible difference in the results. The isotopic content of O^{16} was 99.76%. Dry tank-nitrogen gas, 99.99% chemically pure (manufacturer's specification) and 99.63% isotopically pure, was used for the nitrogen target. Contamination due to leakage and outgassing of the chamber was kept at a predetermined low level by flushing the chamber and changing the scattering gas at a time interval determined from the measured rate of pressure rise of the evacuated chamber.

The pulse-analyzer bias-level was adjusted by analyzing the pulse heights of the protons from the direct beam, greatly reduced in intensity by shutting off the cyclotron arc. The bias-levels at other angles were then calculated relative to the zero-angle level by the conservation laws and set accordingly. To determine the experimental background a voltage gate was usually set on a second pulse analyzer to include voltage pulses corresponding to the valley between the elastic and first inelastic lines in the proton spectra.

The mean range of the incident beam in aluminum was determined by placing aluminum foils in front of the Faraday cup while the beam was monitored with the counter detecting protons scattered at 15° by a thin aluminum target. Several measurements were made at different periods and the energy of the beam evaluated as discussed in Part IV.

IV. RESULTS

The experimental results for oxygen are shown in Fig. 1, and those for nitrogen in Fig. 2. The solid triangular inset in the figures denotes the instrumental resolution. The probable errors of the cross sections ranged from 1% to 4% for O^{16}, 1½% to 4% for nitrogen in the forward angles, and to 6½% at the back angles. These errors are compounded from those arising in the geometrical-factor G, the charge per electrometer discharge, temperature and pressure of the scattering gas, and counting statistics, the main contribution.

The energy of the incident beam was determined from the measured range by extrapolating from the experimental values of Hubbard and MacKenzie (1952) using Wilson's (1947) power-law approximation:

$$E_2 = (R_2/R_1)^{1/1.8} E_1,$$

where E_1 is the known energy at which range R_1 is measured, and E_2 is the energy to be determined from the measured range R_2. This approximation, as used, assumes I is constant between 17.85 Mev. and 20.0 Mev., and when applied as a check to Smith's (1947) value at 17 Mev. to obtain the energy for the range corresponding to 21 Mev., the value thus derived was 0.4% lower.

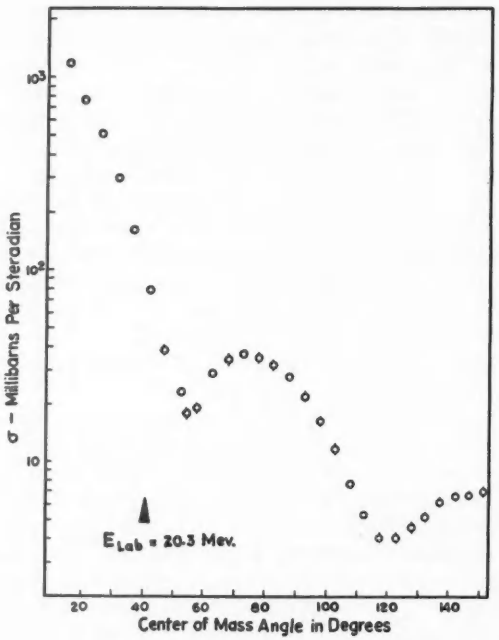

FIG. 1. Differential cross section for O^{16}.

Thus the mid-target energy was found from the above expression to be 20.3 ± 0.5 Mev. for oxygen targets and 19.9 ± 0.3 Mev. for nitrogen. The stated spread includes maximum target thickness, spread in beam energy in excess of straggling, as well as small short-time fluctuations in mean energy due to unstable cyclotron operation.

Measurements on carbon were to be made following those on oxygen and nitrogen. An absolute value of the carbon elastic cross section was measured at 30° using methane gas as target. Simultaneously the cross section for proton–proton scattering was determined for comparison with an accepted value. The carbon angular distribution at other angles was to be determined using a thin carbon target and normalized relative to the absolute value at 30°. After completion of the measurements with the gas target, however, the experiment was discontinued when, upon changing over to the scattering geometry appropriate to a solid target, the external cyclotron beam was found to have changed in energy and direction. This shift in the beam caused the background, which generally was low in comparison when a gas target was used, to increase considerably. The lower background obtained when the scattering was from a gas target was believed to be due either to the fact that the shift had not yet occurred, or to the fact that the two-slit system, in addition to being well shielded, effectively excluded protons from sources other than the scattering volume it defined.

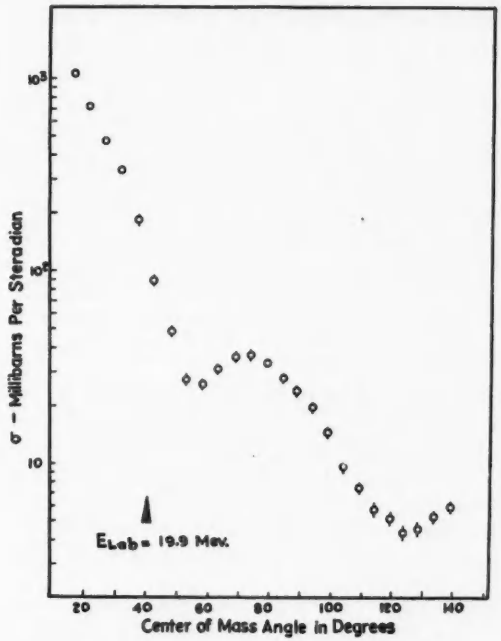

FIG. 2. Differential cross section for N^{14}.

The carbon elastic scattering cross section was found in this experiment to be 376±11 mb. per sterad. C.M.S. at 20.0 Mev. This value can be roughly compared with that of Peelle (1955) who measured the same cross sections for energies ranging from 14.0 Mev. to 19.4 Mev. A reasonable extrapolation to 20.0 Mev. can be obtained only from the results determined at the four highest energies of 17.9, 18.4, 18.9, and 19.4 Mev. Depending upon the curve chosen to fit these points, extrapolated values of 360±24 mb. per sterad. and 385±24 mb. per sterad. were obtainable. The errors shown above include the uncertainty in reading the values off the curves available.

The proton–proton cross section at 20.0 Mev. was found in this experiment to be 24.8±1.0 mb. per sterad., C.M.S. A small correction for the inelastic contribution from the 4.43 Mev. level of carbon in the methane was made using the experimental results of Peelle (1955). A comparison with the proton–proton cross section at 18.2 Mev. determined by Yntema and White (1954) showed excellent agreement when a $1/E$ energy-dependent correction, apparently valid in this angular region (Yntema and White 1954), was applied.

The effect of the finite width of the slit at small-angle scattering was checked at 15° in the laboratory system by using slits with one third the width normally used. The oxygen cross section measured with the narrow slits was 1172±32 mb. per sterad. C.M.S. at 20.0 Mev. as compared to 1160±15 mb. obtained with the wider slits at 20.3 Mev. Correction for energy dependence

was made using assumptions based upon the optical model and correction for effective widening of the slits through slit-edge penetration was made following the treatment of Courant (1951). The values then became respectively 1128 ± 32 mb. and 1153 ± 15 mb. for the narrow and wide slits. Thus, within the statistical error, the results are found to be independent of the width of the slits, and Breit's formula, as applied to the design of the slit system, is verified within experimental error.

Since the beam energy was not monitored continuously while the cross sections were measured, a small discontinuous shift in the beam energy could have given rise to a fairly large error in cross section, particularly at the back angles where the cross section is known to be quite energy sensitive. The magnitude of the error arising from such an effect is largely unknown.

V. THEORY

The elastic scattering of protons by atomic nuclei has up to the present been best described by the optical model of the nucleus. In this model the nucleus is represented by a complex potential characterized by parameters such as those defining the depth, extent, shape, and charge distribution. The imaginary part of the complex potential accounts for absorption due to non-elastic processes, as can be seen from the equation of continuity for probability density and current, readily derived using such a potential:

$$\frac{\partial \rho}{\partial t}+\nabla\cdot\mathbf{J} = -\frac{2\rho W_0}{\hbar}$$

where $\rho = \psi\psi^*$,

$\mathbf{J} = (\hbar/2im)(\psi^*\nabla\psi-\psi\nabla\psi^*)$,

and W_0 is the imaginary part of the potential.

The nucleus thus acts as a sink for incoming particles and probability density is conserved if $W_0 = 0$.

The scattering is described by the stationary solutions to Schrodinger's equation:

$$\nabla^2\psi+\left[k^2-\frac{2m}{\hbar^2}V(\mathbf{r})\right]\psi = 0.$$

For a spherically symmetric potential, $V(\mathbf{r}) = V(r)$, the general solution, valid exterior to the nucleus, is found to be:

$$\psi = \frac{1}{v^{\frac{1}{2}}kr}\sum_{L=0}^{\infty}[a_L F_L(kr)+b_L G_L(kr)]\,P_L(\cos\theta),$$

where k is the magnitude of the propagation vector,

v is the velocity of the incident proton,

P_L is the Legendre polynomial of order L,

L is the angular momentum quantum number,

and F_L and G_L are respectively the regular and irregular Coulomb functions.

The asymptotic form of the solution is required and can be shown to be:

$$\psi \underset{r\to\infty}{\sim} \frac{1}{2ikrv^{\frac{1}{2}}} \sum_{L=0}^{\infty} [(a_L+ib_L)\, e^{iy_L} - (a_L-ib_L)\, e^{-iy_L}]\, P_L(\cos\theta)$$

where $y_L = kr - \frac{1}{2}L\pi - \alpha \ln 2kr + \arg\Gamma(L+1+i\alpha)$ and $\alpha = Ze^2/\hbar v$.

For a pure Coulomb potential, the set of expansion coefficients a_L are equal to some set $a_L{}^c$, whereas the set b_L are identically zero. Further, either in the presence or in the absence of the nuclear potential, the distant incident subwaves of a given angular momentum are identical, since the effects of short-range nuclear forces are not yet felt. This boundary condition shows readily that a_L, b_L, and $a_L{}^c$ are related by a phase shift δ_L as follows:

$$a_L+ib_L = a_L{}^c\, e^{2i\delta_L}.$$

The difference between the asymptotic solutions obtained in the presence and absence of the nuclear potential represents outgoing scattered waves. The total asymptotic solution for the case including the nuclear potential can now be expressed in a more convenient form by superposing the closed forms for the incident distorted plane waves and purely Coulomb-scattered waves, both given by Schiff (1949). Thus:

$$\psi \underset{r\to\infty}{\sim} \left\{1 - \frac{\alpha^2}{ik(r-z)}\right\} \frac{\exp\{i[kz - \alpha \ln k(r-z)]\}}{(v)^{\frac{1}{2}}} + \frac{1}{(v)^{\frac{1}{2}}} \left\{ f_c(\theta) + \frac{1}{2ik} \sum_{L=0}^{\infty} (2L+1)\, e^{2i\eta_L} (e^{2i\delta_L} - 1)\, P_L(\cos\theta) \right\} \times \frac{\exp[i(kr - \alpha \ln 2kr)]}{r}.$$

The resultant scattering amplitude is readily identified and the expression for the elastic scattering cross section obtained:

$$\sigma(\theta) = \left| f_c(\theta) + \frac{1}{2ik} \sum_{L=0}^{\infty} (2L+1)\, e^{2i\eta_L} (e^{2i\delta_L} - 1)\, P_L(\cos\theta) \right|^2.$$

The nuclear effects are contained in δ_L, determined by requiring that the logarithmic derivatives of the exact solutions for the regions inside and outside the nucleus be continuous across the connecting region. When δ_L is zero, the expression for the cross section becomes that for a pure Coulomb potential, as it must.

VI. DISCUSSION

A comparison of the two angular distributions shows them to be quite similar except for the deeper first minimum in oxygen. This feature was confirmed in an independent test using the gas cell. The results of Burcham *et al.* (1953) and Freemantle *et al.* (1954) showed that at 9.5 Mev. the difference in depth of the first minima is still greater. Because O^{16} is a doubly closed-shell nucleus while N^{14} lacks a nucleon in each of the same shells, one is inclined to attribute the difference to possible shell effects, particularly since for a given bombarding energy a difference of about 6½ Mev. excitation energy exists

between the corresponding compound nuclei, O^{15} and F^{17}, so that the level densities in these nuclei at corresponding levels of excitation might be quite different especially if the bombarding energy is sufficiently low. At 20 Mev. bombarding energy, however, it is doubtful that such an effect, if it existed, would be detectable. At 12 Mev., a search by Shaw *et al.* (1956) for shell effects failed to reveal any, at least for elements with atomic number equal to that of iron or higher.

On the other hand, such local variations for light nuclei are not unexpected. In view of the complexity of the computational problem, no attempt was made to try to determine which parameter of the diffuse-surface optical model might be responsible in the present instance.

The present results fit quite well into the general scheme which appears to exist for elastic scattering from various nuclei in this energy range, particularly at not-too-large angles. For instance, Cohen and Neidigh (1954) found that when their results were expressed relative to Rutherford cross sections the maxima and minima occurred at positions such that the relationship $\theta = K\lambda/R$, where K is approximately constant, seems to hold. Such a relation suggests the pattern to arise from diffraction phenomena. The apparent shift towards smaller angles of the O^{16} pattern relative to N^{14} in this experiment tends to support this argument. Furthermore, the position of the maxima and minima of the ratio-to-Rutherford curves for the present results can be fairly well predicted by applying the above relationship using a value of K interpolated from the results of Cohen and Neidigh or from those of Schrank (Melkanoff *et al.* 1955). The expression $R = (1.35A^{1/3} \times 10^{-13} + \lambda)$ cm. was used for the nuclear radius. The results are compared in Table I.

TABLE I

COMPARISON OF ANGULAR POSITION OF MAXIMA AND MINIMA PREDICTED FROM $\theta = K\lambda/R$ WITH EXPERIMENTALLY DETERMINED VALUES

Elements	Order	Predicted values in degrees		Experimental value in degrees
		Cohen and Neidigh	Schrank	
Oxygen	1st max.	33	33	36
	1st min.	53	52	54
	2nd max.	81	84	89
	2nd min.	103	113	120
Nitrogen	1st max.	35	35.4	34
	1st min.	55	54	54
	2nd max.	85	88.0	86
	2nd min.	108	118.0	122

The above predictions were made more or less empirically. However, Kinsey and Stone (1956) pointed out that from the elementary diffraction theory of Placzek and Bethe (1940) the differential cross section is given by:

$$\sigma = k^2 R'^4 [J_1(x)/x]^2$$

where k is the wave number, in the center-of-mass system, R' is equal to $(1.35A^{1/3}\times10^{-13}+\lambda\!\!\!^{-})$, and $x = 2kR'\sin\theta/2$. The positions of the maxima and minima predicted by this theory for the angular distributions are compared with the experimental values in Table II.

TABLE II

COMPARISON OF ANGULAR POSITIONS OF MAXIMA AND MINIMA AS PREDICTED BY SIMPLE DIFFRACTION THEORY (PLACZEK AND BETHE 1940)

Order	Predicted values in degrees		Experimental values in degrees	
	O^{16}	N^{14}	O^{16}	N^{14}
1st min.	54.5	57.2	54	56
1st max.	77.6	81.8	74	72
2nd min.	115.0	123.6	120	125

The values of the cross section at the first maxima in units of $k^2R'^4$ are 0.84×10^{-2} for O^{16} and 1.2×10^{-2} for N^{14}. When these values are included in Fig. 9 of the article by Kinsey and Stone (1956), they seem to fit in quite well with respect to the neighboring elements and with respect to the 31.5 Mev. results.

Evidently the result of the present experiment is consistent with the proposal that the structures in the angular distribution curves are caused by some simple diffraction phenomena.

ACKNOWLEDGMENTS

Interest in this experiment was greatly stimulated by discussions with Professors D. S. Saxon, S. A. Moszkowski, and R. D. Woods. Fruitful suggestions were offered by Professor K. R. MacKenzie. The program was expedited by the efforts of the cyclotron and machine shop staffs.

REFERENCES

ASHBY, V. J. 1951. University of California Radiation Laboratory Report, UCRL-1414.
BREIT, G., THAXTON, H. M., and EISENBUD, L. 1939. Phys. Rev. **55**, 1018.
BROMLEY, D. A., HASHIMOTO, Y., and WALL, N. S. 1956. Phys. Rev. **102**, 1560.
BURCHAM, W. E., GIBSON, W. M., HOSSAIN, A., and ROTBLAT, J. 1953. Phys. Rev. **92**, 1266.
BURKIG, J. W. and WRIGHT, B. T. 1951. Phys. Rev. **82**, 451.
CALDWELL, D. C. and ROYDEN, H. N. 1956. Rev. Sci. Instr. **27**, 91.
COHEN, B. L. and NEIDIGH, R. U. 1954. Phys. Rev. **93**, 282.
COURANT, E. D. 1951. Rev. Sci. Instr. **22**, 1003.
DAYTON, I. E. 1954. Phys. Rev. **95**, 754.
DICKENSON, W. D. and DODDER, D. C. 1953. Rev. Sci. Instr. **24**, 428.
FREEMANTLE, R. G., PROWSE, D. J., and ROTBLAT, J. 1954. Phys. Rev. **96**, 1268.
HERB, R. G., KERST, D. W., PARKINSON, D. B., and PLAIN, G. I. 1939. Phys. Rev. **55**, 998, 603A.
HUBBARD, E. L. and MACKENZIE, K. R. 1952. Phys. Rev. **85**, 107.
KINSEY, B. B. and STONE, T. 1956. Phys. Rev. **103**, 975.
MELKANOFF, M. A. *et al.* 1955. Tech. Rept. 7-12-55, University of California, Los Angeles, Calif.
PEELLE, R. 1955. Phys. Rev. **98**, 1184A, and private communication.
PLACZEK, G. and BETHE, H. 1940. Phys. Rev. **57**, 1075A.
SAXON, D. S. and LELEVIER, R. E. 1952. Phys. Rev. **87**, 40.
SAXON, D. S., MELKANOFF, M. A., MOSZKOWSKI, S. A., and NODVIK, J. 1956. Phys. Rev. **101**, 507L.

SAXON, D. S. and WOODS, R. D. 1954. Phys. Rev. **95**, 577.
SCHIFF, L. I. 1949. Quantum mechanics (McGraw-Hill Book Co., Inc., New York), p. 116.
SCHRANK, G. 1955. Phys. Rev. **99**, 640A.
SHAW, H. C., CONZETT, H. E., SLOBODRIAN, R. J., and SUMMERS-GILL, R. G. 1956. Bull. Am. Phys. Soc. **1**, No. 5, 253, F9.
SMITH, J. H. 1947. Phys. Rev. **71**, 32.
WILSON, R. R. 1947. Phys. Rev. **71**, 385.
WORTHINGTON, H. R., MCGRUER, J. H., and FINDLEY, D. E. 1953. Phys. Rev. **90**, 899.
YNTEMA, J. L. and WHITE, M. G. 1954. Phys. Rev. **95**, 1226.

ESTIMATED FISSION FRAGMENT MASSES[1]

I. W. Hay and T. D. Newton

ABSTRACT

The mass excesses, $M-A$, of atoms in the fission fragment region have been empirically estimated by extrapolation of β-decay Q-values using the regularities found by Way and Wood (1954). The resulting estimates of the energy release in fission may indicate the most probable charge and, roughly, the range of charge for a given mass ratio of primary fission fragments.

METHOD OF COMPUTATION

The primary fission fragments whose ground state masses we wish to estimate lie outside the range of near stable atoms whose masses may be obtained from mass spectroscopic measurements combined with measured β-decay and reaction Q-values (Wapstra 1955; Huizenga 1955). It is therefore necessary to extrapolate in some fashion. The procedure which can be most closely tied to experimental results is the extrapolation of β-decay Q-values.

The systematics of these Q-values has been frequently studied. We use a slight extension of the regularity found by Way and Wood (1954), who also list references to other studies; the method consists in the extrapolation, for fixed Z, of the observed Q values as a function of N. A second estimate can be obtained by extrapolation at fixed N of Q as a function of Z. The Z (N) are the proton (neutron) numbers of the parent nucleus.

By the Q-value of a β-decay we mean the difference between the ground state masses of the parent and daughter atoms. We have used the Q-values adopted by King (1954). With this definition a mass difference derived from either negaton or positon emission can be written as the sum of the difference between the masses of the neutron and the hydrogen atom, and the difference between the proton and neutron binding energies. The latter can be separated into a change of the specifically nuclear binding and a change in the Coulomb energy of the system. If we write the mass of an atom as

$$m(ZN) = Zm_{\mathrm{H}}+Nm_{\mathrm{n}}-b(ZN)+CZ^2A^{-1/3} \tag{1}$$

in which m_{H}, m_{n} are the hydrogen atom and neutron masses, $b(ZN)$ is the total nuclear binding energy, and $CZ^2A^{-1/3}$ the total Coulomb energy, then the Q-value of the transition $Z^A \rightarrow (Z+1)^A$ is

$$Q(ZN) = m_{\mathrm{n}}-m_{\mathrm{H}}+b(Z+1, N-1)-b(ZN)-C(2Z+1)A^{-1/3}. \tag{2}$$

The difference between two Q's for which the parents contain the same number of protons but have neutron numbers differing by 2 is denoted by $S(ZN)$,

$$\begin{aligned} S(ZN) &= Q(ZN)-Q(Z, N-2) \\ &= \{b(Z+1, N-1)-b(Z+1, N-3)\}-\{b(ZN)-b(Z, N-2)\} \\ &\qquad +2C/3(2Z+1)A^{-4/3}. \end{aligned} \tag{3}$$

[1]Manuscript received September 20, 1956.
Contribution from Theoretical Physics Branch, Atomic Energy of Canada Limited, Chalk River, Ontario.
Issued as A.E.C.L. No. 390.

The term in $A^{-4/3}$ is the first approximation to the change of the Coulomb term due to the change in A. The terms neglected are smaller by a factor A^{-1}. Apart from this Coulomb term $S(ZN)$ is the difference between the nuclear binding of the last pair of neutrons in the nuclei $(Z+1)^A$ and Z^A.

The observation made by Way and Wood (1954) from a study of experimental material is that $S(ZN)$ at fixed Z varies but little with N.

In a similar fashion when Z changes by 2 we define the difference $T(ZN)$:

$$(4)\quad T(ZN) = -Q(Z-1, N+1)+Q(Z-3, N+1)$$
$$= +\{b(Z-1, N+1)-b(Z-3, N+1)\}-\{b(ZN)-b(Z-2, N)\}$$
$$+4CA^{-1/3}-2/3C(2Z-5)A^{-4/3}.$$

Here there are two Coulomb terms, one arising from the change in Z, and one from the change in A, together with the difference in nuclear binding of the last pair of protons in the nuclei $(Z-1)^A$ and Z^A.

On the postulate of charge symmetry of nuclear forces, the nuclear binding of a pair of neutrons in a system of X protons and Y neutrons should be the same as the nuclear binding of a pair of protons in a system of Y protons and X neutrons. Hence from (3) and (4) we obtain:

$$(5)\quad S(XY)-T(YX) = -4C(X+Y)^{-1/3}+2/3C(X+Y)^{-4/3}(2X+1+2Y-5)$$
$$\approx -8/3C(X+Y)^{-1/3}$$

in which the term $-8/3C(X+Y)^{-4/3}$ has been neglected.

We have obtained a table of 225 values of $S(ZN)$ and 160 values of $T(ZN)$ from the experimental values given by King (1954). In constructing these tables no differences were used which involved a change in N or Z across a magic number. The values of S vary from about 20 Mev. near $A = 10$ to a fraction of an Mev. for $A > 200$. The product AS, however, usually lies between 100 and 200 Mev. This indicates that the variation with A^{-1} which one derives from the semiempirical mass formula is followed in a general way. However the fluctuations are large, considerably larger than is contained in the quoted experimental values of the Q's. Some part of the residual variation is removed by parabolic dependence on $A = N+Z$. There is no clear dependence on N and Z separately, so we finally adopted the form

$$(6a)\qquad S(ZN) = S(A) = 117.5A^{-1}+0.01(A-100)^2A^{-1}\ \text{Mev.}$$

in which the constants are fitted to the values of $S(ZN)$ for $0 < A < 200$; the parabolic term appears to be too large for $A > 200$ to permit a good fit of the form (6) in that region. We then examined the values of

$$117.5A^{-1}+0.01(A-100)^2A^{-1}-T(ZN),$$

which, according to (5) and (6a), should equal $-8/3CA^{-1/3}$. We found the average value

$$(7)\qquad 8/3C = 3.078\ \text{Mev.}$$

This is a curiously large value. It would imply that the nuclear radius is $R = 0.748A^{1/3}$ fermis, which is much smaller than that found by any method

of measurement. However, the determination of C as the difference between two averages is not such as to give any physical significance to this result. It probably is an indication of the obvious fact that the form (6a) is not an accurate representation of S. For our purposes (7) is a parameter to be adjusted in order that we may find the local average rate of change of Q with Z and N. The results we obtain are reasonably consistent. This serves as the only justification for our rather arbitrary procedure.

From (5), (6a), and (7) it follows that

$$T(ZN) = T(A) = +117.5A^{-1}+0.01(A-100)^2A^{-1}+3.078A^{-1/3}. \tag{6b}$$

Equations (6a) and (6b) represent the experimental values of S and T only on the average; the fluctuations from these smoothed averages are great and should be so since these forms take no account of the local peculiarities of nuclear structure. It would have been extremely difficult to separate the real fluctuations from the frequently large experimental uncertainties in the differences S and T. Since our aim was to extrapolate across fairly large differences of neutron and proton number it seemed best to ignore these details except for the pronounced effect on Q at magic N or Z.

We found no detectable change in S with the even or odd character of N or Z, or in passing from one side to the other of a magic number. However, there is often a large change in Q at such a passage (Way and Wood 1954). The average value of this "jump" at those magic numbers needed for our purposes has been found using equations (6) with each possible measured Q to estimate Q values on each side of a magic number. The average "jumps" so found are given in Table I. The numbers in Table I, like the constants of equation (6), are those used in the computation and do not represent their experimental significance. Individual "jumps" estimated from two experimental Q values at the same N but on opposite sides of a magic proton number differ from the quoted average by factors of 2 in some cases.

TABLE I

MAGIC JUMPS IN Q (MEV.)

Z	M_Z	N	M_N
28	0.980	50	1.780
50	1.739	82	1.534

Having determined the forms (6a), (6b), and Table I, it is possible to estimate an unknown Q value in two ways, using either (3) or (4): i.e.

$$Q(ZN) = Q(Z, N-2k)+\sum_{j=0}^{k-1} S(A-2j)+M_N \tag{8}$$

or

$$Q(ZN) = Q(Z-2k, N)+\sum_{j=0}^{k-1} T(A-2j)+M_Z. \tag{9}$$

In (8) the term M_N is the "magic jump" of Table I and is to be included for those cases when a magic neutron number occurs between $N-2k$ and N. The term M_Z in (9) is the similar jump for a magic proton number.

To obtain the starting values for (8) we constructed a table containing for each Z ($25 \leqslant Z \leqslant 65$) a base value of Q for N odd and another for N even. Q for each (Z, N) was estimated using (8) with each possible experimental value for $Q(Z, N-2k)$. The resulting estimates of the required $Q(ZN)$ were then averaged. For example, at $Z = 32$, we used the base value $Q(32, 38) = -6.271$ Mev., obtained by averaging values of this number derived from experimental values (King 1954) of $Q(32, 40)$, $Q(32, 42)$, and $Q(32, 44)$; and the base value $Q(32, 39) = -2.358$ Mev. derived from experimental values of $Q(32, 43)$ and $Q(32, 45)$. A similar table was constructed for (9); for each N ($29 \leqslant N \leqslant 96$) base values for both odd and even Z were obtained. In some cases for which there is no measurement in King's (1954) tabulation from which to estimate a base value for (8), say, a preliminary interpolation by means of (9) has been made, and inversely to fill gaps in base values for (9).

With these base values each of (8) and (9) may be used to estimate Q-values in the region of fission fragments. Then from the two estimates of Q for each member of a family of isobaric atoms in which at least one member has a measured mass, two estimates for the mass of each member of the family can easily be obtained by addition. The so-estimated mass excesses $M-A$, expressed in Mev., are given in Table II. The estimates using (8) (column (*a*)) and those using (9) (column (*b*)) are given separately. The initial mass excess value is taken from Wapstra (1955) and is indicated in the table by a W. An X in the table shows the occurrence of a Q value obtained from a double use of (8) and (9) as described in the last paragraph.

The comparison of the two columns gives a possible indication of their accuracy. There is, of course, no theoretical basis for the use of (6*a*) and (6*b*) and it is quite possible that the true values are not bracketed by these values. The difference in the two estimates of the same mass is of the order of 10 Mev. at about 7 neutrons away from the measured mass. Column (*a*) obtained from (8) is always larger than column (*b*), and the difference increases with the extrapolation distance from measured values. The increasing spread presumably represents the increasing difference of structure between the nuclei on which the extrapolations of Q are based.

While the difference in the estimates of a given fission fragment mass is often quite large, the estimated releases of energy in fission using Huizenga's (1955) value for the mass excess of the fissioning atom combined separately with the fission fragment masses estimated by (8) and by (9) differ near the maximum energy release for any given mass ratio by amounts usually less than 2 Mev. This arises because the maximum energy release occurs at fragments only 3 to 5 neutrons away from stability (see Table III).

Since statistical factors should have some effect on the fission process, the most probable charge ratio at a given mass ratio would be expected to occur at the maximum energy release, and neighboring charges should also occur if their energy release is decreased by less than, say, the excitation above threshold, i.e. for thermal fission of U^{235}, about 1 Mev. The only published treatment of statistical factors of fission is by Fong (1956), and if the masses found here are used with the level density formula which fits slow neutron

TABLE II

MASS EXCESSES (IN MEV.) OF FISSION FRAGMENTS

The initial values (marked W) are from Wapstra (1955). Column (*a*) gives mass excesses estimated by isotopic extrapolation using equation (8); column (*b*), by isotonic extrapolation using equation (9). Values marked X have been obtained using doubly extrapolated Q value

A	Z	(*a*)	(*b*)
70	25	1.93	− 7.05
	26	−15.97	−22.37
	27	−27.05	−28.90
	28	−39.00	−40.09
	29	−42.77	−42.58
	30	−48.95 W	−48.95 W
	31	−47.66	−47.07
	32	−49.62	−48.72
71	25	5.32	− 5.27
	26	−10.90	−17.95
	27	−23.87	−28.46
	28	−34.75	−37.09
	29	−42.28	−42.96
	30	−46.47	−46.91
	31	−49.01 W	−49.01 W
	32	−48.59	−48.76
72	25	12.15	− 0.83 X
	26	− 7.49	−16.31
	27	−20.31	−24.69
	28	−34.00	−36.88
	29	−39.52	−39.95
	30	−47.43	−47.68
	31	−47.89	−47.69
	32	−51.58 W	−51.58 W
73	26	− 1.92	−10.89
	27	−16.60	−22.41
	28	−29.18	−32.65
	29	−38.43	−39.73
	30	−44.32	−44.93
	31	−48.57	−48.36
	32	−49.86 W	−49.86 W
	33	−49.21	−49.52
74	25	23.89	7.04
	26	2.56	− 8.98
	27	−11.93	−18.76 X
	28	−27.30	−31.84
	29	−34.50	−36.82
	30	−44.10	−45.62
	31	−46.23	−46.28
	32	−51.60 W	−51.60 W
	33	−48.75	−49.20
75	25	28.64	10.54
	26	8.12	− 3.69
	27	− 8.20	−16.40
	28	−22.43	−27.15
	29	−33.33	−35.31
	30	−40.87	−42.18
	31	−46.77	−46.88
	32	−49.71 W	−49.71 W
	33	−50.71	−50.76
	34	−49.78	−49.88
76	25	35.82	17.18
	26	12.87	− 1.44
	27	− 3.24	−12.52
	28	−20.23	−26.20
	29	−29.05	−32.65 X
	30	−40.27	−42.39
	31	−44.02	−45.03
	32	−51.02	−51.48
	33	−49.79 W	−49.79 W
	34	−52.62	−52.76
	35	−47.84	−48.01
77	25	44.55	23.98
	26	20.66	5.51
	27	0.95	− 9.57
	28	−14.87	−21.49
	29	−27.36	−30.90
	30	−36.50	−38.35
77	31	−44.00	−44.19
	32	−48.53	−48.75
	33	−51.13 W	−51.13 W
	34	−51.79	−51.64
	35	−50.42	−50.37
78	25	52.19	30.07
	26	27.67	10.69
	27	8.21	− 3.23
	28	−12.13	−19.57
	29	−22.51	−27.38
	30	−35.30	−37.79
	31	−40.62	−41.95 X
	32	−49.19	−49.41
	33	−49.52	−49.75
	34	−53.92 W	−53.92 W
	35	−50.71	−49.94
79	25	61.24	36.61
	26	35.81	18.16
	27	14.56	2.41
	28	− 4.59	−13.79
	29	−20.40	−25.64
	30	−31.08	−34.32
	31	−40.12	−41.47
	32	−46.20	−46.66
	33	−50.34	−50.24
	34	−52.54 W	−52.54 W
	35	−52.71	−52.66
80	25	69.31	43.71
	26	43.27	23.18
	27	22.29	7.86
	28	0.43	− 9.28
	29	−13.25	−19.99
	30	−29.33	−33.12
	31	−36.17	−38.69
	32	−46.26	−46.88
	33	−48.12	−48.81 X
	34	−54.03 W	−54.03 W
	35	−52.33	−52.14
	36	−54.33	−54.07
81	25	78.53	48.74
	26	51.60	29.61
	27	28.86	13.31
	28	8.21	− 2.92
	29	− 9.09	−15.49
	30	−23.05	−28.51
	31	−35.37	−38.15
	32	−42.94	−44.63
	33	−48.57	−49.58
	34	−52.27	−52.55
	35	−53.93 W	−53.93 W
	36	−54.19	−54.02
82	25	86.71	56.63
	26	59.20	35.03
	27	36.74	19.93
	28	13.41	1.57
	29	− 1.74	−10.58
	30	−19.30	−24.56
	31	−29.39	−33.10
	32	−42.72	−44.05
	33	−46.05	−47.44
	34	−53.44 W	−53.44 W
	35	−53.22	−53.19 X
	36	−56.69	−56.23
83	25	95.95	62.20
	26	67.58	42.40
	27	43.37	24.54
	28	21.28	7.56
	29	2.52	− 5.59
	30	−12.88	−18.69
83	31	−26.65	−29.11
	32	−37.45	−39.97
	33	−46.31	−47.46
	34	−51.46	−51.78
	35	−54.57 W	−54.57 W
	36	−56.28	−55.39
84	25	104.88	71.11
	26	75.94	48.40
	27	52.05	32.16
	28	27.29	12.68
	29	10.70	0.70
	30	− 8.28	−14.54
	31	−19.80	−24.57
	32	−34.56	−36.42
	33	−41.10	−42.82
	34	−51.70	−51.64
	35	−52.90 W	−52.90 W
	36	−57.80	−56.77
	37	−55.57	−54.39 X
85	26	85.26	55.66
	27	59.65	36.80
	28	36.15	19.10
	29	15.98	4.34
	30	− 0.83	− 9.54
	31	−16.00	−20.60
	32	−28.21	−31.59
	33	−38.49	−39.89
	34	−46.82	−48.65
	35	−53.12	−54.03
	36	−56.24 W	−56.24 W
	37	−56.63	−56.92
86	26	93.65	61.60
	27	68.38	44.48
	28	42.22	23.85
	29	24.25	10.67
	30	3.87	− 5.73
	31	− 9.03	−15.63
	32	−25.18	−28.78
	33	−33.11	−36.73
	34	−45.10	−46.49
	35	−49.47	−50.81
	36	−57.54 W	−57.54 W
	37	−56.70	−56.72
	38	−58.61	−58.50
	39	−54.35	
87	27	74.75	48.78
	28	49.88	30.36
	29	28.35	14.54
	30	10.16	− 0.10
	31	− 6.38	−12.80
	32	−19.95	−24.62
	33	−31.60	−33.61
	34	−41.31	−42.54
	35	−48.98	−48.78
	36	−55.24	−55.47
	37	−58.78 W	−58.78 W
	38	−59.59	−58.93
	39	−57.90	−57.54
88	27	83.73	56.42
	28	56.22	35.05
	29	36.89	20.95
	30	15.17	3.35
	31	0.90	− 7.78
	32	−16.59	−22.14
	33	−25.87	−30.00
	34	−39.21	−41.11
	35	−44.94	−47.01
	36	−54.36	−54.73
	37	−56.65	−57.00
	38	−61.69 W	−61.69 W
	39	−58.79	−58.82

TABLE II (*continued*)

MASS EXCESSES (IN MEV.) OF FISSION FRAGMENTS (*continued*)

A	Z	(a)	(b)
89	27	90.89	60.58
	28	64.68	41.95
	29	41.81	25.14
	30	22.29	9.72
	31	4.41	− 4.06
	32	−10.50	−16.68
	33	−23.47	−27.36
	34	−34.52	−37.16
	35	−43.52	−44.13
	36	−51.12	−51.03
	37	−55.99	−55.25
	38	−59.92 W	−59.92 W
	39	−61.34	−61.21
	40	−59.39	−59.33
90	27	101.88	68.93
	28	71.27	47.01
	29	50.63	32.32
	30	27.58	13.94
	31	12.00	1.84
	32	− 6.81	−13.75
	33	−17.41	−22.88
	34	−32.06	−35.24
	35	−39.10	−41.09
	36	−49.84	−50.20
	37	−53.45	−54.09
	38	−59.81 W	−59.81 W
	39	−60.00	−60.08
	40	−62.43	−62.76
	41	−57.99	−57.89
91	28	80.49	53.22
	29	56.32	35.66
	30	35.50	20.00
	31	16.32	5.18
	32	0.11	− 8.25
	33	−14.16	−20.06
	34	−26.51	−30.70
	35	−36.81	−39.39
	36	−45.71	−47.21
	37	−51.88	−52.19
	38	−57.11 W	−57.11 W
	39	−59.83	−59.34
	40	−60.96	−62.03
	41	−59.75	−61.33
92	29	65.56	44.51
	30	41.23	25.54
	31	24.37	12.82
	32	4.26	− 3.59
	33	− 7.61	−13.72
	34	−23.55	−27.35
	35	−31.87	−34.52
	36	−43.90	−44.91
	37	−48.79	−48.80
	38	−56.43	−55.94
	39	−57.91	−57.87
	40	−61.62 W	−61.62 W
	41	−60.24	−59.92
	42	−60.98	−60.64
93	29	71.02	47.92
	30	48.93	30.63
	31	28.48	15.02
	32	11.00	1.31
	33	− 4.54	−11.56
	34	−18.15	−23.04
	35	−29.73	−32.91
	36	−39.90	−41.60
	37	−47.34	−48.35
	38	−53.83	−54.21
	39	−57.82	−57.25
	40	−60.22 W	−60.22 W
	41	−60.28	−60.50
	42	−59.82	−61.24
94	30	56.16	37.55
	31	38.04	23.96
	32	16.68	6.93
	33	3.55	− 3.86
	34	−13.63	−18.35
	35	−23.22	−26.55
94	36	−36.49	−38.25
	37	−42.64	−43.48
	38	−51.54	−51.94
	39	−54.27	−53.90
	40	−59.23	−59.11
	41	−59.11 W	−59.11 W
	42	−61.10	−60.93
95	30	63.72	43.55
	31	42.03	27.08
	32	23.31	11.71
	33	6.52	− 1.98
	34	− 8.32	−13.78
	35	−21.13	−24.74
	36	−32.54	−34.31
	37	−41.22	−42.26
	38	−48.96	−49.04
	39	−54.18	−53.87
	40	−57.82 W	−57.82 W
	41	−59.12	−58.94
	42	−59.90	−60.00
	43	−58.44	−58.37
96	30	71.27	49.17
	31	51.92	34.93
	32	29.34	16.87
	33	14.98	5.19
	34	− 3.43	− 9.94
	35	−14.24	−18.84
	36	−28.74	−31.43
	37	−36.11	−37.73
	38	−46.24	−47.53
	39	−50.20	−50.87
	40	−56.39	−57.44
	41	−57.49 W	−57.49 W
	42	−60.70	−60.81
	43	−58.12 X	−58.91
97	31	56.21	39.24
	32	36.27	22.98
	33	18.28	8.39
	34	2.21	− 5.08
	35	−11.80	−16.90
	36	−24.42	−26.82
	37	−34.31	−35.90
	38	−43.26	−43.59
	39	−49.70	−49.65
	40	−54.55 W	−54.55 W
	41	−57.06	−57.50
	42	−59.05	−59.57
	43	−58.81	−58.81
98	31	66.75	47.86
	32	42.96	28.87
	33	27.40	16.49
	34	7.78	0.30
	35	− 4.21	− 9.51
	36	−19.92	−22.78
	37	−28.49	−29.81
	38	−39.81	−40.53
	39	−44.97	−44.97
	40	−52.36	−52.90
	41	−54.66	−54.37
	42	−59.07 W	−59.07 W
	43	−57.68 X	−57.26
	44	−59.22	−58.71
99	32	51.32	36.66
	33	32.14	21.26
	34	14.89	6.84
	35	− 0.31	− 5.88
	36	−14.12	−17.52
	37	−25.20	−27.48
	38	−35.33	−35.55
	39	−42.96	−42.78
	40	−49.00	−48.61
	41	−52.69	−52.83
	42	−55.87 W	−55.87 W
	43	−56.82	−56.97
	44	−57.16	−57.19
100	32	56.31	45.35
	33	39.58	26.75
	34	18.78	9.59
	35	5.60	− 0.93
	36	−11.27	−15.29
	37	−21.01	−23.27
	38	−33.51	−34.70
	39	−39.84	−39.90
	40	−48.41	−48.78
	41	−51.88	−51.37
	42	−57.47 W	−57.47 W
	43	−57.26 X	−57.10
	44	−59.97	−59.96
	45	−56.53	
102	33	53.01	38.10 X
	34	31.07	20.06
	35	16.73	8.71
	36	− 1.29	− 6.63
	37	−12.18	−15.35
	38	−25.83	−27.89
	39	−33.32	−34.06
	40	−43.03	−43.69
	41	−47.66	−47.07
	42	−54.40	−54.14
	43	−55.34 X	−54.92
	44	−59.21 W	−59.21 W
	45	−56.92	−57.03
103	33	57.58	43.55
	34	38.02	27.22
	35	20.50	12.60
	36	4.39	− 0.79
	37	− 8.98	−12.56
	38	−21.42	−23.35
	39	−31.35	−32.47
	40	−39.70	−40.48
	41	−45.69	−46.82
	42	−51.18	−51.26
	43	−54.43	−54.87
	44	−57.08 W	−57.08 W
	45	−57.90	−57.67
104	33	67.26	50.40
	34	44.18	31.50
	35	28.72	18.92 X
	36	9.56	2.67
	37	− 2.46	− 6.88
	38	−17.24	−20.44
	39	−25.85	−27.38
	40	−36.70	−38.14
	41	−42.46	−42.52
	42	−50.33	−50.36
	43	−52.40 X	−51.96
	44	−57.40	−57.24
	45	−56.24 W	−56.24 W
	46	−58.61	−58.74
105	34	51.23	39.39
	35	32.59	23.78
	36	15.36	9.22
	37	0.85	− 3.62
	38	−12.70	−15.24
	39	−23.75	−25.25
	40	−33.21	−34.27
	41	−40.33	−41.60
	42	−46.94	−47.84
	43	−51.31	−52.41
	44	−55.08 W	−55.08 W
	45	−57.02	−56.91
	46	−57.63	−57.35
	47	−56.54	−56.17
106	34	57.06	42.81
	35	40.48	29.25
	36	20.21	12.11
	37	7.07	1.30 X
	38	− 8.81	−13.18
	39	−18.54	−20.98
	40	−30.50	−32.78
	41	−37.37	−37.96
	42	−46.36	−46.95

TABLE II (*continued*)

MASS EXCESSES (IN MEV.) OF FISSION FRAGMENTS (*continued*)

A	Z	(a)	(b)
106	43	−49.54 X	−49.57
	44	−55.65 W	−55.65 W
	45	−55.60	−55.49
	46	−59.08	−59.01
	47	−56.11	−56.24
107	35	45.51	35.25 X
	36	27.17	20.11
	37	11.56	6.25
	38	− 3.09	− 6.55
	39	−15.24	−17.64
	40	−25.81	−27.52
	41	−34.03	−35.77
	42	−41.74	−43.04
	43	−47.22	−48.63
	44	−52.09	−53.11
	45	−55.13	−55.93
	46	−56.85 W	−56.85 W
	47	−56.86	−56.93
	48	−55.56	−55.62
108	36	32.31	23.14
	37	18.07	11.32
	38	1.09	− 4.07
	39	− 9.73	−13.14 X
	40	−22.78	−25.89
	41	−30.75	−31.95
	42	−40.82	−42.01
	43	−45.10 X	−45.45
	44	−52.31	−52.70
	45	−53.35	−53.58
	46	−57.92 W	−57.92 W
	47	−56.05	−56.02
	48	−57.86	−57.80
109	36	39.47	32.19
	37	22.78	17.40 X
	38	7.03	3.99
	39	− 6.20	− 8.13
	40	−17.85	−19.21
	41	−27.16	−28.58
	42	−35.95	−36.72
	43	−42.51	−43.25
	44	−48.47	−48.78
	45	−52.60	−52.64
	46	−55.40 W	−55.40 W
	47	−56.50	−56.49
	48	−56.28	−55.68
110	36	45.62	35.41
	37	30.31	22.86
	38	12.25	6.67
	39	0.35	− 3.42
	40	−13.77	−17.10
	41	−22.82	−24.45 X
	42	−33.97	−35.49
	43	−39.32 X	−39.83
	44	−47.61	−48.17
	45	−49.73	−49.88
	46	−55.38	−55.42
	47	−54.58 W	−54.58 W
	48	−57.47	−57.20
111	36	52.40	43.78
	37	34.64	28.14
	38	17.82	14.12
	39	3.51	1.04 X
	40	− 9.20	−10.65
	41	−19.58	−21.07
	42	−29.44	−30.44
	43	−37.07	−38.10
	44	−44.10	−44.54
	45	−49.29	−49.35
	46	−53.16	−53.18
	47	−55.33 W	−55.[illegible] W
	48	−56.18	−56.38
	49	−55.45	−55.76
112	37	41.94	33.12
	38	22.81	16.29
	39	9.85	5.45
	40	− 5.33	− 9.03
112	41	−15.44	−17.42
	42	−27.65	−29.40
	43	−34.07 X	−35.06 X
	44	−43.41	−44.39
	45	−46.59	−47.03
	46	−53.30	−53.67
	47	−53.57	−53.69
	48	−57.52 W	−57.52 W
	49	−54.64	−54.98
113	37	46.81	39.36
	38	28.94	24.43
	39	13.58	10.49
	40	− 0.19	− 1.84
	41	−11.62	−13.22 X
	42	−22.54	−23.23
	43	−31.22	−31.96
	44	−39.31	−39.64
	45	−45.56	−45.60
	46	−50.48	−50.35
	47	−53.70	−53.47
	48	−55.61 W	−55.61 W
	49	−55.93	−56.07
114	37	54.70	44.73
	38	34.52	27.06
	39	20.52	15.35
	40	4.28	0.21
	41	− 6.87	− 8.94
	42	−20.13	−21.75
	43	−27.60 X	−28.46
	44	−37.99	−38.76
	45	−42.22	−42.73 X
	46	−49.98	−50.38
	47	−51.29	−51.33
	48	−56.29 W	−56.29 W
	49	−54.45	−54.62
	50	−56.43	−56.78
	51	−50.66	−50.81
115	37	59.92	50.85
	38	41.01	35.23
	39	24.61	20.70
	40	9.79	7.43
	41	− 2.68	− 4.82
	42	−14.64	−15.48
	43	−24.36	−25.19 X
	44	−33.48	−33.53
	45	−40.77	−40.59
	46	−46.74	−46.59
	47	−51.00	−50.88
	48	−53.95 W	−53.95 W
	49	−55.31	−55.40
	50	−55.61	−55.86
	51	−52.94	−52.91
	52	−48.67	
116	38	46.85	38.36
	39	31.81	25.89
	40	14.53	9.89
	41	2.34	− 0.15
	42	−11.94	−13.62
	43	−20.44 X	−21.11
	44	−31.87	−32.26
	45	−37.14	−37.30
	46	−45.93	−45.93
	47	−48.28	−48.24 X
	48	−54.31	−54.22
	49	−53.51 W	−53.51 W
	50	−56.53	−56.80
	51	−51.79	−51.73
	52	−50.70	−50.48
117	38	53.44	46.04
	39	36.01	30.95
	40	20.16	16.99
	41	6.66	4.11
	42	− 6.32	− 7.48
	43	−17.07	−18.09
	44	−27.22	−27.09
	45	−35.54	−35.14 X
	46	−42.54	−41.83
117	47	−47.83	−47.22
	48	−51.81	−51.57
	49	−54.20 W	−54.20 W
	50	−55.52	−55.61
	51	−53.89	−53.67
	52	−50.64	−50.73
118	40	24.77	19.55
	41	11.56	8.73
	42	− 3.75	− 5.61
	43	−13.28 X	−14.00
	44	−25.73	−25.83
	45	−32.01	−31.67
	46	−41.83	−41.16
	47	−45.20	−44.55
	48	−52.26	−51.53
	49	−52.48	−52.19 X
	50	−56.52 W	−56.52 W
	51	−52.81	−52.42
	52	−52.74	−52.32
119	40	30.93	26.23
	41	16.41	12.78
	42	2.40	0.46
	43	− 9.36	−10.76
	44	−20.53	−20.72
	45	−29.87	−29.69
	46	−37.89	−37.04
	47	−44.19	−43.45 X
	48	−49.19	−48.49
	49	−52.60	−52.24
	50	−54.94 W	−54.94 W
	51	−54.32	−54.19
	52	−52.09	−52.22
120	40	35.61	28.93
	41	21.38	17.11
	42	5.05	2.18
	43	− 5.47 X	− 6.99
	44	−18.94	−19.71
	45	−26.24	−26.47
	46	−37.07	−36.65
	47	−41.45	−40.86
	48	−49.52	−48.71
	49	−50.76	−50.47
	50	−55.81 W	−55.81 W
	51	−53.11	−53.09 X
	52	−54.05	−54.05
121	41	26.79	21.13
	42	11.77	8.04
	43	− 1.00	− 3.76
	44	−13.18	−14.45
	45	−23.52	−24.05
	46	−32.54	−32.38
	47	−39.86	−39.72
	48	−45.86	−45.45
	49	−50.28	−50.22 X
	50	−53.63 W	−53.63 W
	51	−54.02	−54.01
	52	−52.80	−53.35
	53	−50.32	−50.97
122	42	14.75	10.60
	43	3.21 X	0.41
	44	−11.25	−12.89
	45	−19.55	−20.45
	46	−31.39	−31.54
	47	−36.77	−36.67
	48	−45.85	−45.24
	49	−48.08	−47.82
	50	−54.14	−54.05
	51	−52.44 W	−52.44 W
	52	−54.39	−54.42
	53	−50.09	−50.08 X
123	42	21.82	16.15
	43	8.04	3.69
	44	− 5.13	− 7.77
	45	−16.47	−17.97
	46	−26.49	−27.04
	47	−34.81	−35.03

TABLE II (*continued*)

MASS EXCESSES (IN MEV.) OF FISSION FRAGMENTS (*continued*)

A	Z	(a)	(b)
123	48	−41.81	−41.74
	49	−47.22	−47.46
	50	−51.57 W	−51.57 W
	51	−52.96	−52.99 X
	52	−52.74	−53.04
	53	−51.26	−51.81
124	43	12.60 X	7.81
	44	− 2.85	− 5.59
	45	−12.15	−14.17
	46	−24.98	−25.87
	47	−31.36	−31.82
	48	−41.43	−41.30
	49	−44.66	−44.82
	50	−51.71	−51.77
	51	−51.00 W	−51.00 W
	52	−53.94	−53.88
	53	−50.63	−50.66
125	43	17.58	11.77
	44	3.41	− 0.69
	45	− 8.91	−11.55
	46	−19.92	−21.42
	47	−29.23	−30.01
	48	−37.22	−37.47
	49	−43.62	−43.85
	50	−48.96 W	−48.96 W
	51	−51.34	−51.33
	52	−52.11	−52.10
	53	−51.62	−51.91 X
126	43	22.90 X	18.05
	44	6.45	1.84
	45	− 3.82	− 7.61
	46	−17.64	−19.42
	47	−25.01	−26.40
	48	−36.06	−36.50
	49	−40.28	−40.85
	50	−48.31	−48.73
	51	−48.59	−48.91
	52	−52.52 W	−52.52 W
	53	−50.20	−50.15
127	44	14.01	8.79
	45	− 0.83	− 4.53
	46	−12.82	−15.40
	47	−23.11	−24.67
	48	−32.09	−32.94
	49	−39.48	−39.93
	50	−45.80	−45.80
	51	−49.16	−48.85
	52	−50.91	−50.62
	53	−51.40 W	−51.40 W
	54	−50.45	
128	44	17.33	13.06 X
	45	6.07	1.10
	46	−10.25	−13.52
	47	−18.60	−21.38
	48	−30.63	−31.60
	49	−35.82	−36.99
	50	−44.84	−45.50
	51	−46.10	−46.52
	52	−51.01	−51.07
	53	−49.66 W	−49.66 W
	54	−51.21	−51.68
129	44	26.75	20.12
	45	10.92	6.10
	46	− 3.57	− 7.43
	47	−16.37	−19.18
	48	−26.32	−28.47
	49	−34.68	−36.15
	50	−41.98	−42.83
	51	−46.32	−46.50
	52	−49.04	−49.05
	53	−50.51 W	−50.51 W
	54	−50.54	−50.70
130	45	17.97	12.01
	46	0.68	− 3.56 X
	47	−10.17	−13.93
	48	−24.70	−26.98
	49	−30.87	−33.26
	50	−40.86	−41.90
	51	−43.09	−43.98
	52	−48.97	−49.16
	53	−48.60 W	−48.60 W
	54	−51.12	−51.57
	55	−48.06	
131	45	23.52	17.69
	46	8.04	3.37
	47	− 5.71	− 9.06
	48	−18.16	−21.03
	49	−29.03	−31.20
	50	−37.30	−38.91
	51	−42.61	−43.28
	52	−46.30	−46.64
	53	−48.74 W	−48.74 W
	54	−49.74	−49.71
	55	−49.19	
132	46	12.33	7.75
	47	0.51	− 3.59
	48	−14.99	−17.60 X
	49	−23.66	−26.39
	50	−36.14	−37.87
	51	−39.34	−40.84
	52	−46.19	−46.16
	53	−46.79	−46.67
	54	−50.28 W	−50.28 W
	55	−48.19	−48.14
133	46	19.83	14.61
	47	5.10	1.14
	48	− 8.31	−11.60
	49	−20.14	−22.48
	50	−30.91	−32.88
	51	−38.71	−39.74
	52	−43.37	−44.14
	53	−46.78	−46.94
	54	−48.74 W	−48.74 W
	55	−49.16	−49.27
	56	−48.41	
134	46	24.61	19.48
	47	11.82	7.47
	48	− 4.64	− 7.71
	49	−14.27	−17.49
	50	−27.72	−29.94 X
	51	−33.41	−35.43
	52	−42.76	−43.60
	53	−44.32	−45.01
	54	−48.77 W	−48.77 W
	55	−47.64	−47.71
	56	−49.41	−49.76
136	47	23.86	20.66
	48	6.43	3.75
	49	− 4.15	− 6.69
	50	−18.56	−20.33
	51	−25.21	−26.81
	52	−35.52	−35.96 X
	53	−39.57	−39.90
	54	−46.51 W	−46.51 W
	55	−46.34	−46.36
	56	−49.07	−48.56
	57	−46.20	
137	48	14.68	10.99
	49	0.93	− 1.59
	50	−11.75	−13.90
	51	−21.47	−22.51
	52	−29.58	−30.41
	53	−36.44	−36.43
	54	−41.85	−41.97
	55	−45.72 W	−45.72 W
	56	−46.89	−47.01
	57	−46.68	−46.69
138	48	18.07	16.22 X
	49	6.52	4.84
	50	− 8.83	−10.51
	51	−16.45	−17.67
	52	−27.70	−28.02
	53	−32.71	−32.95
	54	−40.61	−40.55 X
	55	−42.93 W	−42.93 W
	56	−48.14	−47.99
	57	−46.23	−46.29
	58	−47.38	
139	49	11.40	8.05 X
	50	− 2.23	− 4.44
	51	−12.91	−13.74
	52	−21.98	−22.76
	53	−29.79	−29.83
	54	−36.16	−36.18
	55	−40.98	−40.65
	56	−44.64 W	−44.64 W
	57	−46.91	−46.84
	58	−46.85	−46.58
140	49	18.12	15.40
	50	1.80	1.05 X
	51	− 6.75	− 7.03
	52	−18.96	−19.11
	53	−24.92	−24.72
	54	−33.78	−33.52
	55	−37.05	−36.90
	56	−43.22	−42.95 X
	57	−43.79 W	−43.79 W
	58	−47.42	−47.31
141	49	23.40	17.87
	50	8.81	5.16
	51	− 2.81	− 4.82 X
	52	−12.83	−14.05
	53	−21.60	−21.80
	54	−28.92	−29.28
	55	−34.70	−34.80
	56	−39.31	−39.60
	57	−42.53 W	−42.53 W
	58	−44.96	−44.98
	59	−45.46	
142	49	30.36	25.95
	50	13.09	11.10 X
	51	3.58	2.07
	52	− 9.58	− 8.99 X
	53	−16.49	−15.54
	54	−26.30	−26.07
	55	−30.52	−30.14
	56	−37.64	−37.40
	57	−39.17	−39.24
	58	−43.75 W	−43.75 W
	59	−43.11	−43.05
143	50	20.91	15.86
	51	8.32	4.48
	52	− 2.64	− 4.94
	53	−12.35	−13.39 X
	54	−20.63	−21.07
	55	−27.35	−27.29
	56	−32.92	−33.23
	57	−37.09	−37.21
	58	−40.47 W	−40.47 W
	59	−41.92	−41.86
	60	−42.74	−42.77
144	50	25.75	22.14
	51	15.29	12.17
	52	1.17	0.59
	53	− 6.68	− 6.89
	54	−17.44	−16.42
	55	−22.61	−21.44
	56	−30.68	−30.43
	57	−33.16	−32.97
	58	−38.69 W	−38.69 W
	59	−39.00	−38.99
	60	−42.10 X	−41.96 X

TABLE II (*concluded*)

MASS EXCESSES (IN MEV.) OF FISSION FRAGMENTS (*concluded*)

A	*Z*	(*a*)	(*b*)
146	52	12.42	10.09 X
	53	3.61	1.65
	54	− 8.10	− 8.38 X
	55	−14.22	−14.34
	56	−23.24	−22.33 X
	57	−26.67	−25.81
	58	−33.15	−33.27
	59	−34.41	−34.27
	60	−38.46 W	−38.46 W
147	53	7.86	4.19
	54	− 2.31	− 5.13
	55	−10.93	−13.45
	56	−18.40	−19.81
	57	−24.47	−25.19
	58	−29.75	−29.81
	59	−33.10	−32.95
	60	−35.82 W	−35.82 W
	61	−36.60	
148	53	14.92	11.63
	54	2.27	0.65 X
	55	− 4.81	− 6.25
	56	−14.50	−14.76 X
	57	−18.88	−19.18
	58	−26.31	−25.64 X
	59	−28.52	−27.59
	60	−33.52 W	−33.52 W
	61	−33.23	−32.99
149	53	19.32	13.95
	54	8.20	4.23
	55	− 1.37	− 4.66
	56	− 9.79	−12.46
	57	−16.81	−19.24
	58	−23.04	−24.07
	59	−27.34	−27.93 X
	60	−31.01 W	−31.01 W
	61	−32.74	−32.62
150	53	25.48	
	54	11.87	7.60 X
	55	3.85	− 0.25
	56	− 7.07	− 9.70 X
150	57	−12.40	−15.08
	58	−20.78	−22.06 X
	59	−23.94	−24.96
	60	−29.89 W	−29.89 W
	61	−30.55	−30.31
	62	−34.57 X	−34.71
152	53	38.15	
	54	23.59	
	55	14.62	
	56	2.76	− 2.12 X
	57	− 3.52	− 8.45
	58	−12.86	−16.38 X
	59	−16.96	−20.22
	60	−23.87 X	−25.68 X
	61	−25.47	−27.04
	62	−30.45 W	−30.45 W
154	54	34.22	
	55	24.29	
	56	11.47	
	57	4.24	
	58	− 6.05	−10.00 X
	59	−11.11	−14.80
	60	−18.96 X	−21.20 X
	61	−21.52	−23.52
	62	−27.45 W	−27.45 W
	63	−28.14	−27.29
155	54	40.36	
	55	27.93	
	56	16.66	
	57	6.79	
	58	− 2.29	
	59	− 9.45	−11.99
	60	−15.97	−17.13
	61	−20.56	−21.44
	62	−24.67 W	−24.67 W
	63	−26.65	−26.87
156	54	46.40	
	55	35.52	
	56	21.74	
	57	13.56	
156	58	2.32	
	59	− 3.69	
	60	−12.50	−15.19 X
	61	−16.02	−18.47
	62	−22.90	−23.34 X
	63	−23.92	−24.14
	64	−26.54 W	−26.54 W
157	54	50.24	
	55	36.86	
	56	24.63	
	57	13.80	
	58	3.76	
	59	− 4.34	
	60	−11.82	
	61	−17.36	−18.72
	62	−22.43	−22.33
	63	−25.37	−25.12
	64	−26.82 W	−26.82 W
158	54	57.76	
	55	45.92	
	56	31.19	
	57	22.05	
	58	9.85	
	59	2.88	
	60	− 6.89 X	
	61	−11.36	
	62	−19.20 X	−19.65 X
	63	−21.18	−21.40
	64	−24.75 W	−24.75 W
160	55	58.58	
	56	42.89	
	57	32.79	
	58	19.64	
	59	11.71	
	60	0.98	
	61	− 4.45	
	62	−13.25	
	63	−16.19	
	64	−20.72 W	−20.72 W
	65	−21.17	−20.95

data (Newton 1956) one does not obtain general agreement with the experimental fission yield curve. However it may still be true that the energy release affects the local distributions of yield. It is not the purpose of this paper to attempt to develop a theory of fission, but as an example of the possibility of such use of our mass estimates, Table III lists the energy releases for spontaneous fission of U^{236}. To find the energy release in thermal fission of U^{235} one, of course, must add the neutron binding energy 6.43 Mev.*

Recently Levy (1955) has constructed a completely empirical mass formula containing a pairing energy term, a constant, and terms proportional to each of A, Z, AZ, Z^2, and A^2. The form is fitted separately to the known masses in each region of the N–Z plane bounded by magic neutron and proton numbers. We have computed by his formula the masses of a few sets of isobars in the fission fragment region. For A near 96 his masses follow very closely column (*b*) of Table II, while for A near 140 his masses are more nearly those of column (*a*); however in this region columns (*a*) and (*b*) are very similar.

*Similar tables of energy release have been computed for 23 other fissile nuclei. These may be obtained from Atomic Energy of Canada Ltd., Chalk River, Ontario.

TABLE III

ENERGY RELEASES (IN MEV.) IN SPONTANEOUS FISSION OF U^{236}

Column (*a*) gives energy release derived from mass excesses listed in column (*a*) of Table II; columns (*b*) also correspond

A_H	A_L	Z_H	Z_L	(*a*)	(*b*)
118	118	46	46	195.02	193.68
		47	45	188.57	187.58
		48	44	189.35	188.72
		49	43	177.12	177.55
		50	42	171.63	173.49
		51	41	152.61	155.05
		52	40	139.33	144.13
119	117	40	52	131.07	135.86
		41	51	148.84	152.25
		42	50	164.48	166.51
		43	49	174.92	176.32
		44	48	183.70	183.65
		45	47	189.06	188.27
		46	46	191.79	190.23
		47	45	191.09	189.95
		48	44	187.77	186.94
		49	43	181.03	181.69
		50	42	172.62	173.78
		51	41	159.02	161.44
		52	40	143.29	146.59
120	116	40	52	126.45	132.91
		41	51	141.77	145.98
		42	50	162.84	165.98
		43	49	170.34	171.86
		44	48	184.61	185.29
		45	47	185.88	186.07
		46	46	194.36	193.94
		47	45	189.95	189.52
		48	44	192.75	192.33
		49	43	182.56	182.94
		50	42	179.11	180.79
		51	41	162.13	164.60
		52	40	150.88	155.52
121	115	41	51	137.51	143.14
		42	50	155.20	159.18
		43	49	167.67	170.52
		44	48	178.49	179.76
		45	47	185.88	186.29
		46	46	190.64	190.33
		47	45	191.99	191.67
		48	44	190.70	190.34
		49	43	186.00	186.77
		50	42	179.63	180.47
		51	41	168.06	170.19
		52	40	154.37	157.28
		53	39	137.07	141.63
122	114	42	50	153.04	157.54
		43	49	162.60	165.57
		44	48	178.90	180.54
		45	47	182.20	183.14
		46	46	192.73	193.28
		47	45	190.35	190.76
		48	44	195.20	195.36
		49	43	187.04	187.64
		50	42	185.63	187.16
		51	41	170.67	172.74
		52	40	161.47	165.57
		53	39	140.93	146.09
123	113	42	50		
		43	49	159.25	163.74
		44	48	172.10	174.74
		45	47	181.53	182.80
		46	46	188.33	188.75
		47	45	191.73	191.99
		48	44	192.48	192.74
		49	43	189.80	190.78
		50	42	185.47	186.16
		51	41	175.94	177.57
		52	40	164.29	166.24
		53	39	149.04	152.68
124	112	43	49	153.40	158.53
		44	48	171.73	174.47
		45	47	177.08	179.22
		46	46	189.64	190.90
		47	45	189.31	190.21
		48	44	196.20	197.05
		49	43	190.09	191.24
		50	42	190.72	192.53
		51	41	177.80	179.78
		52	40	170.63	174.27
		53	39	152.14	156.57
125	111	43	49	149.23	155.35
		44	48	164.13	168.43
		45	47	175.60	178.24
		46	46	184.44	185.96
		47	45	189.88	190.72
		48	44	192.68	193.37
		49	43	192.05	193.31
		50	42	189.76	190.76
		51	41	182.28	183.76
		52	40	172.67	174.11
		53	39	159.47	162.23
126	110	43	49		
		44	48	162.38	166.72
		45	47	169.76	173.55
		46	46	184.38	186.20
		47	45	186.10	187.64
		48	44	195.03	196.03
		49	43	190.96	192.04
		50	42	193.64	195.58
		51	41	182.77	184.72
		52	40	177.65	180.98
		53	39	161.21	164.93
127	109	44	48	153.63	158.25
		45	47	168.69	172.38
		46	46	179.58	182.16
		47	45	187.07	188.67
		48	44	191.92	193.08
		49	43	193.35	194.54
		50	42	193.11	193.88
		51	41	187.68	188.79
		52	40	180.12	181.19
		53	39	168.96	170.89
		54	38	154.78	
128	108	44	48	151.89	156.10
		45	47	161.34	166.28
		46	46	179.53	182.80
		47	45	183.31	186.32
		48	44	194.30	195.66
		49	43	192.28	193.80
		50	42	197.02	198.87
		51	41	188.21	189.83
		52	40	185.15	188.32
		53	39	170.75	174.16
		54	38	161.48	167.11
129	107	44	48	140.17	146.86
		45	47	157.30	162.19
		46	46	171.78	175.64
		47	45	182.86	186.47
		48	44	189.77	192.94
		49	43	193.26	196.14
		50	42	195.08	197.23
		51	41	191.71	193.63
		52	40	186.21	187.93
		53	39	177.11	179.51
		54	38	164.99	168.61
130	106	45	47	149.50	155.59
		46	46	169.76	173.93
		47	45	177.13	180.78
		48	44	191.71	193.99
		49	43	191.77	194.19
		50	42	198.58	200.21

TABLE III (*continued*)

ENERGY RELEASES (IN MEV.) IN SPONTANEOUS FISSION OF U^{238} (*continued*)

A_E	A_L	Z_H	Z_L	(a)	(b)
130	106	51	41	191.82	193.30
		52	40	190.83	193.30
		53	39	178.50	180.94
		54	38	171.29	176.11
		55	37	152.35	
131	105	45	47	144.38	149.84
		46	46	160.95	165.34
		47	45	174.09	177.33
		48	44	184.60	187.47
		49	43	191.70	194.97
		50	42	195.60	198.11
		51	41	194.30	196.24
		52	40	190.87	192.27
		53	39	183.85	185.35
		54	38	173.80	176.31
		55	37	159.70	
132	104	46	46	157.64	162.35
		47	45	167.09	171.19
		48	44	183.75	186.20
		49	43	187.42	189.71
		50	42	197.83	199.59
		51	41	193.16	194.72
		52	40	194.25	195.66
		53	39	184.00	185.41
		54	38	178.88	182.08
		55	37	162.01	166.38
133	103	46	46		
		47	45	164.16	167.89
		48	44	176.75	180.04
		49	43	185.93	188.71
		50	42	193.45	195.50
		51	41	195.76	197.92
		52	40	194.43	195.98
		53	39	189.49	190.77
		54	38	181.52	183.45
		55	37	169.50	173.19
		56	36	155.38	
134	102	46	46		
		47	45	156.46	160.92
		48	44	175.21	178.28
		49	43	180.97	183.77
		50	42	193.48	195.44
		51	41	192.43	193.86
		52	40	197.15	198.65
		53	39	189.00	190.43
		54	38	185.96	188.02
		55	37	171.18	174.42
		56	36	162.06	167.75
136	100	47	45	144.03	
		48	44	164.90	167.57
		49	43	172.77	175.15
		50	42	187.39	189.16
		51	41	188.45	189.54
		52	40	195.29	196.10
		53	39	190.77	191.16
		54	38	191.38	192.57
		55	37	178.71	180.99
		56	36	171.70	175.21
		57	35	151.96	
137	99	48	44	153.84	157.56
		49	43	167.25	169.92
		50	42	178.98	181.13
		51	41	185.52	186.70
		52	40	189.94	190.38
		53	39	190.76	190.57
		54	38	188.54	188.88
		55	37	182.28	184.56
		56	36	172.37	175.89
		57	35	158.35	163.93
138	98	48	44	152.51	153.85
		49	43	162.52	163.78
		50	42	179.26	180.94
		51	41	182.47	183.40
		52	40	191.42	192.28
		53	39	189.04	189.28
		54	38	191.78	192.44

A_H	A_L	Z_H	Z_L	(a)	(b)
138	98	55	37	182.78	184.10
		56	36	179.42	182.13
		57	35	161.80	167.16
		58	34	150.96	
139	97	49	43	158.77	162.12
		50	42	172.64	175.37
		51	41	181.33	182.60
		52	40	187.89	188.67
		53	39	190.85	190.84
		54	38	190.78	191.13
		55	37	186.65	187.91
		56	36	180.42	182.82
		57	35	170.07	175.10
		58	34	156.00	163.02
140	96	49	43	151.36	154.87
		50	42	170.26	171.12
		51	41	175.60	175.88
		52	40	186.71	187.91
		53	39	186.48	186.95
		54	38	191.38	192.41
		55	37	184.52	185.99
		56	36	183.32	185.74
		57	35	169.39	173.99
		58	34	162.21	168.61
141	95	49	43	146.40	151.86
		50	42	162.45	166.20
		51	41	173.29	175.12
		52	40	182.01	183.23
		53	39	187.14	187.03
		54	38	189.24	189.68
		55	37	187.28	188.42
		56	36	183.21	185.27
		57	35	175.02	178.63
		58	34	164.64	170.12
		59	33	150.30	
142	94	49	43		
		50	42	159.37	161.19
		51	41	166.89	168.40
		52	40	180.17	179.46
		53	39	182.12	180.80
		54	38	189.20	189.37
		55	37	184.52	184.98
		56	36	185.49	187.01
		57	35	173.75	177.15
		58	34	168.74	173.46
		59	33	150.92	158.27
143	93	50	42	150.27	156.74
		51	41	163.32	167.38
		52	40	174.22	176.52
		53	39	181.53	182.00
		54	38	185.82	186.64
		55	37	186.05	187.00
		56	36	184.18	186.19
		57	35	178.18	181.48
		58	34	169.98	174.87
		59	33	157.82	164.78
		60	32	143.10	152.82
144	92	50	42	146.59	149.86
		51	41	156.31	159.11
		52	40	171.81	172.39
		53	39	175.95	176.12
		54	38	185.23	183.72
		55	37	182.76	181.60
		56	36	185.94	186.70
		57	35	176.39	178.85
		58	34	173.60	177.40
		59	33	157.97	164.07
		60	32	149.20	156.91
146	90	52	40	161.38	164.03
		53	39	167.76	169.79
		54	38	179.27	179.55
		55	37	179.03	179.79
		56	36	184.44	183.89
		57	35	177.13	178.26
		58	34	176.57	179.87
		59	33	163.18	168.51
		60	32	156.63	163.57

TABLE III (*concluded*)

ENERGY RELEASES (IN MEV.) IN SPONTANEOUS FISSION OF U^{238} (*concluded*)

A_H	A_L	Z_H	Z_L	(*a*)	(*b*)
147	89	53	39	164.84	168.38
		54	38	173.59	176.41
		55	37	178.28	180.06
		56	36	180.88	182.20
		57	35	179.35	180.68
		58	34	175.63	178.33
		59	33	167.93	171.67
		60	32	157.68	163.86
		61	31	143.55	
148	88	53	39	154.96	158.55
		54	38	170.52	172.40
		55	37	172.54	174.61
		56	36	180.22	180.85
		57	35	175.18	177.55
		58	34	176.88	178.11
		59	33	165.75	168.95
		60	32	161.47	167.02
		61	31	143.69	152.13
149	87	53	39	149.94	154.95
		54	38	162.75	166.06
		55	37	171.51	174.80
		56	36	176.39	179.29
		57	35	177.15	179.38
		58	34	175.71	177.97
		59	33	170.30	172.90
		60	32	162.32	166.99
		61	31	150.48	156.78
150	86	53	39	140.24	
		54	38	158.11	162.26
		55	37	164.22	168.33
		56	36	175.97	178.60
		57	35	173.23	177.25
		58	34	177.24	179.91
		59	33	168.41	173.05
		60	32	166.43	170.03
		61	31	150.94	157.30
		62	30	142.06	151.80
152	84	53	39		
		54	38		
		55	37	152.31	
		56	36	166.41	170.25
		57	35	167.78	172.71
		58	34	175.92	179.38
		59	33	169.42	174.40
		60	32	169.79	173.46
		61	31	156.63	162.97
		62	30	150.09	156.35
154	82	54	38		
		55	37		
		56	36	156.59	
		57	35	160.35	
		58	34	170.85	174.80
		59	33	168.52	173.60
		60	32	173.04	176.61
		61	31	162.27	167.98
		62	30	158.11	163.37
		63	29	140.62	149.23
155	81	54	38		
		55	37		
		56	36	148.89	
		57	35	158.50	
		58	34	165.92	
		59	33	169.38	172.93
		60	32	170.27	173.12
		61	31	167.29	170.95
		62	30	159.08	164.54
		63	29	146.31	153.72
156	80	54	38		
		55	37		
		56	36	143.96	
		57	35	150.14	
		58	34	163.08	
		59	33	163.17	
		60	32	170.12	173.43
		61	31	163.55	168.52
		62	30	163.59	167.82
		63	29	148.53	155.49
		64	28	137.47	147.18
157	79	54	38		
		55	37		
		56	36		
		57	35	150.27	
		58	34	160.14	
		59	33	166.04	
		60	32	169.38	
		61	31	168.84	171.55
		62	30	164.87	168.01
		63	29	156.34	162.12
		64	28	141.98	151.97
158	78	54	38		
		55	37		
		56	36		
		57	35	140.03	
		58	34	155.44	
		59	33	158.01	
		60	32	167.44	
		61	31	163.34	
		62	30	165.86	168.80
		63	29	155.05	160.14
		64	28	148.24	155.68
160	76	55	37		
		56	36		
		57	35	126.42	
		58	34	144.35	
		59	33	149.45	
		60	32	161.41	
		61	31	159.83	
		62	30	164.88	
		63	29	156.60	
		64	28	152.31	158.28
		65	27	135.77	144.83

Cameron (1956), who has made quite extensive calculations with Levy's formulae, points out that to obtain the masses near $A = 96$ an extrapolation at constant N is required to proceed from the measured masses to fission fragment masses within the appropriate Levy region. Hence it is reasonable that his masses agree with our column (*b*). In other parts of the table of nuclei, extrapolation at constant Z is required by Levy and, according to Cameron, the agreement is then better with our column (*a*).

These tables are not recommended for estimating detailed differences such as neutron or proton binding energies. Their method of construction carries

over the irregularities of one position in the periodic table (at which the base Q's apply) to another part, and consequently one cannot be confident that the individual differences have physical meaning. Perhaps greater confidence can be placed in the general trends shown by such differences; e.g. the rather rapid decrease in neutron binding energy as one moves away from the stable nuclei. In the same way the individual estimates of energy release in fission may not be relatively very accurate but the location of the maximum and the width of the distribution of energy as a function of charge at a given mass ratio are probably more reliable.

We wish to acknowledge that the suggestion for this method of estimating fission fragment masses was made to us by Dr. L. G. Elliott, to whom we are grateful.

The final calculations were made on I.B.M. accounting machines. We wish to thank R. J. Montgomery, C. M. Rioux, and others of that section for advice and assistance.

REFERENCES

CAMERON, A. G. W. 1956. Private communication.
FONG, P. 1956. Phys. Rev. **107**, 434.
HUIZENGA, J. R. 1955. Physica, **21**, 410.
KING, R. W. 1954. Revs. Mod. Phys. **26**, 327.
LEVY, H. B. 1955. University of California Radiation Laboratory, Livermore, Calif., Report UCRL–4588 (unpublished).
NEWTON, T. D. 1956. Can. J. Phys. **34**, 804.
WAPSTRA, A. H. 1955. Physica, **21**, 367, 385.
WAY, K. and WOOD, M. 1954. Phys. Rev. **94**, 119.

THE INFLUENCE OF IMPURITIES ON THE MACROMOSAIC STRUCTURES OF TIN AND LEAD[1]

H. A. ATWATER[2] AND B. CHALMERS

ABSTRACT

The properties and characteristics of arrays of low-angle boundaries which appear upon freezing of single crystals of tin and lead from the melt are shown to be dependent upon the amount and kind of impurities in the freezing liquid. The boundary-direction angle as a function of lattice orientation and impurity content in crystals frozen at speeds greater than 18–20 mm./minute is employed as an observational quantity. Measurements of boundary-direction are given for various impurity concentrations and types. Mechanisms for the determining of the boundary directions are proposed.

INTRODUCTION

A macromosaic structure which appears under certain conditions of freezing of tin crystals from the melt has been described by Teghtsoonian and Chalmers (1951, 1952). In the work reported by these authors, a melt of 99.987% tin was solidified by the passage of the solid–liquid interface along a horizontal graphite boat. The lattice orientation was determined by a seed crystal so that the [001] axis was vertical in the boat, and a ⟨110⟩ axis rotated in the horizontal plane by an angle ϕ measured away from the axis of growth. Crystals grown in this manner exhibit a macromosaic structure, called striations, which consists of long, continuous, low-angle grain boundaries. These boundaries represent a lattice rotation of up to a few degrees around the interface-normal direction. When $\phi = 0°$, the striations are parallel to the specimen axis. For $\phi > 0°$, the striations diverge from the specimen axis

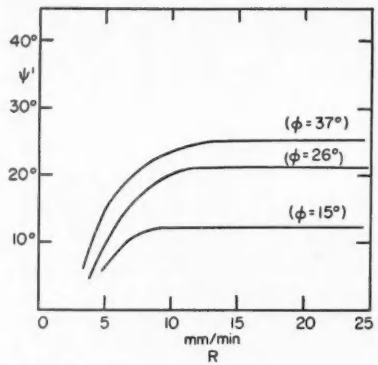

FIG. 1. Direction of striation lines in tin, as a function of growth rate for different ⟨110⟩ orientations. (After Teghtsoonian and Chalmers (1951).)

[1]Manuscript received September 19, 1956.
Contribution from the Gordon McKay Laboratory, Harvard University, Cambridge, Massachusetts.
[2]Now at University of Oregon, Eugene, Oregon.

toward the ⟨110⟩ direction, taking up an angle with respect to the axis which will here be called ψ'. In general, ψ' depends upon ϕ and the rate of growth, R, in the manner indicated in Fig. 1 for a typical case (after Teghtsoonian and Chalmers 1951). For R greater than 15 to 20 mm. per minute, the striation direction angle assumes a final value ψ (unprimed), which is independent of the rate of growth. Angle definitions are as indicated in Fig. 6.

It has been determined in the present research that the typical regular character of the striation arrays, as well as the particular values obtained for the ψ' vs. R relation, is dependent upon the amount and kind of metallic impurities present in the melt from which the crystal is frozen, over an impurity-concentration range of about 0.001% to 0.1%.

OBSERVATIONS ON TIN

Figure 7A shows a tin crystal prepared from "Spectrographically Pure" tin supplied by A. D. Mackay, Inc., New York, stated to be of 99.998% purity. Table I indicates the supplier's analysis of the "Spec. Pure" tin, and also the

TABLE I

Impurity	"Spec. Pure" tin* (A. D. Mackay, Inc.)	"Chempur" tin† (Johnson, Matthey Co.)
Sb	0.0005%	0.0032%
As		0.0001%
Pb	0.0005%	0.0082%
Bi		0.0009%
Cu		0.0007%
Fe	0.0002%	0.0005%
S		0.0003%
Other	0.0008%	

*Impurity analysis furnished by A. D. Mackay, Inc., New York.
†Estimated probable impurity analysis furnished by the Tin Research Institute, Greenford, England.

estimated probable impurity content of the Johnson and Matthey "Chempur" tin used in the earlier work cited (Teghtsoonian and Chalmers 1951). The crystal of Fig. 7A was frozen at about 5 mm. per minute, with the [001] axis vertical, and a ⟨110⟩ axis parallel to the specimen axis ($\phi = 0°$). As may be seen in the figure, the small-angle boundaries visible at the surface of the etched crystal are non-straight and discontinuous. When about 0.005 atomic per cent of pure lead was added to a melt of tin of this purity, and the crystal frozen under the same conditions as above, the resulting striation boundaries were then continuous and nearly-straight lines, as indicated by Fig. 7E. The addition of intermediate quantities of impurity produces intermediate amounts of influence on boundary uniformity, as indicated by the sequence of crystals in Figs. 7A to 7E containing increasing concentrations of added lead. Other elements used as additive impurities have effects comparable to that of lead on the subboundaries observed in tin crystals.

A quantitative measure of the influence of solute impurities upon the striations was obtained by observing ψ, the final maximum striation angle

reached at speeds of growth greater than 15 to 20 mm. per minute, as a function of orientation angle, ϕ. In these observations, the angles ψ and ϕ were measured with respect to the interface-normal direction, as indicated by ripple marks on the crystal surface, established by occasionally agitating the melt. The striations were observable as boundary grooves on the surface of the unetched crystal, so that their direction could be measured without removing the crystal from the boat.

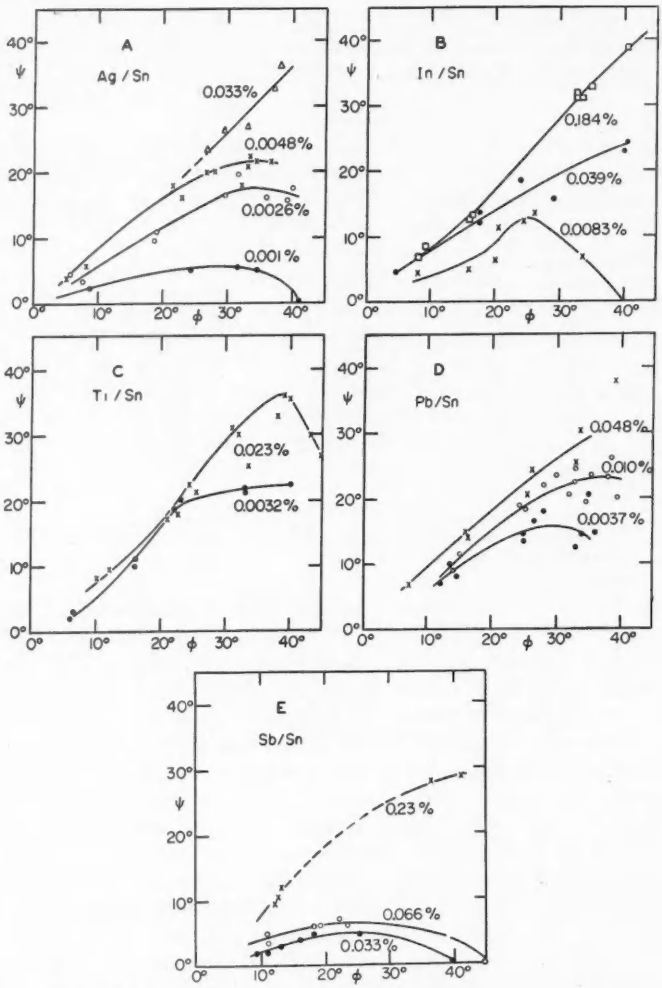

FIG. 2. A to E. Direction of striation lines in tin at growth rates above 18 mm./minute as a function of ⟨110⟩ orientation, for different impurity amounts and types. Amounts of added impurity are given in atomic percentages.

The variation of ψ as a function of ϕ was measured for various levels of impurity concentration, when indium, silver, antimony, thallium, and lead were used as the impurity element. The results of the measurements are shown in Figs. 2A to 2E. For all of these cases, crystals were grown at speeds greater than 18 mm. per minute, in which range a further increase in growth rate produced no observable increase in ψ'. A stream of cooling air was directed onto the solid in order to attain these growth rates, and no effect upon striation direction was observed to result from such variations in temperature gradient as were caused by moderate variations in the intensity of cooling.

Corrugations were also visible at the surface for all except the lower impurity levels used in these crystals. The corrugations are the surface manifestation of the cellular structure, the prismatic substructure due to linear distributions of impurity in the solid, described by Rutter and Chalmers (1953). The corrugations and striation boundaries, when they appeared simultaneously on these crystals, were essentially always parallel, each striation boundary occurring in one of the cell-boundary regions, and travelling with it as growth proceeds. Typical cases of these structures are shown in Figs. 8 and 9.

The distribution coefficient of a binary metallic system is defined as the ratio of solute in the solid phase to solute in the contiguous liquid, in equilibrium. A correlation was established between the distribution coefficients of the impurity metals used in this work with tin, and the concentration of these impurities necessary to produce a given effect on the striation boundaries. All of the curves of ψ vs. ϕ for all the impurities used were brought into comparison, and from these were selected the impurity concentrations, c_0^*, necessary to cause the striation-angle curve to run an arbitrarily selected

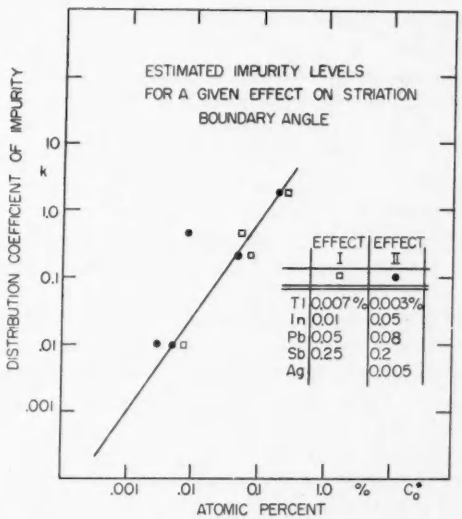

FIG. 3. Relation of distribution coefficient and concentration, for the amounts of various impurities needed to produce a given effect on striation line directions in tin crystals.

course in the ψ vs. ϕ diagram, for each of the impurities used. This was repeated for two ψ vs. ϕ courses, and the resulting pairs of c_0^*, k values plotted logarithmically. The result is as shown in Fig. 3, being reasonably well represented by the straight line:

$$\log k = 1.2+1.4 \log c_0^*. \tag{1}$$

OBSERVATIONS ON LEAD

The striations which form in lead crystals were found to have characteristics analogous in most respects to those of tin. Lead crystals were grown in a horizontal graphite boat, with the [001] axis vertical, and [100] deviating from the interface-normal direction by angle ϕ in the horizontal plane. When the starting material was "Spec. Pure" lead, furnished by A. D. Mackay, New York, stated to be of 99.999% purity, it was found to be necessary to add an impurity metal in order to obtain straight, uniform striations over the range of growth speeds investigated here, of about 5 to 30 mm. per minute. When straight striations form, the striation angle tends toward the [100] axis direction, reaching a steady value at growth speeds above 18 to 20 mm. per minute. The ψ' vs. R relationship for a lead crystal with 0.0017 atomic per cent of silver added is shown in Fig. 4 for two values of orientation angle ϕ.

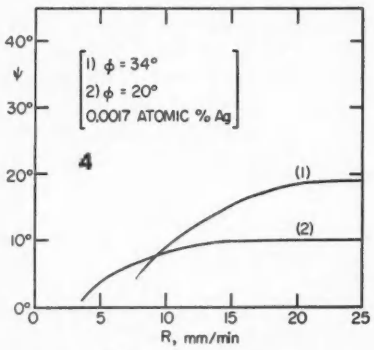

FIG. 4. Direction of striation lines in lead, as a function of growth rate for different ⟨100⟩ orientations.

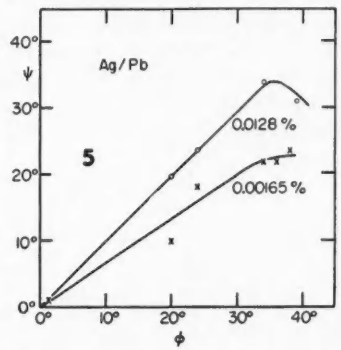

FIG. 5. Direction of striation lines in lead at growth rates above 18 mm./minute as a function of ⟨100⟩ orientations, for different amounts of silver impurity.

The striations in lead show a ψ vs. ϕ characteristic similar in nature to that of tin. Fig. 5 shows the ψ vs. ϕ relationship for two levels of silver impurity in "Spec. Pure" lead. Typically striated lead crystals are shown in Fig. 10.

DISCUSSION

Straight, uniform striations appear in lead and tin crystals when there exists an impurity, or solute metal, content of the order of 0.001% to 0.1%. The striation lines tend toward the direction of the ⟨001⟩ axes in lead, and of the ⟨110⟩ axes in tin. The closeness of "coupling" of the striation directions to

these axes depends upon the orientation of the axes with respect to the growth direction, and upon the speed of growth, and the amount and kind of solute metal present. The mechanism which determines the direction and straightness of the striation boundaries must depend on these quantities.

The striation boundaries are equivalent to arrays of dislocations (Teghtsoonian and Chalmers 1952). The misorientation of the boundary is observed to be predominantly a rotation around the direction of growth, as shown schematically in Fig. 6. When $\phi = 0°$ and $\psi = 0°$, the boundary is a pure tilt

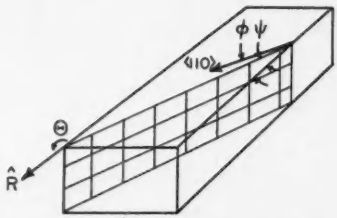

FIG. 6. Striation boundary in a tin crystal; schematic.

boundary consisting only of edge dislocations. When $0° < \phi < 45°$, and $0° < \psi < \phi$, the boundary will contain a twist component, which can be composed of a crossed grid of screw dislocations having [001] and ⟨110⟩ Burgers vectors. In the latter case, however, there is still required an edge-dislocation component in the dislocation array of the boundary.

It has been shown that a misfitting spherical solute atom interacts with the stress field of an edge dislocation, but not with that of a screw dislocation (Cottrell 1953). It may likewise be shown that such a solute atom interacts with the stress field of a vertical array of edge dislocations, or a tilt boundary.

The impurity atoms can reduce the energy of the edge-dislocation components of the striation boundary arrays by migrating to that region of the stress field which permits of the greatest amount of stress relaxation. The hypothesis may be made that the dislocation arrays during freezing of an impure crystal take up that direction which minimizes the dislocation energy per unit length of crystal frozen. Then it may be expected that the striations will assume a direction that represents a balance between the tendency toward increasing the stress reduction of the edge components, and simultaneously decreasing the screw-dislocation components of boundary energy, while introducing the least possible boundary area per unit length of crystal. The boundary area varies as $1/\cos \psi$ for a plane interface.

It has been shown, however, (Rutter and Chalmers 1953) that the interface of a crystal solidifying under conditions such that the cellular structure forms is not planar, but is composed of convex regions at the cell ends, separated by grooves, which are the terminations of the cell boundaries at the interface. The presence of these grooves will cause the striation boundary area to change more rapidly than $1/\cos \psi$ as the boundary termination moves across the groove.

The distribution of impurity concentration in the melt, as a function of distance, x, ahead of an advancing solid–liquid interface in steady-state freezing, is (Tiller *et al.* 1953)

$$c_L(x) = c_0\{1+[(1-k)/k]e^{-(R/D)x}\}, \tag{2}$$

in which k is the distribution coefficient for the solute, R the rate of advance of the interface, D the diffusion coefficient of the solute in the liquid, and c_0 the mean impurity concentration in the specimen. This equation may be written, in terms of concentration at $x = 0$:

$$c_L(x)-c_L(0) = c_0[(k-1)/k]\,(1-e^{-(R/D)x}). \tag{3}$$

Equation 3 implies that the gradient of impurity density in the liquid ahead of the interface increases asymptotically towards a maximum value as larger values of R are used in freezing.

This dependence upon R is of the same character as that shown by the striation-boundary direction angle, ψ. The mechanism for the correlation of these two quantities is furnished if it is assumed that the impurity distribution in the melt in the neighborhood of the cell-boundary grooves on the interface determines the impurity density established in the cell-boundary regions of the solid. Since the striation boundaries essentially always occur in the cell walls, the amount of interaction energy between the dislocation arrays and the impurity atoms will depend upon the impurity density established in the cell boundaries, thus leading to the hypothesized correlation.

The observations have shown that the corrugations, and hence the cellular structure, have a well-defined direction which is the same as that of the striation boundaries. It is to be expected that the cellular boundaries also have a dislocation content, as a geometrical consequence of the matching of crystal regions having different effective lattice constants due to differences in concentration of impurity atoms. If the impurity atoms in the cell boundaries are smaller than the solvent atoms in the lattice, there will be a decreased lattice constant in the boundary material. This change of lattice constant can be effected with minimum elastic strain by a distribution of dislocations, as indicated schematically in Fig. 11. The density of dislocations necessary to accomplish a solute-concentration change of Δc can be represented by (Goss, Benson, and Pfann 1956):

$$\delta = A[d(1/a_0)/dc]\Delta c, \tag{4}$$

where c is solute concentration, a_0 is lattice constant, and A is a geometrical constant depending upon the relation of the Burgers vector of the dislocations to the lattice constant. In the simple case in which $b = a_0 = 3\times10^{-8}$ cm., $A = 1$, and $da_0/dc = 10^{-8}$ cm./100%, $\delta = 10^4$ dislocations per cm. along the boundary between the material of higher purity and that of lower purity, for a concentration change of 0.1%.

Dislocation distributions of opposite sign are required along opposite sides of the cell boundary, each in the order of density given above. Therefore, if the direction assumed by the substructures in the crystal depends upon the energy balance of dislocation lines, although these are not coupled into small-

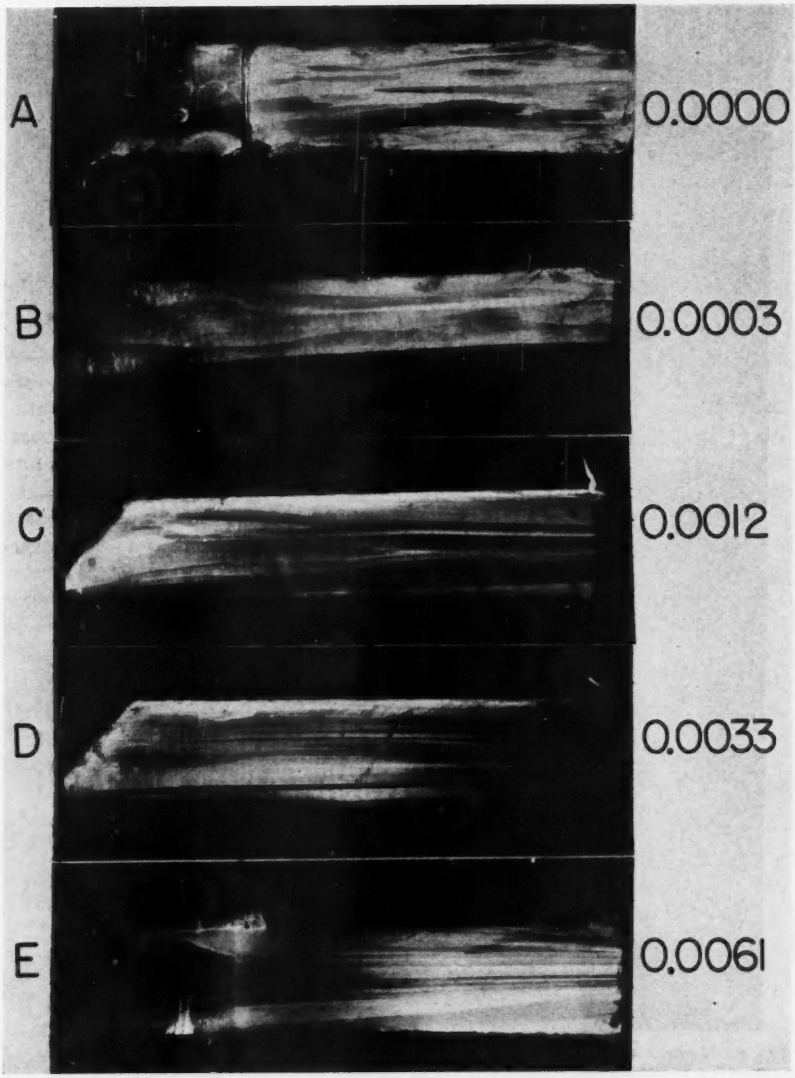

FIG. 7. Influence of increasing amounts of added lead impurity upon the substructures of tin crystals. Amounts of added lead are given in atomic percentages.

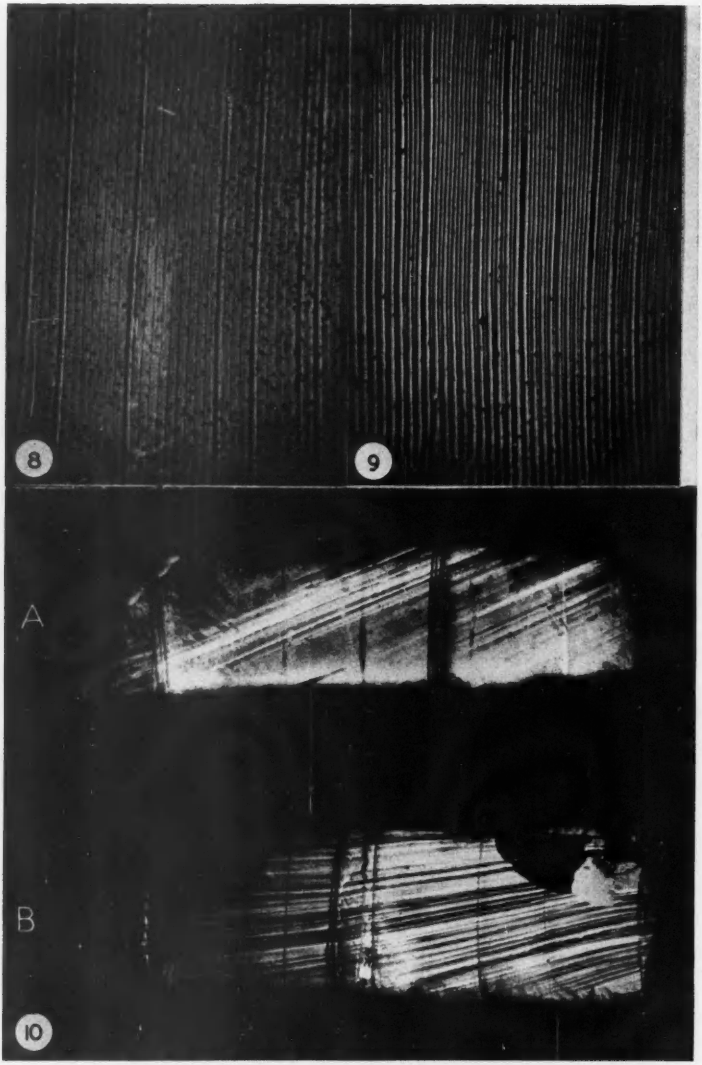

FIG. 8. Typical striation boundary grooves and corrugations on top surface of impure tin crystal. Magnification 35×.

FIG. 9. Striation boundary grooves and corrugations on impure tin, showing transfer of striation boundary to adjacent cell boundary. Magnification 35×.

FIG. 10. Striated lead crystals. Added silver impurity: A, 0.028%; B, 0.187%. Effect of growth-speed variations at $\dot{R}$ less than 15 mm./minute are visible in B.

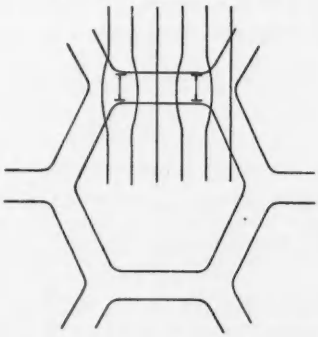

FIG. 11. Dislocations in cell boundaries. Schematic; not to scale.

angle boundaries, the cellular structure may be determined in direction by dislocations.

It must be remarked that the observations on striation directions which have been reported here are not sufficient to determine whether the direction and rectilinearity of these substructures in the presence of impurities are the consequence of a minimization of the volume elastic energy of dislocation arrays, or are the result of the behavior of the surface configuration at the solid–liquid interface. It has been shown (Rutter and Chalmers 1953) that a freezing crystal may exhibit a regular pattern of projections separated by grooves, on the liquid–solid interface. It may be assumed that this pattern of cell-boundary groove sites moves transversely across the interface at a fraction of the speed of interface advance. If the lateral speed of the groove pattern depends asymptotically upon rate of growth, R, this model results in the formation of cellular structure having the characteristic direction angle ψ. If it is further postulated that the striation boundaries occur in the cell walls since they can have minimum boundary energy there, the directional properties of the striations then would appear as a consequence of interface phenomena.

REFERENCES

COTTRELL, A. H. 1953. Dislocations and plastic flow in crystals (Oxford University Press, London).
GOSS, A. J., BENSON, K. E., and PFANN, W. G. 1956. Acta Met. **4**, 333.
RUTTER, J. W. and CHALMERS, B. 1953. Can. J. Phys. **31**, 15.
TEGHTSOONIAN, E. and CHALMERS, B. 1951. Can. J. Phys. **29**, 370.
——— 1952. Can. J. Phys. **30**, 388.
TILLER, W. A., JACKSON, K. A., RUTTER, J. W., and CHALMERS, B. 1953. Acta Met. **1**, 428.

EMISSION BAND SPECTRA OF NITROGEN

A STUDY OF SOME SINGLET SYSTEMS[1]

ALF LOFTHUS

ABSTRACT

Ten bands of Gaydon's and Herman's singlet systems and eight new bands have been photographed under high resolution and analyzed in detail. Two of the new transitions were shown to be $^1\Sigma_u^+$—$a\ ^1\Pi_g$, the upper state being in one case identical with Watson's and Koontz's state g, and one new transition to be $^1\Delta_g$—$w\ ^1\Delta_u$ in type. It is proposed that the new state $^1\Delta_g$ has the same electron configuration as the $x\ ^1\Sigma_g^-$ state. Two bands in the red and one band in the ultraviolet could not be assigned with certainty. Local perturbations in the $b'\ ^1\Sigma_u^+$ state were observed and shown to be caused by the $v = 1$ level of the $b'\ ^1\Sigma_u^+$ state. Observed pecularities in the rotational structure of most of the upper states are proposed to be indicative of a transition from case b' to d' coupling. In some cases pronounced decreases in branch intensities were observed, indicating predissociations probably caused by "forbidden" intercombination processes. Identification of the electronic structure of the higher singlet states in terms of Rydberg orbitals is discussed. Rotational and vibrational constants and excitation energies are presented.

INTRODUCTION

The emission band spectrum of nitrogen in the visible and near ultraviolet region produced under ordinary a-c. or d-c. discharge at low gas pressure consists mainly of a part of the Lyman–Birge–Hopfield system, the fifth positive system, and Gaydon's and Herman's systems, all singlets, and of the first, the second, and the fourth positive systems, all triplets.

The nitrogen band spectra have been the subject of numerous investigations through decades, but most of the measurements were done under rather limited resolution.[2] The present author has recently made an extensive study of all the singlet systems from 2000 to 9000 Å under ordinary a-c. discharge at low gas pressure, and analyzed under very high resolution the fine structure of all bands sufficiently free from overlapping structures. In three previous papers the results of this study were presented for the fifth positive system (Lofthus 1956*a*), the Lyman–Birge–Hopfield system (Lofthus 1956*b*), and Kaplan's first and second systems (Lofthus and Mulliken 1957). (Hereafter referred to as Parts I, II, and III.) In this paper results are presented for the analysis of Gaydon's and Herman's systems, and of some new bands.

The group of Gaydon's and Herman's singlet systems, which all involve the $a\ ^1\Pi_g$ state[3] as the lower state, was first studied independently by Gaydon

---

[1]Manuscript received October 29, 1956.
Contribution from Department of Physics, University of Oslo, Blindern, Norway.
This work was supported by the Norwegian Research Council of Science and the Humanities.

[2]For references of the works on the nitrogen spectra up to 1950, cf. the books by Herzberg (1950) and Pearse and Gaydon (1950).

[3]At the time Gaydon's and Herman's systems were first studied the a state was believed to be $^1\Pi_u$. However, as Herzberg (1946) has shown, this state must be $^1\Pi_g$ in type, and the symmetry notations for the upper states have been changed accordingly. The letters used in designating the electronic states in the present work are those adopted in Herzberg's book (1950).

(1944) and by Herman (1945) (Gaydon and Herman 1946), who assigned eight systems to this group. Herman analyzed only the vibrational structures, but Gaydon also analyzed the rotational structures of some of the bands. Some of these systems have also been studied by Janin (1943*a*, *b*, 1945, 1946*a*, *b*, 1950) and Janin and Crozet (1946), who also added three new systems to the same group. Attempts to identify some of the upper levels involved in these systems with levels known from the absorption measurements of Watson and Koontz (1934) and of Worley (1943) and to fit others into Rydberg series have been made by several authors (in addition to references just cited, see Gaydon and Worley 1944; Herzberg 1946; Setlow 1948; Tschulanowsky 1935; Worley 1944).

The present author obtained altogether 10 bands belonging to five of Gaydon's and Herman's systems, and eight bands belonging to five new transitions, which were sufficiently free from overlapping structures and otherwise well developed to be analyzed in detail. Owing to the high resolution used in the present work, fairly reliable rotational constants and band origins could be evaluated. Strong perturbations and other forms of irregularities in the rotational structure in most of the upper states were observed and will be discussed.

EXPERIMENTAL

All bands except two were photographed in the second order of a 21-ft. grating spectrograph with a dispersion of 0.65 Å/mm., and a resolving power of about 250,000. Two bands in the red and infrared were photographed in the first order of another 21-ft. grating spectrograph with a dispersion of 2.6 Å/mm. and a resolving power of about 50,000. The plates used were Kodak Spectrum Analysis No. 1, Type F, and Type N in the ultraviolet, the visible, and the infrared region, respectively. The excitation conditions were exactly the same as described in Part I of this series.

GAYDON'S AND HERMAN'S SYSTEMS

The fine structure analysis of five of Gaydon's and Herman's systems is presented in this section. Appropriate rotational constants and vibrational intervals as given in Table XI show clearly that all the systems have $a\ ^1\Pi_g$ as the lower state. In the case of $^1\Sigma$—$^1\Pi$ transitions there was observed an intensity alternation: even J strong, odd J weak for P and R branches, and even J weak, odd J strong for Q branches. Usually the intensity distribution between the branches was $Q > P > R$ for the $^1\Sigma$—$^1\Pi$ transitions, except in two cases where it was $Q \approx P \gg R$, and $P \approx R$ for the $^1\Pi$—$^1\Pi$ transition. According to these observations it can be concluded that the upper states must be $^1\Sigma_u^+$ in type in the case of $^1\Sigma$—$^1\Pi$, and $^1\Pi_u$ in the case of $^1\Pi$—$^1\Pi$ transitions.[3]

The wave numbers and intensities for individual lines of the bands are given in Tables I to X. The maximum density of each line was measured from photometer curves and converted into intensity, and the strongest line in each band was set equal to 10.0. Such intensity measurements are of course not very accurate, but a correct qualitative picture can apparently be given.

More or less pronounced peculiarities in the rotational structures and in the branch intensities were observed in most of these systems. In the cases where shifts of the observed rotational levels from their "normal" positions $F_v(J) = B_vJ(J+1)$ were found, these shifts were calculated using ν_0 and B_v values evaluated from the present measurements, and are listed in the last column of the wave number tables, and shown graphically in Figs. 1 and 2. The nature of these peculiarities will be discussed more fully in a later section.

Rotational and vibrational constants were evaluated from the wave number measurements by the usual methods as outlined by Herzberg (1950), and are given at the end of the corresponding wave number table. A summary of all the evaluated constants is also given in Tables XI and XII. Since most of the upper states were perturbed in some way, the combination differences $\Delta_1F'(J)$ and $\Delta_2F'(J)$ versus $(J+1)^2$ and $(J+\frac{1}{2})^2$, respectively, did not at all form straight lines; consequently the evaluations of the rotational constants and band origins were encumbered with somewhat greater uncertainty than usual. An estimate of the uncertainty is given in each case.

1. The System $p'\ ^1\Sigma_u^+$—$a\ ^1\Pi_g$

A progression of the six bands λλ 2827.1 (0, 0), 2967.0 (0, 1), 3118.6 (0, 2), 3283.3 (0, 3), 3463.3 (0, 4), and 3661.1 Å (0, 5), all degraded to the red, has been reported and assigned to this system. Gaydon (1944) analyzed the rotational structure of the (0, 0) band and found indication of a perturbation in the upper state about $J = 10$; the same perturbation was also observed by Janin (1946*a*) and by Setlow (1948).

Also in this case the (0, 0) band was the only one sufficiently free from overlapping structure to be analyzed in detail. Table I gives the observed wave

TABLE I

WAVE NUMBERS AND INTENSITIES OF THE BAND LINES IN THE p'--a SYSTEM OF N_2

	$\lambda_{BH} = 2827.1$ Å (0, 0), $\nu_0 = 35371.2$ cm^{-1}						
J	$Q(J)$	Int. Q	$R(J)$	Int. R	$P(J)$	Int. P	$F'(J)_{obs}-F'(J)_{calc}$
1	35371.86	1.3	b*		b		0.02
2	373.17	1.2	b		b		0.05
3	375.08	5.6	35390.46	7.2	b		0.04
4	377.62	2.0	396.86	2.1	b		0.01
5	380.77	10.0	403.86	b	b		−0.02
6	384.60	3.8	411.38	3.0	35361.50	6.0	−0.06
7	388.90	10.0	419.44	1.4	362.17	b	−0.24
8	393.73	3.8	427.93	2.8	363.15	4.0	−0.51
9	399.02	7.1	b		364.79	1.2	−0.99
10	403.98	2.0	b		366.87	3.0	−2.38
11	415.44	3.2			368.66	0.7	2.03
12	422.94	5.0			376.88	1.1	1.82

*In this and in subsequent tables b indicates blended lines.

$B_0' = 1.929 \pm 0.005$ cm^{-1}, $\nu_{00}(p'—a) = 35371.2 \pm 0.2$ cm^{-1}.

numbers and intensities of the individual lines, and the rotational constants and band origins as evaluated from these measurements.

The perturbation in the upper state was readily observed, the maximum perturbation lying between $J = 10$ and $J = 11$ at an energy of 25604.3 cm^{-1} above the $a\ ^1\Pi_g$ state, or 104557.3 cm^{-1} above the ground state. After the

maximum perturbation the intensity of the lines decreased abruptly, and the branches could not be followed after $J = 12$.

The shifts of the observed rotational levels from their calculated positions, $\Delta\nu = F'(J)_{obs} - F'(J)_{calc}$, are listed in the last column of Table I and also shown in Fig. 1. As will be seen, over the measured J region (J up to 12) this

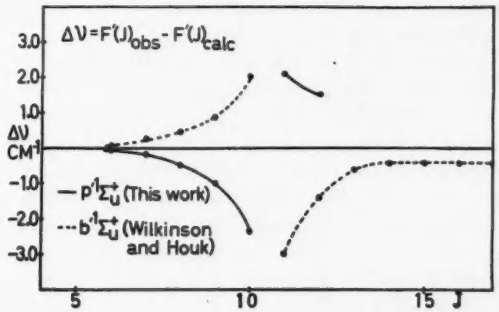

FIG. 1. The mutual perturbation between the $v = 0$ level of the $p'\,{}^1\Sigma_u^+$ state and the $v = 1$ level of the $b'\,{}^1\Sigma_u^+$ state of nitrogen. The difference between the observed and calculated position of the rotational levels is plotted against J. The maximum perturbation occurs between $J' = 10$ and $J' = 11$.

perturbation is the same in magnitude, but opposite in direction, as the perturbation in the $v = 1$ level of the $b'\,{}^1\Sigma_u^+$ state, as observed by Wilkinson and Houk (1956), and almost exactly at the same position (104552.8 cm^{-1}). It might therefore be concluded that there is a mutual perturbation between the p' and b' states, as also suggested by Setlow (1948). However, Wilkinson and Houk concluded that the b' state might be perturbed by a $^1\Pi_u$ state rather than by the $p'\,{}^1\Pi_u^+$ state, since it was found that the rotational levels do not return to normal position after the perturbed region, but are shifted downward by 0.45 cm^{-1}. If this permanent shift is real,[4] and since there can be no doubt that there is a local perturbation between p' ($v = 0$) and b' ($v = 1$), then there must be one or more $^1\Pi_u$ states in the neighborhood which perturb both p' and b'. In fact, Janin (1950) has reported such a state ($l\,{}^1\Pi_u$) at 104141 cm^{-1}, exhibiting a large Λ-type splitting (the Π^+ levels are below Π^-) which in turn indicated perturbation by a $^1\Sigma_u^+$ state (tentatively identified as the p' state by Janin). Since the $l\,{}^1\Pi_u$ state is below $b'\,{}^1\Sigma_u^+$, we should expect the permanent shift of the rotational levels to be pointed upwards, not downwards as actually observed. However, the whole problem is likely to be more complicated, since other $^1\Pi_u$ and $^1\Sigma_u^+$ states than those already observed may lie in the same region (for instance higher vibrational levels of the $b\,{}^1\Pi_u$ state). Also, shifts due to uncoupling phenomena, as observed in the

[4] It seems possible to eliminate this shift by even a very slight change in the rotational constants involved in the calculations of $F'(J)$ for the relatively short J region (16–26) under consideration, without affecting the shift of the lower levels perceptibly. Also, as Dr. Wilkinson has pointed out (private communication), an error of only 0.003 Å in one of the vacuum standards could easily explain the existence of an apparent shift of this magnitude.

TABLE II

WAVE NUMBERS AND INTENSITIES OF THE BAND LINES IN THE m—a SYSTEM OF N_2

	λ_{BH} = 2746.2 Å (0, 0), ν_0 = 36394.5 cm^{-1}				λ_{BH} = 2877.9 Å (0, 1), ν_0 = 34728.4 cm^{-1}				λ_{BH} = 3020.3 Å (0, 2), ν_0 = 33090.0 cm^{-1}			
J	$R(J)$	Int. R	$P(J)$	Int. P	$R(J)$	Int. R	$P(J)$	Int. P	$R(J)$	Int. R	$P(J)$	Int. P
1	b		—		b		—		b		—	
2	b		36387.67	b	b		b		b		33082.40	3.5
3	b		383.53	b	b		b		b		078.79	4.3
4	b		378.84	5.0	b		34712.91	2.6	b		074.69	6.5
5	b		373.75	8.3	b		707.92	4.6	b		069.94	5.5
6	36403.49	10.0	368.07	7.0	34737.89	10.0	702.52	5.8	33100.33	10.0	064.74	4.1
7	402.69	8.4	361.88	6.3	737.42	9.1	696.63	4.5	099.95	7.9	059.11	5.6
8	401.51	6.0	355.24	5.6	736.51	7.6	690.30	5.1	099.30	6.8	053.03	4.6
9	399.69	b	348.08	5.8	735 05	7.6	683.47	5,1	098.20	5.9	046.50	4.7
10	397.70	b	340.47	5.1	733.27	4.7	676.29	9.1	096.74	6.8	039.64	4.1
11	394.67	b	332.28	5.3	730.89	3.4	668.44	5.4	094.83	4.1	032.23	5.7
12	391.69	5.0	323.69	5.3	727.99	b	660.32	4.3	092.52	3.6	024.54	3.7
13			314.49	b	724.65	2.9	651.58	3.8				
14							642.74	b				
15							632.78	b				

$B_0' = 1.361 \pm 0.001$ cm^{-1}, $\nu_{00}(m—a) = 36394.5 \pm 0.2$ cm^{-1}.

other $^1\Sigma_u^+$ states, may also be present. A possible permanent shift of the rotational levels of the $p'\ ^1\Sigma_u^+$ state could, because of the very short branches observed, unfortunately not be confirmed.

2. The System $m\ ^1\Pi_u$—$a\ ^1\Pi_g$

A progression of the four bands λλ 2746.2 (0, 0), 2877.9 (0, 1), 3020.4 (0, 2), and 3174.8 Å (0, 3), all degraded to the red, has been reported and assigned to this system. Janin (1943*a*, *b*, 1946*a*), however, treated these bands as the $v' = 1$ progression of the system d—$a\ ^1\Pi_g$, but so far no rotational analysis of any band belonging to the $v' = 0$ progression of this last system has been done which could support Janin's suggestion.

Gaydon (1944) analyzed the rotational structure of the (0, 0) and (0, 1) bands and found indications of a perturbation in the upper state about $J = 12$ and a resolution into two Λ-components. However, the existence of this perturbation could not be confirmed because of overlapping structure and limited resolving power.

Also in this case the present system was badly masked by stronger structure, but still an analysis of the (0, 0), (0, 1), and (0, 2) bands could be carried out. The observed wave numbers and intensities of the lines of the P and R branches are given in Table II. A very weak Q branch was probably present in all bands, but could not be measured with certainty.

The combination differences indicated no obvious perturbation in the upper state about $J = 12$; the intensity of the branch lines however seemed to decrease considerably about this point and the branches could not be followed any longer, a fact which might indicate a predissociation at about 13.08 ev. Unfortunately, none of the bands belonging to this system were sufficiently resolved from their overlapping structure, so that nothing more definite about possible irregularities could be said.

3. The System $r'\ ^1\Sigma_u^+$—$a\ ^1\Pi_g$

The two bands λλ 2671.8 (0, 0) and 2796.0 Å (0, 1) (Q heads) have been assigned to this system. In this case only the (0, 0) band was sufficiently free from overlapping structure to be analyzed. This band is slightly degraded to the violet, the Q branch being strongly piled-up but still resolved. The observed wave numbers and intensities are given in Table III.

TABLE III

WAVE NUMBERS AND INTENSITIES OF THE BAND LINES IN THE r'—a SYSTEM OF N_2

	$\lambda_{QBH} = 2671.7$ Å (0, 0). $\nu_0 = 37417.1$ cm^{-1}						
J	$Q(J)$	Int. Q	$R(J)$	Int. R	$P(J)$	Int. P	$F'(J)_{obs} - F'(J)_{calc}$
1	37417.38	2.0	b		37413.95	1.0	0
2	417.71	1.9	37427.94	1.7	410.85	b	0
3	418.32	5.5	431.90	1.2	408.04	1.5	0
4	419.07	2.8	436.05	2.2	405.44	3.4	−0.08
5	419.95	10.0	440.24	1.7	402.96	1.9	−0.18
6	420.99	4.3	444.56	2.7	400.68	5.4	−0.34
7	422.04	10.0	448.91	1.5	398.49	2.6	−0.72
8	423.19	4.3	453.23	2.5	396.37	6.2	−1.21
9	424.30	10.0	457.38	1.2	392.26	2.9	−1.94
10	425.32	5.6	461.34	2.0	392.19	6.2	−3.05
11	426.33	10.0			389.87	b	−4.44
12					387.45	6.2	

$B_0' = 1.711 \pm 0.002$ cm^{-1}, $\nu_{00}(r'$—$a) = 37417.1 \pm 0.2$ cm^{-1}.

The predissociation in the upper state indicated in Gaydon's (1944) measurements showed up very clearly in this case as a sharp cutting-off of all branches above $J' = 11$; at least the intensities had decreased so much that the branches could not be followed after this point. Since $F'(11)$ is at 106591.3 cm^{-1} and $F'(12)$ at 106630.4 cm^{-1}, we have a predissociation limit at 106611 ± 20 $cm^{-1} = 13.214 \pm 0.003$ ev.

The observed predissociation limit is very close to another predissociation at 13.233 ± 0.002 ev. observed in the $v = 4$ level of the $b'\ ^1\Sigma_u^+$ state by Wilkinson and Houk (1956) and discussed in some detail by them. It might therefore be concluded that the r' and b' states are predissociated by the same state.[5]

TABLE IV

WAVE NUMBERS AND INTENSITIES OF THE BAND LINES IN THE s'—a SYSTEM OF N_2

	λ_{QBH} = 2397.0 Å (0, 0), ν_0 = 41705.3 cm^{-1}						
J	$Q(J)$	Int. Q	$R(J)$	Int. R	$P(J)$	Int. P	$F'(J)_{obs} - F'(J)_{calc}$
1	b		b		b		0
2	b		41715.13	2.5	41699.19	4.4	0
3	b		718.31	2.4	695.92	3.0	0
4	b		721.43	3.0	692.67	6.3	0
5	b		724.42	1.6	689.39	3.2	0
6	b		727.33	3.9	686.05	7.1	0
7	41704.93	b	730.46	1.6	682.66	3.6	0
8	704.51	5.1	732.78	3.7	679.19	7.4	−0.13
9	703.89	8.6	b		675.56	3.9	−0.49
10	702.98	5.1	737.03	2.7	671.72	7.4	−1.16
11	701.73	8.5	b		667.64	3.6	−2.12
12	699.96	4.4	739.31	b	663.16	6.9	−3.50
13	697.59	10.0	b		658.25	3.6	−5.58
14	694.36	3.8	738.35	3.2	652.59	7.4	−8.33
15	690.15	6.1	b		646.24	b	−12.17
16	684.68	3.1	732.27	2.6	638.79	5.2	−17.13
17	677.75	5.6			630.14	b	−23.68
18	669.13	2.8			619.97	4.4	−31.67
19	658.70	5.3			608.22	2.7	−41.68
20	646.24	b					−53.58
21	631.97						−67.26
22	615.64						−82.84

	λ_{QBH} = 2603.3 Å (0, 2). ν_0 = 38400.5 cm^{-1}					
J	$Q(J)$	Int. Q	$R(J)$	Int. R	$P(J)$	Int. P
1	b		b		b	
2	b		38410.41	5.8	38394.35	3.0
3	b		b		391.34	3.0
4	b		416.92	b	388.39	b
5	b		420.66	1.4	385.39	b
6	b		423.97	3.0	382.57	7.2
7	38402.03	b	b		379.75	5.5
8	402.03	b	430.31	4.5	376.80	7.8
9	402.03	b	b		373.84	5.6
10	b				370.72	8.4
11	401.48	b			367.42	b
12	b				363.84	10.0
13	399.17	8.1			359.75	6.0
14	396.94	4.6			355.22	9.2
15	393.82	6.8			349.85	6.7
16	389.50	4.5			343.60	9.1
17	383.77	5.8			336.15	4.7
18	376.50	b			327.38	8.0
19	367.42	b			316.79	b
20					304.74	5.5

$B_0' = 1.595 \pm 0.005$ cm^{-1}, $\nu_{00}(s'—a) = 41705.3 \pm 0.2$ cm^{-1}.

[5]Wilkinson and Houk (1956) suggested that the predissociation in the b' state is an accidental one, i.e., perturbation by a predissociating state, and that this state is $C\ ^3\Pi_u$.

The shifts of the rotational levels of the $r'\ ^1\Sigma_u^+$ state, which are listed in Table III, are pointed downwards.

4. The System $s'\ ^1\Sigma_u^+$—$a\ ^1\Pi_g$

Three bands λλ 2397.1 (0, 0), 2496.8 (0, 1), and 2603.3 Å (0, 2) (Q heads), all degraded to the red, have been reported. In this case the (0, 0) and (0, 2) bands could be analyzed; the wave numbers and intensities of these are given in Table IV.

In both these bands the first lines of the Q branches were strongly piled-up but soon became more open, a fact which is obviously due to pronounced irregularities in the rotational structure of the upper state. The shifts of the rotational levels of the $s'\ ^1\Sigma_u^+$ state are listed in Table IV, and, as can be seen, these shifts are very large and pointed downwards.

As also observed by Gaydon (1944), there was an anomalous intensity distribution between the branches for this transition. The R branch was very weak, but the P branch had about the same over-all intensity as the Q branch, whereas in normal cases the intensity distribution $Q > P > R$ should be expected for a $^1\Sigma$—$^1\Pi$ transition. Gaydon pointed out that this is a similar effect to one observed for NiH (Gaydon and Pearse 1935) which he ascribed to the unusual structure of the initial state.

5. The System $h\ ^1\Sigma_u^+$—$a\ ^1\Pi_g$

A progression of the five bands λλ 2281.5 (0, 0), 2371.6 (0, 1), 2569.6 (0, 3), 2678 (0, 4), and 2795.6 Å (0, 5) (Q heads) has been reported as belonging to this system. The (0, 2) band, which should lie at about 2469 Å, could definitely not be seen. Certainly this region was strongly masked, but not so badly that the (0, 2) band should not be seen if it had normal intensity. Gaydon (1944) also pointed out this peculiar fact that the (0, 2) band seemed to be absent.

The (0, 0), (0, 1), and (0, 3) bands could be analyzed in this case. They were all slightly degraded to the red, and showed strongly piled-up Q branches. Only for the (0, 3) band was the Q branch sufficiently resolved to be measured; however, for this same band the R branch was too weak. Also for the (0, 0) and (0, 1) bands the R branches were weaker than expected, so that the system is in this respect similar to the s'—a system. This anomalous intensity distribution between the branches might also in this case be attributed to an unusual form of the rotational structure of the upper state.

The shifts of the rotational levels in the upper state are listed for the (0, 1) band in Table V. As can be seen, these shifts are also in this case very large, and pointed downwards.

There was a clear indication of a not too sharp predissociation in the upper state. The branches had a normal intensity up to $J' = 10$, from where the intensity decreased markedly. Since $J' = 10$ is at 112915.3 cm^{-1} and $J' = 11$ is at 112948.5 cm^{-1}, we can put the predissociation limit at 112932 ± 17 cm^{-1} = 14.004 ± 0.002 ev.

TABLE V

WAVE NUMBERS AND INTENSITIES OF THE BAND LINES IN THE h—a SYSTEM OF N_2

	λ_{QBH} = 2281.5 Å (0, 0), ν_0 = 43816.5 cm^{-1}				λ_{QBH} = 2569.8 Å (0, 3), ν_0 = 38901.5 cm^{-1}			
J	$R(J)$	Int. R	$P(J)$	Int. P	$Q(J)$	Int. Q	$P(J)$	Int. P
1	b		b		38901.54	b	b	
2	43826.72	b	b		901.80	5.3	38889.19	5.6
3	830.77	5.5	b		902.35	6.0	892.39	3.4
4	833.69	6.5	43804.16	b	903.10	b	889.85	b
5	836.98	b	801.27	6.8	903.88	7.2	887.45	5.3
6	840.23	b	798.41	10.0	904.81	6.5	885.22	7.3
7	b		795.36	b	905.77	10.0	883.02	6.2
8	846.30	6.6	792.37	b	906.45	b	880.76	8.2
9			789.05	7.7	906.93	9.1	878.39	b
10			785.35	9.3			875.85	7.5
11			783.11	6.4			b	
12			780.88	7.4			868.57	6.0
13							864.96	5.4

	λ_{QBH} = 2371.7 Å (0, 1), ν_0 = 42150.5 cm^{-1}				
J	$R(J)$	Int. R	$P(J)$	Int. P	$F'(J)_{obs} - F'(J)_{calc}$
1	b		b		0
2	42160.83	0.5	42144.25	3.7	0
3	164.40	b	141.34	2.5	0
4	168.01	1.8	138.48	5.5	−0.12
5	171.64	b	135.74	3.1	−0.30
6	175.23	3.1	133.04	10.0	−0.61
7	178.59	b	130.35	4.5	−1.11
8	181.56	5.5	127.54	7.9	−1.95
9	183.89	1.1	124.56	3.9	−3.28
10	185.34	0.7	121.21	6.9	−5.38
11	b		117.25	2.4	−8.56
12	186.40	0.5	112.27	3.8	−12.47
13			106.38	0.8	−16.95
14			100.83	1.7	

$B_0' = 1.655 \pm 0.002$ cm^{-1}, $\nu_{00}(h—a) = 43816.5 \pm 0.2$ cm^{-1}.

NEW BANDS

In this section are presented the results of the fine structure analysis of the eight new singlet bands λλ 2054.1(R), 2368.8(V), 2477.3(V), 2498.6(R), 2524.9(R), 2753.8(R), 6895.2(V), and 8937.0(V) Å (R and V indicating that bands are degraded to the red and to the violet, respectively).

6. The 2498.4 Å Band

This band,[6] degraded to the red, was very weak and short but showed clearly one P, one R, and one Q branch with intensity alternation: even J strong, odd J weak for the P and R branches; odd J strong, even J weak for the Q branch. It was hard to tell which of the branches P or R was the stronger, because the R lines which formed the head were piled-up and blended, but probably the intensity distribution was $Q > P > R$. Wave numbers and intensities of the branch lines are given in Table VI. Appropriate combination differences showed clearly that the lower level is $v = 0$ of the $a\ ^1\Pi_g$ state. The upper state must therefore be $^1\Sigma_u^+$ in type.

The upper state of this new band is at 108953.0 cm^{-1} above the ground state. This is very close to the value 108950 cm^{-1} reported (Herzberg 1950, p. 552) for the g state observed in emission to the ground state by Watson and Koontz (1934). It is therefore proposed that the two states are identical, so that the new transition can be written $g\ ^1\Sigma_u^+$—$a\ ^1\Pi_g$. There seemed to be

[6]A band at 2498 Å has also been mentioned by Gaydon (1944) but was not analyzed by him.

TABLE VI

WAVE NUMBERS AND INTENSITIES OF THE BAND LINES IN THE g—a SYSTEM OF N_2

$\lambda_{BH} = 2498.6$ Å (0, 0), $\nu_0 = 40000.7$ cm^{-1}

J	$Q(J)$	Int. Q	$R(J)$	Int. R	$P(J)$	Int. P	$F'(J)_{obs} - F'(J)_{calc}$
1	40000.26	2.2	40005.63	b	b		0.06
2	39999.25	b	007.41	b	39993.81	2.4	0.07
3	997.74	5.3	008.64	b	989.59	1.9	0.08
4	995.78	3.4	009.43	b	984.85	4.0	0.14
5	993.33	7.1	b		979.69	b	0.22
6	990.47	4.3	009.70	b	974.00	4.4	0.41
7	987.20	10.0	b		967.96	2.5	0.67
8	983.59	4.7	008.64	b	961.49	3.8	1.14
9	979.69	b	007.55	b	954.69	2.1	1.77
10	975.52	2.7	006.48	2.2	947.57	3.2	2.66
11	971.16	3.0			940.17	b	3.86
12					932.63	1.4	

$B_0' = 1.356 \pm 0.003$ cm^{-1}, $\nu_{00}(g—a) = 40000.7 \pm 0.2$ cm^{-1}.

a breaking-off of all branches above $J' = 11$, but the lines from $J' = 10$ and $J' = 11$ were already somewhat weakened, which should indicate the presence of a weak predissociation. Placing the predissociation limit between $J' = 9$

TABLE VII

WAVE NUMBERS AND INTENSITIES OF THE BAND LINES IN THE k—a SYSTEM OF N_2

$\lambda_{BH} = 2524.9$ Å (0, 0), $\nu_0 = 39593.5$ cm^{-1}

J	$Q(J)$	Int. Q	$R(J)$	Int. R	$P(J)$	Int. P	$F'(J)_{obs} - F'(J)_{calc}$
1	39593.11	b	b		b		−0.04
2	592.28	b	b		b		−0.12
3	591.21	b	b		39582.72	b	−0.20
4	589.71	2.7	b		578.33	3.3	−0.30
5	587.73	b	b		573.59	b	−0.48
6	585.49	3.7	39605.28	b	568.50	4.1	−0.63
7	582.72	b	605.28	b	563.03	3.4	−0.94
8	579.65	b	604.85	b	557.07	5.1	−1.28
9	576.00	8.0	603.93	b	550.69	3.2	−1.77
10	571.88	3.7	602.55	b	543.87	6.7	−2.38
11	567.25	8.4	600.60	b	536.57	3.9	−3.15
12	562.02	4.1	597.91	b	528.72	8.4	−4.16
13	556.20	8.4	594.63	b	520.29	3.4	−5.46
14	549.66	3.7	590.43	2.8	511.23	8.4	−7.08
15	542.37	10.0	585.49	b	501.49	3.7	−9.16
16	534.27	3.1	579.65	b	491.01	6.6	−11.69
17	525.22	5.9	573.59	b	479.66	3.1	−14.78
18	515.24	2.8			467.43	4.7	−18.20
19	504.14	3.9					−22.86

$\lambda_{BH} = 2753.8$ Å (0, 2), $\nu_0 = 36288.6$ cm^{-1}

J	$Q(J)$	Int. Q	$R(J)$	Int. R	$P(J)$	Int. P
1	b		b		b	
2	36287.63	0.6	b		b	
3	286.75	2.8	b		b	
4	285.51	2.3	b		b	
5	283.97	4.3	b		36269.74	2.0
6	282.06	3.4	b		265.11	3.6
7	279.88	5.6	b		260.08	2.2
8	277.30	2.9	b		254.73	3.6
9	274.31	8.8	36302.49	3.2	248.98	2.8
10	270.93	3.4	301.78	4.0	242.90	5.2
11	267.09	10.0	300.50	3.2	236.40	3.0
12	262.73	3.8	298.62	4.0	229.40	5.5
13	257.82	8.8	296.22	2.7	221.95	3.7
14	252.28	4.1	293.14	3.5	213.90	8.4
15	246.08	10.0	289.22	2.6	205.20	2.9
16	239.05	3.9	284.60	2.7	195.85	6.4
17	231.31	8.4	278.99	2.3	185.76	b
18	222.58	4.3	272.44	2.6	174.82	5.2
19	212.90	6.8				
20	202.14	3.3				
21	190.29	7.3				
22	177.25	3.2				

$B_0' = 1.435 \pm 0.005$ cm^{-1}, $\nu_{00}(k—a) = 39593.5 \pm 0.2$ cm^{-1}.

and $J' = 10$, we have, since $J' = 9$ is at 109077.5 cm^{-1} and $J' = 10$ at 109105.5 cm^{-1}, for this limit 109092 ± 14 cm^{-1} or 13.528 ± 0.002 ev.

The shifts of the rotational levels of the $g\ ^1\Sigma_u^+$ state, as shown in Table VI, are in this case pointed upwards.

7. The Bands 2524.9 and 2753.8 Å.

These two bands, degraded to the red, were fairly well developed, and showed one R, one P, and one Q branch with intensity alternation: even J strong, odd J weak for P and R, and even J weak, odd J strong for the Q branch. The intensity relation between the branches was $Q > P > R$. Wave numbers and intensities are given in Table VII.

Appropriate combination differences showed clearly that the two bands have the same upper level, and that the lower levels are the $v = 0$ and $v = 2$ levels, respectively, of the $a\ ^1\Pi_g$ state. Other bands of the same progression could not be seen. Since the lower state is $a\ ^1\Pi_g$, the upper state must be $^1\Sigma_u^+$ in type.

From the rotational constants and band origins as given in Table VII, it can not be concluded that this system is part of any other known system. It is therefore probably best to treat it as a separate system. The letter k is proposed to designate the upper state, so that the transition can be written $k\ ^1\Sigma_u^+ — a\ ^1\Pi_g$.

The shifts of the rotational levels of the $k\ ^1\Sigma_u^+$ state were calculated from the (0, 0) bands of this system, the results of which are given in Table VII. The shifts are pointed downwards.

8. The 2368.8 and 2477.3 Å *Bands*

The first of these bands, which was rather weak, but still fairly well developed, showed only one single branch (head-forming), without intensity alternation. However, assuming that there were both a P and an R branch that coincided, the band could be analyzed. A very weak Q branch was possibly present, but could not be observed with certainty. No perturbations or Λ-type splitting could be observed.

Wave numbers and intensities for the branch lines are given in Table VIII. The combination differences evaluated for the lower state are comparable equally well with those for the $v = 3$ level of the $a'\ ^1\Sigma_u^-$ states and with those for the $v = 4$ level of the $w\ ^1\Delta_u$ state (Parts I and III) as shown in Table VIII*b*. The possibility that the transition is $^1\Sigma_g^- — a'\ ^1\Sigma_u^-$ can be ruled out, since this would lead to coincidence of P and R lines of the same parity, thus giving rise to strong intensity alternations, and a $^1\Pi_g — a'\ ^1\Sigma_u^-$ or $^1\Pi_g — w\ ^1\Delta_u$ transition can also be ruled out, because of the absence of a strong Q branch. A possibility left is that the transition is from a new upper state $^1\Delta_g$ to the $v = 4$ level of the $w\ ^1\Delta_u$ state: $^1\Delta_g(v = ?) — w\ ^1\Delta_u(v = 4)$.[7]

The second of these bands, 2477.3 Å,[8] was somewhat stronger than the

[7]The best clue as to the type of transition would of course be given by determining the number of missing lines near the zero gap. Unfortunately, this could not be done with certainty in this case.

[8]A band at 2477 Å has been mentioned by Kaplan (1934*a*), but not analyzed by him.

TABLE VIII

WAVE NUMBERS AND INTENSITIES OF THE BAND LINES IN THE z—a SYSTEM OF N_2

	λ_{BH} = 2368.8 Å (3, 4), ν_0 = 42210.3 cm^{-1}				λ_{BH} = 2477.3 Å (0, 2), ν_0 = 40362.5 cm^{-1}			
J	$R(J)$	Int. R	$P(J)$	Int. P	$R(J)$	Int. R	$P(J)$	Int. P
1	?		?		?		?	
2	42222.35		?		40374.77	b	b	
3	227.45		42203.44		380.24	5.4	b	
4	233.30		202.30		386.11	5.6	b	
5	239.43		201.75		392.62	6.9	b	
6	246.07		201.75		399.78	6.9	40354.20	b
7	253.48		202.30		407.47	b	354.96	b
8	261.44		203.44		415.86	8.0	356.28	7.1
9	269.88		205.17		424.87	9.2	358.25	7.6
10	279.08		207.45		434.44	10.0	360.86	7.1
11	288.77		210.28		444.65	8.0	363.97	8.5
12	299.07		213.67		b		367.77	7.6
13	309.97		217.70		466.83	8.7	372.17	7.8
14			222.35				377.17	8.0
15			227.45				382.78	8.0
16							389.06	7.7
17							395.81	8.0
18							403.29	8.0
19							411.36	7.7
20							420.06	7.7
21							429.33	b
22							439.35	8.0
23							449.79	7.7
24							460.98	6.9

$B_0' = 1.753 \pm 0.002$ cm^{-1}, $B_2' = 1.707 \pm 0.002$ cm^{-1}, $\nu_{00}(z—a) = 43667.0 \pm 0.2$ cm^{-1}.

b. COMBINATION DIFFERENCES, $\Delta_2F''(J)$ (cm^{-1})

J	2368.8 Å	2477.3 Å	$a'\,{}^1\Sigma_u^-$ $v = 3$	$w\,{}^1\Delta_u$ $v = 4$	$w\,{}^1\Delta_u$ $v = 2$
1					
2					
3	20.05				
4	25.70				
5	31.55	31.91		31.30	
6	37.13	37.66	37.00	36.94	
7	42.63	43.50	42.62	42.58	43.68
8	48.31	49.22	48.27	48.36	49.57
9	53.99	55.00	54.03	54.04	55.29
10	59.60	60.90	59.91	59.68	
11	65.41	66.67	65.73	65.37	66.88
12	71.07	72.48	71.08		72.76
13	76.72		76.79	76.76	78.40
14	82.43	84.05	82.31	82.33	83.85

former, and showed two branches of about the same over-all intensity. The branches were obviously one R and one P branch (head-forming). No strong Q branch could be present, but possibly a very weak one. Wave numbers and intensities of the branch lines for this band are also given in Table VIII.

The combination differences for the lower state of this band are comparable with those for the $v = 2$ level of the $w\,{}^1\Delta_u$ state as shown in Table VIII*b*, although there seems to be a small but systematic difference between the two columns. From similar considerations as above it may be concluded that this band is due to a transition from a new ${}^1\Delta_g$ state to the $v = 2$ level of the $w\,{}^1\Delta_u$ state: ${}^1\Delta_g(v = ?)$—$w\,{}^1\Delta_u(v = 2)$.

From the rotational constants and vibrational intervals as given in Table VIII, it seems reasonable to conclude that the two bands belong to the same system. If so, and since the difference between the two vibrational levels is 4802.2 cm^{-1}, the difference between the vibrational quantum numbers is most probably 3, giving a ω_e of about 1600–1700 cm^{-1}, and a α_e of 0.0153 cm^{-1},

which should be reasonable for a state with B_e about 1.75 cm^{-1}. The letter z is proposed to designate the new state, so that the transition can be written $z\ ^1\Delta_g$—$w\ ^1\Delta_u$.

If real, this new state $z\ ^1\Delta_g$ can be interpreted as originating from the $^2D+^2P$ limit at 15.713 ev. Two $^1\Delta_g$ states can originate from this combination; the only other low energy atomic combination that can yield $^1\Delta_g$ states is $^2D+^2D$; however, this limit is at 14.522 ev., i.e., below both of the observed levels.

The existence of such a $^1\Delta_g$—$w\ ^1\Delta_u$ transition was also discussed in Part III. It was there pointed out that one must expect, among others, a $^1\Delta_g$ state of the same electron configuration as the $x\ ^1\Sigma_g^-$ state ($\ldots \pi_u^3\ \sigma_g^2\ R\pi_u$). The identification of the new z state as the expected $^1\Delta_g$ state is supported by the fact that B_e and ω_e for $z\ ^1\Delta_g$ (B_e = 1.761 cm^{-1}, ω_e = 1600–1700 cm^{-1}) are close to B_e and ω_e for $x\ ^1\Sigma_g^-$ (B_e = 1.750 cm^{-1}, ω_e = 1910.0 cm^{-1}) as expected for states of the same configuration.

9. The Band 2054.1 Å

This band was very weak, degraded to the red, and showed one R and one P branch with intensity alternation, but no Q branch could be seen. The transition is therefore most probably $^1\Sigma$—$^1\Sigma$ in type. The observed wave numbers of the branch lines are given in Table IX.

TABLE IX

WAVE NUMBERS OF THE LINES OF THE 2054.1 Å N_2 BAND
$\nu_0 = ca.$ 48600 cm^{-1}

R	P
48668.10 *w*	48596.25 *w*
667.03 *s*	593.82 *s*
665.49 *w*	591.46 *w*
663.58 *s*	589.16 *s*
661.33 *w*	586.54 *w*
658.67 *s*	583.97 *s*
655.74 *w*	581.04 *w*
652.78 *s*	577.88 *s*
649.56 *w*	574.30 *w*
646.41 *s*	570.31 *s*
643.17 *w*	565.80 *w*
639.88 *s*	560.71 *s*
	554.96 *w*

s and *w* indicate strong and weak lines.

Unfortunately, only the first part of the P branch and the last part of the R branch (after the head) were free from overlapping structure, so that no pair of lines to evaluate combination differences was available. The second differences ($= 2(B'-B'')$) could however easily be found for both branches, and showed that at least one of the states involved in the transition was strongly perturbed. Since the band origin is about 48600 cm^{-1}, or 6.03 ev., the upper state must at least be 14–15 ev. above the ground state.

10. The Bands 6895.5 and 8937.0 Å

These two bands, both degraded to the violet, were fairly well developed. They showed clearly one Q and one P branch, but the positions of the stronger parts of the R branches were completely masked by strong first positive

bands; consequently no R branches could be observed. The intensity of the P branches seemed to exceed that of the Q branches, which is unexpected.

Wave numbers and intensities of the branch lines are given in Table X.

TABLE X

WAVE NUMBERS AND INTENSITIES OF THE LINES OF THE 6895.5 Å AND 8937.0 Å N_2 BANDS

λ_{BH} = 6895.5 Å, ν_0 = 14508.7 cm^{-1}				λ_{BH} = 8937.0 Å, ν_0 = 11200.3 cm^{-1}			
Q	Int. Q	P	Int. P	Q	Int. Q	P	Int. P
14508.94	b	14498.18	b	11200.72	b	11186.37	b
509.36	1.0	498.50	b	201.57	1.0	186.77	2.0
510.02	b	499.08	3.0	202.83	1.8	187.37	1.0
510.97	1.0	499.87	b	204.41	1.1	188.20	3.1
512.19	2.0	500.84	3.4	206.34	3.5	189.28	1.3
513.66	1.7	501.99	1.3	208.63	1.4	190.59	8.7
515.41	2.4	503.38	3.5	211.26	9.0	192.09	1.4
517.53	b	504.84	1.5	214.22	1.6	193.80	10.0
519.75	3.0	506.66	b			195.71	1.8
522.32	1.5	508.55	b			197.75	9.0
525.14	4.3	510.59	6.4			199.96	b
528.21	b	512.79	2.0			202.33	10.0
531.59	4.3	515.10	10.0			204.80	1.4
535.22	1.4	517.53	b			207.39	10.0
539.12	4.3	520.06	10.0			210.10	1.2
543.25	b	522.69	3.2			212.89	1.9
547.68	3.9	525.37	7.0				
552.31	b	528.13	b				
557.20	2.2	530.90	3.2				
		533.75	1.0				
		536.61	1.3				

No J-numbering is given in this table. However, it is just possible that both of the Q branches given there start with $J = 1$. (The given ν_0's depend of course upon the correctness of this J-numbering.) Owing to a perturbation in either or both of the states involved in the transition, and to the absence of the R branches, no reasonable J-numbering could be found for the observed parts of the P branches.

The only conclusion which can be drawn from these measurements is that the two bands may be part of the same system, and that the transition may be $^1\Sigma$—$^1\Pi$ or $^1\Pi$—$^1\Sigma$ in type, the states both having fairly low B values (1.00–1.20 cm^{-1}).

THE $a\ ^1\Pi_g$ STATE

The rotational constants, B_v, for the $a\ ^1\Pi_g$ state were determined from the mean value of combination relations $\Delta_1F''(J)$ and $\Delta_2F''(J)$ from all appropriate bands studied in this work. In a similar way the vibration intervals, $\Delta G(v)$, were determined as the mean difference between band origins of consecutive members of the various progressions. The results are presented in Table XI. For comparison, the same constants derived from the high pre-

TABLE XI

ROTATIONAL CONSTANTS AND VIBRATIONAL INTERVALS FOR THE $a\ ^1\Pi_g$ STATE OF N_2 (cm^{-1})

v	B_v		$G(v)$	
	Part II	This work	Part II	This work
0	1.6090	1.608±0.001	1666.05	1666.2±0.2
1	1.5907	1.590±0.001	1638.40	1638.4±0.2
2	1.5724	1.573±0.001	1610.75	1610.6±0.2

cision measurements of the a—X system in Part II are listed in the same table. As can be seen, there is, within the limit of error, complete agreement between the two sets of measurements.

Owing to the very short bands observed for these transitions, the Λ-type splitting in the $a\ ^1\Pi_g$ state could not be measured.

SUMMARY AND DISCUSSION

The observed molecular constants for the singlet states of N_2 studied in the present work and in the previous three parts of this series are collected in Table XII. In order to make this table more complete, the results obtained

TABLE XII

SUMMARY OF CONSTANTS FOR SINGLET STATES OF N_2 (cm^{-1})

State	ν_0[a]	B_0	B_e	α_e	ω_e	Remarks
$z\ ^1\Delta_g$	(118134)	1.753	1.761	0.0153	~1700	New state
$y\ ^1\Pi_g$	(116944)	1.792c			1707.9	Part III
		1.770d			($\Delta G_{1/2}$)	
$x\ ^1\Sigma_g^-$	(115990)	1.739	1.750	0.0225	1910.0	Part I
$h\ ^1\Sigma_u^+$	112769.5	1.655				
$s'\ ^1\Sigma_u^+$	110658.3	1.595				
$g\ ^1\Sigma_u^+$	108953.7	1.356				
$d'\ ^1\Pi_u$	108698.0	1.797				Janin (1950)
$k\ ^1\Sigma_u^+$	108546.5	1.435				New state
$r'\ ^1\Sigma_u^+$	106370.1	1.711				
$o\ ^1\Pi_u$	105684	1.694			2020.00	Janin (1950), Worley (1953)
$m\ ^1\Pi_u$	105347.5	1.361				
$p'\ ^1\Sigma_u^+$	104324.2	1.929				
$l\ ^1\Pi_u$	104141.0	1.502c				Janin (1950)
		1.486d				
$b'\ ^1\Sigma_u^+$	103672.1	1.152	1.154	0.0048	751.64	Wilkinson and Houk (1956)
$w\ ^1\Delta_u$	(74467)	1.490	1.498	0.0166	1548.0	Part III
$a'\ ^1\Sigma_u^-$	(70517)	1.472	1.480	0.0164	1530.0	Part I
$a\ ^1\Pi_g$	68953.00	1.6090	1.6181	0.0183	1693.70	Part II
$X\ ^1\Sigma_g^+$	0	1.9897	1.9983	0.01709	2358.07	Part II

[a]The values in parentheses are lower limits based upon the assumption that the $v = 0$ level of the a' state is at 70517 + C cm^{-1}, where C most likely is very small (Lofthus and Mulliken 1957).

in other high resolution work have been added. These are for the $d'\ ^1\Pi_u$, $o\ ^1\Pi_u$, and $l\ ^1\Sigma_u^+$ states studied by Janin (1950),[9] and for the $b'\ ^1\Sigma_u^+$ state studied by Wilkinson and Houk (1956). The two new states observed here, $^1\Delta_g$ and $^1\Sigma_u^+$, have tentatively been designated z and k, respectively.

As was shown in the preceding descriptions of the various systems, there are pronounced shifts of the rotational levels from their "normal", calculated positions in the p', r', s', h, g, and $k\ ^1\Sigma_u^+$ states. In the case of $p'\ ^1\Sigma_u^+$ these shifts were shown to be caused by a local perturbation from the $b'\ ^1\Sigma_u^+$ state, but in the other cases the form and magnitude of the shifts (see Fig. 2) indicate strongly a transition from case b' toward case d' coupling. For such high energy levels as these, and where in addition the levels may be members

[9]The state $d\ ^1\Pi_u$ observed by Janin is here designated d' in order to avoid confusion with the state d at 104718 cm^{-1} listed in Herzberg's book (1950, p. 553). The state $o\ ^1\Pi_u$ was designated o' by Janin, the present designation being in accordance with Worley's (1953).

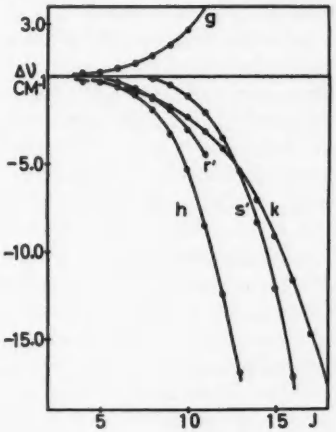

FIG. 2. Shifts of the rotational levels from their "normal" positions, $\Delta\nu = F'(J)_{obs} - F'(J)_{calc}$, for the r', k, g, s', and $h\ ^1\Sigma_u^+$ states of nitrogen, plotted against J. Qualitatively, these curves can be represented by polynomials of third degree, as expected in the cases where transition from case b' to d' coupling takes place.

of Rydberg series, an uncoupling is indeed to be expected, thus leading to an unusual rotational band structure.

In the case of singlet states the rotational term values can usually be written

$$F_v(J) = B_vJ(J+1) - D_vJ^2(J+1)^2 ,$$

but in the case of uncoupling we have to add a certain "uncoupling term" $\Phi(J)$. According to Mulliken (1930, 1931), the following expression for $\Phi(J)$ can be used if the uncoupling does not go very far:

$$\Phi(J) = \kappa + \epsilon J + \delta J(J+1) + \eta J^3 ,$$

where κ, ϵ, δ, and η are constants.

As can be seen from Fig. 2, the observed shifts have the expected form; however attempts to reproduce these shifts by formulae of the type just mentioned, with fixed constants, were not completely successful, nor could any definite correlation be found between the magnitude of the shifts in the various states and the energies and constants of the same states. However, there is no reason to believe that uncoupling is the only phenomenon that affects the rotational levels in these cases. In the energy region under consideration (12–15 ev.) there certainly are numerous states of the proper symmetry type to perturb each other. Also, three or four of the observed states are most likely predissociated over a potential hill. In the vicinity of such a hill a potential curve deviates strongly from its normal course, and a certain shift of the rotational levels might thus be accounted for. Thus there are various possibilities for explaining shifts of rotational levels, but apparently no single possibility can explain everything.

The observed predissociations were in the h, g, and $r'\ ^1\Sigma_u^+$ states at 14.00, 13.53, and 13.21 ev., respectively, and possibly in the $m\ ^1\Pi_u$ state at 13.08 ev. Since none of these predissociations coincide with any dissociation limit, we must have predissociations over potential hills, caused by repulsive states. Assuming the repulsive states to originate from the first dissociation limit below the predissociation limit, the h and $g\ ^1\Sigma_u^+$ states should dissociate into a pair of $^4S+^2P$ atoms at 13.330 ev., and the $r'\ ^1\Sigma_u^+$ and $m\ ^1\Pi_u$ states into $^4S+^2D$ at 12.139 ev., over potential hills 0.67, 0.20, 1.07, and 0.94 ev., respectively.

The only electronic states resulting from $^4S+^2D$ are triplets and quintets; consequently the predissociations must be "forbidden" intercombination processes ($\Delta S \neq 0$). The conclusion that the predissociations are forbidden is also supported by the fact that, except in the r'—a bands, the cutting-off of the branches was never really sharp. The states with the proper symmetry to cause the observed predissociations are $^{3,5}\Pi_u$ resulting from $^4S+^2P$, and $^{3,5}\Pi_u$ and $^{3,5}\Sigma_u^+$ from $^4S+^2D$ (if they are repulsive).

In three of these cases the potential hills are rather high. As Wilkinson and Houk (1956) have pointed out, high potential hills can best be understood if the predissociations considered are accidental ones; i.e. perturbation by a predissociating state. The same authors observed a predissociation in the $v = 4$ level of the $b'\ ^1\Sigma_u^+$ state at 13.23 ev., which, as already mentioned, is very close to the predissociation in $r'\ ^1\Sigma_u^+$ at 13.21 ev., and suggested that this predissociation is accidental, caused by the $C\ ^3\Pi_u$ state.

With regard to the electronic structure of the observed singlet states, it was shown in Part III that the $x\ ^1\Sigma_g^-$ and $y\ ^1\Pi_g$ states could be obtained by adding an electron in a Rydberg orbital to the electronic core of the $A\ ^2\Pi_u$ state of N_2^+, so that $x\ ^1\Sigma_g^-$ is $\ldots \pi_u^3\, \sigma_g^2\, R\pi_u$ and $y\ ^1\Pi_g$ is $\ldots \pi_u^3\, \sigma_g^2\, R\sigma_u$, and that one must expect $^3\Sigma_g^-$, $^3\Delta_g$, $^1\Delta_g$, $^3\Sigma_g^+$, and $^1\Sigma_g^+$ states of the same configuration as x, and a $^3\Pi_g$ state corresponding to y (of which only $^1\Delta_g$ and $^1\Sigma_g^+$ can be expected to be stable). As was shown in the previous section, the observed $z\ ^1\Delta_g$ state had molecular constants very similar to those of x and y, and therefore it might reasonably be concluded that $z\ ^1\Delta_g$ is $\ldots \pi_u^3\, \sigma_g^2\, R\pi_u$.

Now it is interesting to see whether other states can be identified in which an electron in a Rydberg orbital is present. In fact, there seem to be a few more cases in which such an identification can be made. First, if we add a σ_g electron to the $\ldots \pi_u^3\, \sigma_g^2$ core, we shall have $^1\Pi_u$ and $^3\Pi_u$ states of the configuration $\ldots \pi_u^3\, \sigma_g^2\, R\sigma_g$ with molecular constants similar to those of the x and y states. The $o\ ^1\Pi_u$ state with $B_0 = 1.694\ \text{cm}^{-1}$, $\omega_e = 2020\ \text{cm}^{-1}$, might possibly be this expected $^1\Pi_u$ state, and in fact Worley (1953) has shown that the $v = 1$ level of this state is the upper term for the first band in a new Rydberg series converging to the $A\ ^2\Pi_u$ state of N_2^+. In a similar way, the observed $r'\ ^1\Sigma_u^+$ state, with $B_0 = 1.711\ \text{cm}^{-1}$, might account for the $^1\Sigma_u^+$ state which can be obtained by adding a π_g electron to the same core.[10] Second, the

[10]Professor Mulliken has pointed out (private communication) that it is not quite probable that there should be two Rydberg states o and r', one $^1\Pi_u$ and one $^1\Sigma_u^+$, close together and both belonging to a $^2\Pi_u$ ion. Unless, possibly, the $r'\ ^1\Sigma_u^+$ state is really $^3\Pi_{0u}^+$, which might mix somewhat with various $^1\Sigma_u^+$ states and thus acquire transition probability. One would also have to assume that this $^3\Pi_{0u}^+$ is part of $^3\Pi_u$ located somewhat above $o\ ^1\Pi_u$, which is improbable and would have to be explained by strong perturbing interactions.

$D\ ^3\Sigma_u^+$ ($B_0 = 1.961\ \text{cm}^{-1}$, $\omega_e = ?$) and $p'\ ^1\Sigma_u^+$ ($B_0 = 1.929\ \text{cm}^{-1}$, $\omega_e = 2217\ \text{cm}^{-1}$) states may be obtained by adding a σ_u electron to the ground state of N_2^+ ($B_0 = 1.922\ \text{cm}^{-1}$, $\omega_e = 2207\ \text{cm}^{-1}$). It might perhaps also be pointed out that the B_0 values for the $h\ ^1\Sigma_u^+$ and $s'\ ^1\Sigma_u^+$ states (1.655 and 1.595 cm^{-1}, respectively) are very close to B_0 for the $C\ ^2\Sigma^+$ state of N_2^+ ($\sim 1.65\ \text{cm}^{-1}$). Also the B_0 values for the $g\ ^1\Sigma_u^+$ and $m\ ^1\Pi_u$ states are similar (1.356 and 1.361 cm^{-1}, respectively). However, these and the rest of the observed singlet states can not be compared with any known state of N_2^+.

Whereas the correctness of the vibrational numbering in the $a\ ^1\Pi_g$ state might be beyond doubt, this is far from certain for most of the higher singlet states. In most cases only one upper vibrational level has been observed, which was given $v = 0$, and in the rest of the cases where more than one level has been observed, the lowest of them was given $v = 0$. However, it might be a reasonable question whether some of the states treated separately really are different vibrational levels of the same electronic state. Intensity considerations based on the Frank–Condon principle can hardly be trusted in these cases to establish the vibrational numbering, since intensity anomalies and predissociations are to be expected, and indeed have been observed in some cases. The only thing that could settle these questions definitely would be to measure a possible vibrational isotopic shift in the bands of the $N^{14}N^{15}$ molecule; at present it is probably best to treat the observed states separately.

Many more singlet bands than those already reported can be predicted for nitrogen. In addition, all other levels reported on the basis of vacuum ultraviolet absorption spectra should have the proper symmetry to combine with the $a\ ^1\Pi_g$ state, thus giving bands mostly in the more accessible ultraviolet region. States of the type $^1\Sigma_g^-$ and $^1\Pi_g$ should combine with $a'\ ^1\Sigma_u^-$, and states of the type $^1\Pi_g$ and $^1\Delta_g$ with $w\ ^1\Delta_u$, also giving bands in the near ultraviolet. Transitions between the numerous levels above *ca.* 12 ev. should give rise to bands in the visible and near infrared region. Since in such cases both levels can be expected to be perturbed, the bands may be very difficult to analyze. Of special interest are the transitions a'—a and w—a, which have been predicted to lie in the red and infrared (Part III), but have so far not been observed.[11] However, many of these predicted bands will undoubtedly be very weak.

The present results seem to be the most that can be obtained with this type of excitation (ordinary discharge at low pressure). For example, one particular difficulty in the present work was the very strong first and second positive bands which almost completely dominated the visible and part of the near ultraviolet region, thus preventing the observation of many weaker bands undoubtedly present. Using other types of excitation, further high resolution work on nitrogen bands would be highly desirable. In fact, numerous additional bands obtained under various conditions have been reported, notably by Kaplan (1934*a*, *b*), Gaydon (1944), Janin (1943 *a*, *b*, 1945, 1946 *a*, *b*, 1950), Carroll and Sayers (1953), Brook (1955), and others, but none of these bands have been analyzed in detail.

[11]Four new bands, 6897, 7788, 8247, and 8459 Å, all degraded to the red, have been observed in the N_2 afterglow spectrum by Brook (1955). It is just possible that some of these bands might belong to the predicted systems.

ACKNOWLEDGMENTS

Most of the plates studied in the present work were taken during the author's stay at the Laboratory of Molecular Structure and Spectra, The University of Chicago, and the author would like to express his sincere gratitude for the great hospitality shown him.

Further, the author greatly acknowledges the value of correspondence with Professor R. S. Mulliken and Dr. P. G. Wilkinson (Chicago). Finally, thanks are due to Mrs. and Dr. J. G. Hauge for a critical reading of the manuscript.

REFERENCES

BROOK, M. 1955. University of California, Institute of Geophysics Progress Report No. 11, Contract No. AF 19 (122) 453.
CARROLL, P. K. and SAYERS, N. D. 1953. Proc. Phys. Soc. A, **66**, 1138.
GAYDON, A. G. 1944. Proc. Roy. Soc. A, **182**, 286.
GAYDON, A. G. and HERMAN, R. 1946. Proc. Phys. Soc. **58**, 292.
GAYDON, A. G. and PEARSE, R. W. B. 1935. Proc. Roy. Soc. A, **148**, 321.
GAYDON, A. G. and WORLEY, R. E. 1944. Nature, **153**, 747.
HERMAN, R. 1945. Ann. phys. (11), **20**, 241.
HERZBERG, G. 1946. Phys. Rev. **69**, 362.
———1950. Spectra of diatomic molecules (D. Van Nostrand Co., Inc., New York).
JANIN, J. 1943*a*. Cahiers phys. **16**, 73.
———1943*b*. Compt. rend. **217**, 392.
———1945. Compt. rend. **220**, 218.
———1946*a*. Ann. phys. **1**, No. 12, 538.
———1946*b*. Compt. rend. **223**, 321.
———1950. J. recherches centre natl. recherche sci. **12**, 1.
JANIN, J. and CROZET, A. 1946. Compt. rend. **223**, 1114.
KAPLAN, J. 1934*a*. Phys. Rev. **46**, 631.
———1934*b*. Phys. Rev. **46**, 534; **47**, 259.
LOFTHUS, A. 1956*a*. J. Chem. Phys. **25**, 494.
———1956*b*. Can. J. Phys. **34**, 780.
LOFTHUS, A. and MULLIKEN, R. S. 1957. J. Chem. Phys. **26** (In press).
MULLIKEN, R. S. 1930. Phys. Rev. **2**, 60, 506.
———1931. Phys. Rev. **3**, 102.
PEARSE, R. W. B., and GAYDON, A. G. 1950. The identification of molecular spectra (Chapman and Hall, Ltd., London).
SETLOW, R. B. 1948. Phys. Rev. **74**, 153.
TSCHULANOWSKY, W. M. 1935. Bull. Acad. Sci. U.R.S.S. **1**, 1313.
WATSON, W. W. and KOONTZ, P. G. 1934. Phys. Rev. **46**, 32.
WILKINSON, P. G. and HOUK, N. B. 1956. J. Chem. Phys. **24**, 528.
WORLEY, R. E. 1943. Phys. Rev. **64**, 207.
———1944. Phys. Rev. **65**, 249.
———1953. Phys. Rev. **89**, 863.

NOTES

HIGH RESISTANCE MEASUREMENTS*

A. F. DUNN

Despite everyone's familiarity with the Wheatstone Bridge network, the suggestion by Schuster (1895) and Callandar (1909) that the sensitivity of the network may be increased by a factor of approximately two when the ratio arms (A and B) are made proportionately smaller than the measuring arms (X and S) appears to have been overlooked. Under certain conditions it is also possible to obtain another increase of nearly two in sensitivity by making the ratio of the bridge network ($X/S = A/B$) greater than unity. It is the purpose of this note to describe a bridge built in this laboratory of readily available equipment which takes advantage of both these factors, and which is capable of measuring resistances up to 10^{11} ohms with high accuracy.

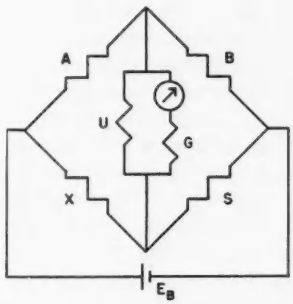

FIG. 1.

Using the notation for the conventional network shown in Fig. 1, it may be readily shown that the expression for the bridge balance is

$$X = (A/B)(S \pm \delta S) = (A/B)S(1 \pm \epsilon)$$

and ϵ, which is the smallest detectable proportional change in the variable arm, and hence in the measured quantity X, is given by

$$\epsilon = X(1+A/X)(1+B/A)\delta I_g/E_B,$$

where δI_g is the minimum detectable change of current through the galvanometer. This simplified expression, which is the same for either the normal or the conjugate connection of the network, is derived on the assumptions $G \ll (A+B)$, or $\ll XS/(X+S)$, or $\ll U$. For any value of X, the value of ϵ decreases, or the sensitivity increases, when A/X is made less than unity and when A/B is made greater than unity.

*Issued as N.R.C. No. 4187.

A high resistance bridge has been constructed using precision radio resistors of 10^3, 10^4, 10^5, 10^6, 10^7 ohms as the ratio arms and a six dial resistance box of maximum value 1.11111×10^7 ohms as the measuring arm. The latter was constructed from a commercial five dial resistance box with a sixth dial of 10^6 ohm precision radio resistors added. The demountable ratio arms allow the observer to measure all the ratio arms by means of the bridge itself, in terms of a known 10^4 ohm standard, as well as to obtain the corrections to the measuring arm by autocalibration.

The insulation between connecting points must be very high (10^{12} ohms or more) so as to introduce no serious errors in the value being measured or in the higher ratio arms. This need for high insulation between components and connecting points is probably the most stringent requirement of the bridge.

As detector, any galvanometer of high current sensitivity is satisfactory provided that it is shunted by the appropriate external critical damping resistance. An increase of five to ten times in the effective sensitivity of the galvanometer may be readily obtained by Dauphinee's (1955) deflection multiplier for reflecting galvanometers. If a suitable double coil galvanometer is available, then the second coil may be shunted by its proper CDRX and the shunt resistor (U) in Fig. 1 eliminated from the working coil.

The sensitivity of this network has been calculated for different values of components assuming a minimum detectable change in galvanometer current of 5×10^{-11} amp., which is the sensitivity available with the galvanometer in use. With a maximum bridge voltage (E_B) of 500 volts, calculation and measurement both show that $\epsilon \leqslant \pm 1 \times 10^{-6} = \pm 0.0001\%$ for X up to 10^7 ohms. As X is increased from 10^7 ohms to 10^{11} ohms, then ϵ, being directly proportional to X, increases from $\pm 0.0001\%$ to $\pm 1\%$, which is about the limit of useful accuracy of the bridge. Above 10^8 ohms the conjugate connection is preferable to the normal as this reduces the voltage drop across the ratio arm resistors and improves their stability.

It is clear that in the past the full capabilities of the Wheatstone network have not been utilized for precise measurement of resistances above 10^6 ohms. The instrument described here permits resistances up to 10^8 ohms to be compared to $\pm 0.001\%$ and 10^{11} ohms to $\pm 1\%$. With equipment readily available in any laboratory, results may be obtained which are superior to most insulation test sets commercially available today, with a net cost which is considerably less.

CALLANDAR, H. L. 1909. Proc. Phys. Soc. (London), **22**, 220.
DAUPHINEE, T. M. 1955. Rev. Sci. Instr. **26**, 873.
SCHUSTER, A. 1895. Phil. Mag. (5), **39**, 175.

RECEIVED AUGUST 13, 1956.
DIVISION OF APPLIED PHYSICS,
NATIONAL RESEARCH COUNCIL,
OTTAWA, CANADA.

A SIMPLE IONIZATION GAUGE CONTROL CIRCUIT WITH OVERLOAD PROTECTION*

P. A. REDHEAD

Protection of vacuum apparatus from accidental pressure surges in the vacuum system is often essential. In particular, protection of the ionization gauge filament from burn-out caused by the accidental admission of air to the system is most desirable. The control circuit described herein regulates the electron current in the gauge, and has a simple and reliable overload protection circuit which switches off the ionization gauge when the pressure in the system rises above any preset value. Provision is also made in the overload circuit to disconnect any auxiliary apparatus.

Fig. 1† shows the circuit for the gauge control unit, which is similar in some respects to the Distillation Products HG–200. The component values have been chosen so that the unit is direct-reading in pressure when used with a VG1A ionization gauge; minor modification would be necessary for other types of gauges with different sensitivities. The electron current is controlled and stabilized by the thyratron (2D21) circuit (Richards and Tuthill 1951). The stability of this method of control is not as good as in some more complicated circuits using vacuum tubes; however the stability is adequate (3% drift in 1 hour) after initial warm-up. The simplicity and reliability of this circuit more than justify its use. The ion current amplifier is of standard design; the tube type 5751 has been found most suitable for this application since it has low grid current and is readily balanced. Provision is also made for outgassing the grid of the gauge.

The overload protection circuit is operated by a contact-type meter (Symplytrol Model 351, with separate holding coil). This meter is calibrated to read pressure directly, and has a movable contact which can be set at any required value of pressure. Closure of this contact caused by a pressure surge operates the holding coil in the meter and closes a small relay. The relay contact removes the filament voltage from the gauge and energizes a pair of terminals which may be used for switching any external apparatus. The contact on the meter remains locked until the overload reset is operated.

The overload protection circuit has proved very satisfactory in service and tests have shown that it will prevent any damage to the ionization gauge if the vacuum system is broken.

RICHARDS, P. I. and TUTHILL, W. A. 1951. Rev. Sci. Instr. **22**, 841.

RECEIVED OCTOBER 10, 1956.
RADIO AND ELECTRICAL ENGINEERING DIVISION,
NATIONAL RESEARCH COUNCIL,
OTTAWA, CANADA.

*Issued as N.R.C. No. 4189.
†See page 238.

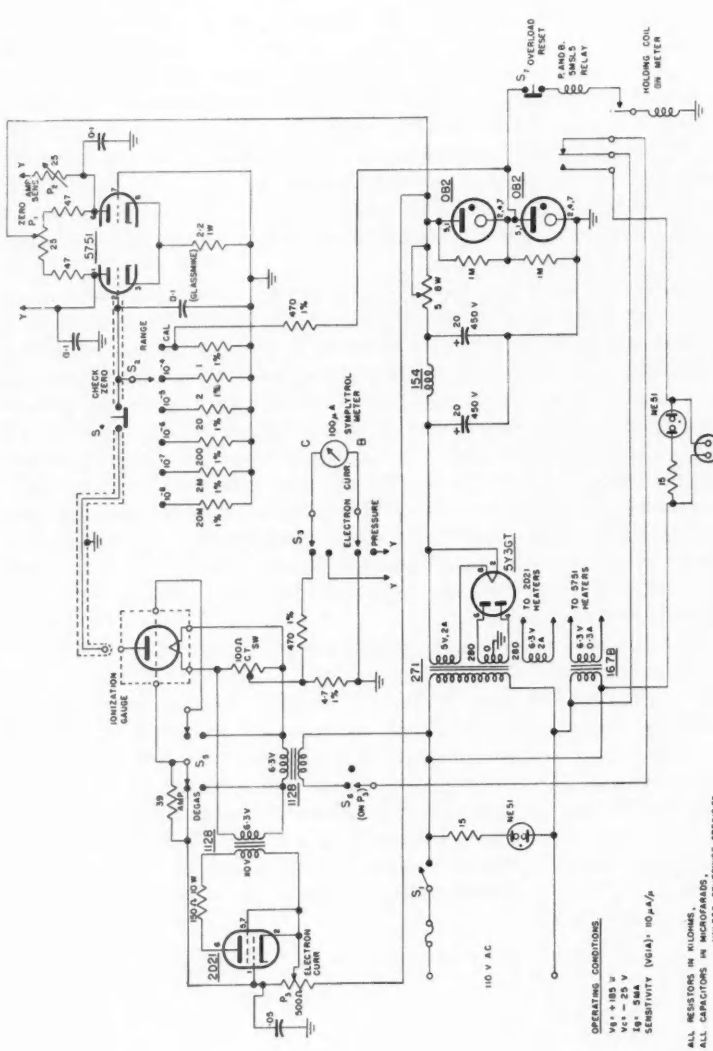
OPERATING CONDITIONS
Vg1 = 185 V
Vc1 = 25 V
Ig1 = 5MA
SENSITIVITY (VG1A) = 110 μA/μ
ALL RESISTORS IN KILOHMS,
ALL CAPACITORS IN MICROFARADS,
UNLESS OTHERWISE SPECIFIED
ALL TRANSFORMERS, HAMMOND MANUFACTURING CO
110 V AC
EXTERNAL OVERLOAD CONTROL
IONIZATION GAUGE
ELECTRON CURR
PRESSURE
100μA SYMPLITROL METER
CHECK ZERO
RANGE
CAL
DEGAS
OVERLOAD RESET
HOLDING COIL ON METER
TO 5751 HEATERS
TO 2021 HEATERS

FIG. 1.

Under this heading brief reports of important discoveries in physics may be published. These reports should not exceed 600 words and, for any issue, should be submitted not later than six weeks previous to the first day of the month of issue. No proof will be sent to the authors.

Controlled Corpuscle Beam Discharges— A Proposed New Method for Attaining High Temperatures and Energy Densities

Recently, with the experimental realization of thermonuclear reactions, the *controlled* fusion of light nuclei has been much discussed (Thirring 1955; Nucleonics Editorials 1955, 1956; Post 1956). A new scheme for the production of a high temperature plasma is proposed here. It is based on controlled discharges of corpuscle beams into gas of high density. It may or may not lead to fusion reactions, but it would certainly produce higher temperatures at higher densities than present methods. The region of hot gas will be far from any walls.

(1) A corpuscle beam is formed and accelerated in a high vacuum. For electrons we can expect to achieve the following values: accelerating voltage $U = 5\times10^5$ v., perveance of the gun $P = 4.4\times10^{-6}$ amp. v.$^{-3/2}$, hence, maximum current $I = 1560$ amp.; focusing ratio cathode area to beam cross section $f = 100:1$, emission $j_0 = 10$ amp./cm.^{2}, hence, current density $j = 1000$ amp./cm.^{2} With $f = 230:1$ (Heil and Ebers 1950) and $j_0 = 60$ amp./cm.^{2} (Danforth 1953) we would even get $j = 13800$ amp./cm.^{2} in the focus. Langmuir's formula gives as a limit $j = 2670$ amp./cm.^{2} or $j = 16020$ amp./cm.^{2} for the two cases assuming the angle of divergence is $\theta = 10^{-2}$ and the cathode temperature is $T = 3000°$ K. For ion beams data are rare. $I = 0.33$ amp. was obtained by Mills and Barnett (1954); a proton gun with $j_0 = 0.23$ amp./cm.^{2} is suggested by Dällenbach (1955).

(2) The beam thus formed is to be led into a gas of high density ρ, for instance 20 times the atmospheric density ρ_0. The technical means to accomplish this, the so-called dynamic pressure stages (Schumacher 1953), has been recently developed. An electron gun working against 10 atmospheres pressure, yielding 200 kev. electrons with $j = 10$ amp./cm.^{2} and $I = 15$ ma., is commercially available (Lorenz 1956). Fig. 1 shows the proposed experimental set-up. The gas jet emerging from the high pressure chamber by-passes the opening of the generator on the side, provided the orifice of the high pressure chamber is properly shaped.

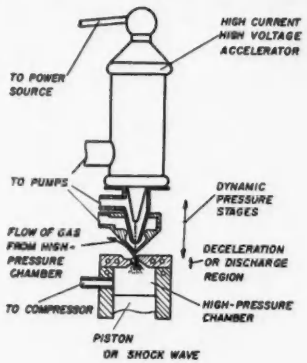

FIG. 1.

(3) The corpuscle beam is stopped in the gas by random scattering. For electrons the specific energy losses are in the order of $\gamma = 10^5$ v./cm. at $\rho = 20\rho_0$, as compared to the gradient of $v = 200\ \gamma$/cm. obtained in arcs and sparks. For ions we can expect $\gamma = 10^6$ v./cm. at $\rho = 2\rho_0$. Gas density and discharge diameter can be chosen freely since nothing which happens in the discharge region will influence the beam formation in the high vacuum. We can call this a *controlled* beam discharge. An electron beam with diameter $d = 0.9$ mm., $j = 10^4$ amp./cm.^{2}, $\gamma = 2.5\times10^5$ v./cm., $I = 60$ amp., $U = 5\times10^5$ v., $N_{tot} = 30$ megawatts, will produce a discharge cylinder approximately 5 mm. long before it spreads over a wider cross section. Assum-

ing this cylinder radiates like a black body, its temperature would be $T = 55000°$ K. The power per surface area would be 5.6×10^7 w./cm.^{2} In sparks 3×10^6 w./cm.^{2} was obtained instantaneously, in arcs 6.3×10^5 w./cm.^{2} Since black body conditions will hardly be reached, the actual temperature will be higher.

Although we have a high density plasma, it is nevertheless difficult to predict whether a suitable number of ions with an energy of 10 kev. or so (see Post 1956) can be produced to give a sufficient reaction density, for instance, for the DT-reaction. In case an ion beam, e.g. T-ions, is shot into high density D-gas we are limited by the low current densities of present-day ion sources; nevertheless, an interesting reaction yield may be achieved, owing to the high target density.

(4) The steady state character of the discharge allows the accumulation of energy over a period of time. It is possible to reduce radiation losses by reflectors and by reflection from the layer of hot gas which builds up around the discharge channel. Then, an additional power pulse, superimposed on the steady state, will not be consumed by ionization processes, and the radiation losses will be reduced by the shield of hot gas already present. This may overcome the "size limit" for microexplosions (Thirring 1955).

(5) The high density in the discharge chamber does not have to be homogeneous. The discharge may be directed into a shock wave moving in opposite direction to the beam, or perpendicular to it. Since the beam particles will pass the low density region in front of the shock wave with negligible energy loss, the reaction will take place in the center of the shock wave and far away from all walls (no "magnetic bottle" would be required!). The shock wave method can eliminate the necessity for high pressures in the discharge chamber (4000 atm. for $T = 50000°$ K., $\rho = 20\rho_0$). Once a reaction has started it would quench itself because of the decrease of density with increasing temperature. It is at present purely speculative, but there seems to be a chance of producing a series of microexplosions with the far-off walls of the reaction chamber as heat exchangers. Regardless of whether or not fusion can finally be achieved, experimental studies of the high density plasma should be interesting for their own sake.

The author is indebted to Dr. A. E. R. Westman and Dr. Ursula Martius for many discussions and encouragement.

DÄLLENBACH, W. 1955. Z. Naturforsch. **10a**, 803.
DANFORTH, W. E. 1953. Thorium oxide and electronics, *in* Advances in electronics, Vol. 5, *edited* by L. Morton (Academic Press Inc., New York).
HEIL, O. and EBERS, J. J. 1950. Proc. I.R.E. **38**, 645.
LORENZ, A. 1956. Paper presented at the Physikertagung, April 27–30, 1956, Bad Nauheim, Germany (Abstract in Physik. Verhandl. **7**, 38 (1956)).
MILLS, C. B. and BARNETT, C. F. 1954. Rev. Sci. Instr. **25**, 1200.
Nucleonics Editorials. 1955. Nucleonics, **13** (10), 9.
——— 1956. Nucleonics, **14** (2), 42.
POST, R. F. 1956. Revs. Mod. Phys. **28**, 338.
SCHUMACHER, B. 1953. Optik, **10**, 116.
THIRRING, H. 1955. Nucleonics, **13** (11), 62.

RECEIVED AUGUST 23, 1956.
B. W. SCHUMACHER
DEPARTMENT OF CHEMISTRY,
ONTARIO RESEARCH FOUNDATION,
43 QUEEN'S PARK,
TORONTO, ONTARIO.

CANADIAN JOURNAL OF PHYSICS

Notes to Contributors

Manuscripts

(i) ***General.*** Manuscripts, in English or French, should be typewritten, double spaced, on paper 8½×11 in. **The original and one copy are to be submitted.** Tables and captions for the figures should be placed at the end of the manuscript. Every sheet of the manuscript should be numbered.

Style, arrangement, spelling, and abbreviations should conform to the usage of this journal. Names of all simple compounds, rather than their formulas, should be used in the text. Greek letters or unusual signs should be written plainly or explained by marginal notes. Superscripts and subscripts must be legible and carefully placed.

Manuscripts and illustrations should be carefully checked before they are submitted. Authors will be charged for unnecessary deviations from the usual format and for changes made in the proof that are considered excessive or unnecessary.

(ii) ***Abstract.*** An abstract of not more than about 200 words, indicating the scope of the work and the principal findings, is required, except in Notes.

(iii) ***References.*** References should be listed **alphabetically by authors' names,** unnumbered, and typed after the text. The form of the citations should be that used in current issues of this journal; in references to papers in periodicals, titles should not be given and only initial page numbers are required. The names of periodicals should be abbreviated in the form given in the most recent *List of Periodicals Abstracted by Chemical Abstracts*. All citations should be checked with the original articles and each one referred to in the text by the authors' names and the year.

(iv) ***Tables.*** Tables should be numbered in roman numerals and each table referred to in the text. Titles should always be given but should be brief; column headings should be brief and descriptive matter in the tables confined to a minimum. Vertical rules should be used only when they are essential. Numerous small tables should be avoided.

Illustrations

(i) ***General.*** All figures (including each figure of the plates) should be numbered consecutively from 1 up, in arabic numerals, and each figure referred to in the text. The author's name, title of the paper, and figure number should be written in the lower left corner of the sheets on which the illustrations appear. Captions should not be written on the illustrations (see Manuscripts (i)).

(ii) ***Line Drawings.*** Drawings should be carefully made with India ink on white drawing paper, blue tracing linen, or co-ordinate paper ruled in blue only; any co-ordinate lines that are to appear in the reproduction should be ruled in black ink. Paper ruled in green, yellow, or red should not be used unless it is desired to have all the co-ordinate lines show. All lines should be of sufficient thickness to reproduce well. Decimal points, periods, and stippled dots should be solid black circles large enough to be reduced if necessary. Letters and numerals should be neatly made, preferably with a stencil (**do NOT use typewriting**) and be of such size that the smallest lettering will be not less than 1 mm. high when reproduced in a cut 3 in. wide.

Many drawings are made too large; originals should not be more than 2 or 3 times the size of the desired reproduction. In large drawings or groups of drawings the ratio of height to width should conform to that of a journal page but the height should be adjusted to make allowance for the caption.

The original drawings and one set of clear copies (e.g. small photographs) are to be submitted.

(iii) ***Photographs.*** Prints should be made on glossy paper, with strong contrasts. They should be trimmed so that essential features only are shown and mounted carefully, with rubber cement, on white cardboard with no space or only a **very** small space (less than 1 mm.) between them. In mounting, full use of the space available should be made (to reduce the number of cuts required) and the ratio of height to width should correspond to that of a journal page (4¾×7½ in.); however, allowance must be made for the captions. Photographs or groups of photographs should not be more than 2 or 3 times the size of the desired reproduction.

Photographs are to be submitted in duplicate; if they are to be reproduced in groups one set should be mounted, the duplicate set unmounted.

Reprints

A total of 50 reprints of each paper, without covers, are supplied free. Additional reprints, with or without covers, may be purchased.

Charges for reprints are based on the number of printed pages, which may be calculated approximately by multiplying by 0.6 the number of manuscript pages (double-spaced typewritten sheets, 8½×11 in.) and including the space occupied by illustrations. An additional charge is made for illustrations that appear as coated inserts. The cost per page is given on the reprint requisition which accompanies the galley.

Any reprints required in addition to those requested on the author's reprint requisition form must be ordered officially as soon as the paper has been accepted for publication.

Contents

Printed in Canada *by* University of Toronto Press